



**University of Tripoli
Faculty of Engineering
Mechanical and Industrial Engineering Department**

**Applying Reverse Engineering in Manufacturing Prototype of Rotor
Components for a Water Pumping Windmill**

Prepared by:

Esmael Mouhammed Hussein Belal

Supervised by:

Dr. Abdulbaset Ali Frefer

**A Thesis submitted in partial fulfillment of the requirements for the
Degree of Master of Science in Industrial Engineering**

Spring 2021– 2022

DECLARATION

I hereby certify that the work contained in this thesis, unless otherwise referenced, is the researcher's own work and has not been previously submitted to meet the requirements of an award at this or any other higher education institution. I furthermore cede the copyright of this thesis in favor of the University of Tripoli.

Esmaeel Mouhammed Belal

Signature

Date/...../2022

الإعتماد النهائي لرسالة الإجازة
العالية (الماجستير) بعد التعديلات
رقم النموذج 101-02-26



جامعة طرابلس
إدارة الدراسات العليا والتدريب

الكلية: الهندسة القسم: الهندسة الميكانيكية و الصناعية

أقر أنا د. عبد الباسط علي فريفر المشرف على رسالة الطالب إسماعيل محمد حسين إبلال المعنونة ب: " تطبيق الهندسة العكسية في تصنيع نموذج اولي لمكونات الجزء الدوار لطحونة ريحية لضخ المياه"

Applying Reverse Engineering in Manufacturing Prototype of Components of a Rotor for Water Pumping Windmill

التي نُوقشت بتاريخ 2022 / 07 / 26م بناءً على قرار السيد رئيس الجامعة رقم (2115) لسنة (2022) بتشكيل لجنة لمناقشتها، بأن الطالب يلتزم بتنفيذ كل التعديلات والتغييرات واستكمل النواقص المطلوبة منه.

توقيع المشرف: د. عبد الباسط علي فريفر

التاريخ 2022 / 8 / 7م

الاعتماد	أعضاء لجنة المناقشة
	1- د. عبد الباسط علي فريفر
	2- أ.د. عثمان محمد عثمان
	3- أ.د. مصطفى عيسى جرناز
	4-

مدير مكتب الدراسات العليا والتدريب بالكلية

الاسم:

التوقيع



رئيس القسم العلمي

الاسم:

التوقيع

عميد الكلية

الاسم:

التوقيع



نسخة الهم:

- 1- منسق الدراسات العليا بالقسم.
- 2- مكتب الدراسات العليا والتدريب بالكلية.
- 3- ثلاثة نسخ لإدارة الدراسات العليا والتدريب بالجامعة.

إدارة الدراسات العليا والتدريب - جامعة طرابلس

Applying Reverse Engineering in Manufacturing Prototype of Rotor Components for a Water Pumping Windmill

Prepared by:
Esmaeel Mouhammed Hussein Belal

Supervised by:
Dr. Abdulbaset Ali Frefer

ABSTRACT

Water-pumping windmills are reliable alternatives to provide water in some areas isolated from the electricity network, especially those with poor wind sources that are insufficient to operate wind turbines to generate electricity. The successful design of windmills for water pumping requires careful study of many variable parameters depending on the wind pattern and topography of the site. However, in this study, the researcher applied the Reverse Engineering (RE) approach, and some activities are usually used as a prerequisite when designing windmills. These activities cannot be neglected when applying RE for successfully manufacturing the windmills for obtaining 3D CAD models of the windmill rotor. The 3D models were the basis for manufacturing the windmill Rotor prototype installed at a pilot site in a suburb of the city of Tajoura. The wind data recorded at the Libyan Center of Solar Energy Research and Studies (CSERS) for several years were used to calculate daily and monthly average wind speed and study the daily wind pattern. The analysis of the collected wind data showed that the minimum and maximum daily average wind speed at Tajoura varies from 2.35m/s to 4.69m/s, and the annual average wind speed is 3.24m/s. Among the design, activities are estimating the wind resources available at the site to size the system to provide the site water requirements of 5 m³/day. From this point on, a commercial water-pumping windmill of 4.88m (16ft) and a standard tower height of 12m was chosen to target a RE application to obtain a CAD model. RE is accomplished in three phases: digitizing the component (part), processing the measured data, and creating the CAD model. To adopt the 3D model for all parts, they must be compared with the original scanned data using Deviation Analysis in CATIA. After adopting the 3D models of all the Rotor components, the 3D assembly models were created based on the RE approach. As for the curving Sails, the researcher applied the reverse engineering approach to design a bending die for curving water pumping windmill Sails, using simulation programming Computerized numerical control (CNC) machines utilizing computer-aided design and computer-aided manufacturing (CAD/CAM) systems and CNC machining technology to manufacture the die. The Computer-Aided Three-Dimensional Interactive Application (CATIA) V5 was used as an integrated CAD/CAM system for designing and developing the die and simulating the operation through graphic models in 3D. Due to the difficulty of manually manufacturing the curving of the Sails based on the available labor, the number of Sails used to produce one unit of the water pumping windmill, and the importance of the Sails in improving the efficiency of the windmill system, the researcher's decision was made to design and manufacture a single-operation die. This die consists of four parts to suit the available CNC machine capacity for curving the Sails using the Sail's 3D model of the RE. A CAM model was prepared to machine the die parts, a tool path simulation was performed using CATIA V5, and all machining operations were programmed. Using a CNC machine center, all the die parts were machined, assembled using welding, and the Sails prototypes were manufactured. Finally, it is worth noting that the windmills for water pumping could not be manufactured solely by just applying reverse engineering.

KEYWORDS: Windmills, Rotor, CAD/CAM, CATIA, Point cloud, RE, Laser Scanning, CNC.

DEDICATION

This thesis is wholeheartedly dedicated to the Almighty God and my beloved parents, who have been my source of inspiration and gave me strength. To my wife and my children, who have always supported me and stood by all my decisions, including choosing my course of study.

ACKNOWLEDGEMENT

It is my duty to dedicate this space of my work to the people who have contributed to its realization with their tireless support. A special thanks to my supervisor for his infinite availability, immense patience, indispensable advice, and the knowledge transmitted throughout every step of the thesis, from the choice of the topic up to the end draft.

A heartfelt thanks to my brothers, sisters, relatives, friends, and classmates who shared their words of advice and encouragement to finish this study.

I thank all the staff of the Trucks and Buses Company staff, the Al-Inma Company, the Libyan Center for Solar Energy Research and Studies, the Higher Technical Center for Training and Production, and the Advanced Center of Technology for hospitality and skills acquired in the field.

CONTENTS

DECLARATION/N.....	I
ABSTRACT	III
DEDICATION	IV
ACKNOWLEDGEMENT.....	V
CONTENTS	1
TABLES	4
FIGURES	5
LIST OF ACRONYMS	8
CHAPTER ONE:.....	10
1 INTRODUCTION	11
1.1 Background.....	11
1.2 Problem Statement.....	13
1.3 Research Objectives.....	14
1.4 Research Limitations	14
1.5 Expected Scientific Contributions	14
1.6 Methodology.....	15
1.7 Potential Contributors to the Research and their Contribution.....	16
CHAPTER TWO:.....	17
2 LITERATURE REVIEW.....	18
2.1 Wind Energy Technology	18
2.2 Reverse Engineering Technology.....	18
2.3 Overview of RE Technology	19
2.4 Applications of RE Process	20
2.5 Rapid Prototyping	20
2.6 Technical Data Development.....	21
2.7 Preparation for RE Process	21
2.7.1 Reverse engineering teams	21
2.7.2 Communication with system users	21
2.7.3 Data collection.....	21
2.7.4 Technical data and manuals.....	21
2.7.5 Data evaluation	22
2.8 Reverse Engineering Cost.....	22
2.9 Determination of Project Type.....	22
2.10 Comparison with the Available Data	23
2.11 Reverse Engineering Process	23
2.11.1 Digitization of the object:	23
2.11.2 Data segmentation.....	24
2.11.3 Creation of CAD model:.....	24
2.12 Physical Mock-Up and Digital Mock-Up	25
2.13 Background of the Windmill.....	25
2.14 Manufacturing Processes Classification.....	26
2.15 Machining Process	27

2.16	Traditional Machining Processes	27
2.16.1	Turning.....	28
2.16.2	Milling	28
2.16.3	Roughing and finishing operations	32
2.17	CNC Machining Process	32
2.18	CAD and Engineering	33
2.19	CAD and Manufacturing Combination	33
2.20	Sheet Metal Cutting and Forming Processes.....	34
2.20.1	Cutting operations.....	35
2.20.2	Cutting forces.....	36
2.20.3	Bending operations	36
2.20.4	Bending force.....	38
2.20.5	Cold stamping operations	38
2.20.6	Die classifications depending on the production quantity of parts	39
2.20.7	Dies types.....	39
2.20.8	Die design: general criteria	39
CHAPTER THREE:		40
3	EXPERIMENTAL PROCEDURE AND ANALYSIS.....	41
3.1	Windmills Water Pumping Rotor Components	41
3.2	Data Presentation	42
3.3	Viability of Wind Pumping.....	42
3.4	Wind Speed Distribution	44
3.5	Selecting the Site and Size of the Windmill	46
3.5.1	Site selection:.....	46
3.5.2	Determining the water demand.....	46
3.5.3	Determination of the hydraulic power.....	46
3.5.4	Wind power potential determination	47
3.5.5	Reference area and size of the windmill.....	48
3.5.6	Determination of the design month	49
3.5.7	Pump selection.....	50
3.6	Acquisition Tools and Equipment	51
3.6.1	Hardware with non-contact techniques	51
3.6.2	Hardware with contact techniques.....	53
3.7	Reverse Engineering Software.....	54
3.8	Digitization of the Component	54
3.8.1	Preparation of the components for scanning	55
3.8.2	Scanning of the physical rotor components.....	56
3.9	Processing the Measured Data	58
3.9.1	Removing error points	59
3.9.2	Filtering points.....	59
3.9.3	Creating mesh	59
3.9.4	Mesh repair	60
3.10	The Hub RE Work.....	61
3.11	The CAD Model Construction	63
3.12	Deviation Analysis Results	66
3.12.1	Sail deviation analysis	67
3.12.2	Sail Tie deviation analysis	68
3.12.3	Sail Rib deviation analysis.....	70
3.12.4	Rotor Arm deviation analysis	71

3.12.5	Outer and Inner Rotor Bands deviation analysis	73
3.12.6	Two-Dimensional manufacturing drawings	74
3.12.7	Rotor components 3D CAD models	74
3.13	Die Design and Manufacturing	76
3.13.1	The Sail die design	76
3.13.2	The die manufacturing	79
3.14	Manufacturing the Rotor Prototype Components	89
3.14.1	Manufacturing of the complete Rotor Sails	94
3.14.2	Manufacturing the Sail Rib	97
3.14.3	Manufacturing the outer Rotor Bands	97
3.14.4	Manufacturing the Inner Rotor Bands	99
3.14.5	Manufacturing the complete Rotor Arms	100
3.15	Sails Section Assembly	101
3.16	Complete Windmill Rotor Assembly	102
3.17	Performance Testing:	105
CHAPTER FOUR:		110
4	CONCLUSIONS AND RECOMMENDATIONS	111
4.1	Conclusions	111
4.2	Recommendations:	112
5	REFERENCES	113
Appendices		123
Appendix (1): CATIA V5 HTML Devietion Analysis report of the Sail		123
Appendix (2): CATIA V5 HTML Devietion Analysis report of the Sail Tie		130
الملخص		139

TABLES

Table 3-1. Windmill Rotor Components Description.	41
Table 3-2. Power Losses in the Windmill.	47
Table 3-3. Determination of Specific Wind Power.	48
Table 3-4. Sheet for Identification of Design Month.	49
Table 3-5. Input Parameters of the Sail Deviation Analysis.	67
Table 3-6. Statistical Results of the Sail Deviation Analysis.	67
Table 3-7. Input Parameters of the Sail Tie Deviation Analysis.	68
Table 3-8. Statistical Results of the Sail Tie Deviation Analysis.....	69
Table 3-9. Input Parameters of Sail Rib Deviation Analysis.	70
Table 3-10. Statistical Results of the Sail Rib Deviation Analysis.	70
Table 3-11. Input Parameters of the Rotor Arm Deviation Analysis.	71
Table 3-12. Statistical Results of the Rotor Arm Deviation analysis.....	72
Table 3-13. Machining Parameters Applied in Preparing CAM Process of the Die Parts..	83
Table 3-14. The Complete Sail's Working Schedule.....	90

FIGURES

Figure 1-1. RE Concept.....	13
Figure 2-1. Steps of the RE process.	19
Figure 2-2. Relationship of cost and risk to data availability.....	22
Figure 2-3. Classification of data acquisition methods.	23
Figure 2-4. The main classification of various types of wind turbines.	26
Figure 2-5. Classification of machining processes.....	27
Figure 2-6. Turning operations that are performed on a lathe.....	28
Figure 2-7. peripheral and face milling cutters.....	29
Figure 2-8. Face milling.	29
Figure 2-9. Profile or contouring milling and partial face milling	30
Figure 2-10. Face milling showing approach and overtravel distances.	31
Figure 2-11. CNC machining process flow.....	33
Figure 2-12. Classification of metal forming processes.....	34
Figure 2-13. Schematic illustration of the shearing process.....	35
Figure 2-14. Shearing operation.	36
Figure 2-15. Sheet metal bending using dies mounted on presses.....	37
Figure 2-16. A bending press is used to create sheet metal bends.	37
Figure 2-17. Die opening dimension D: (a) V-die, (b) wiping die.....	38
Figure 3-1. The main components of the windmill Rotor.	42
Figure 3-2. Monthly variations of wind speed, Tajoura (2017).	43
Figure 3-3. Hourly wind speed variations (Diurnal wind pattern), Tajoura (2017).	43
Figure 3-4. Graphical method of determining Weibull parameters.....	45
Figure 3-5. Weibull distribution to Tajoura (2017) for $k=1.99$, and $c=3.4$	45
Figure 3-6. Baces3D three-coordinate measuring arm.....	51
Figure 3-7. BacesSCAN portable laser scanning system.	52
Figure 3-8. The BacesSCAN laser scanning system is shown in a moment of its use.	52
Figure 3-9. CMM during some measurements of the Hub.....	53
Figure 3-10. Thesis's RE Process Flow Chart.....	55
Figure 3-11. Surface color cause incorrect scanning.....	56
Figure 3-12. The parts of the Rotor were painted white.....	57
Figure 3-13. The Baces3D arm during scanning of the Sail Rib.....	57
Figure 3-14. Applying Remove Command in DSE.....	58
Figure 3-15. Mesh repairing	60

Figure 3-16. Mesh is created by the command of Mesh Creation of DSE CATIA.....	61
Figure 3-17. The repaired mesh of the Sail.	61
Figure 3-18. Disassembled components of the powertrain and brakes group.....	62
Figure 3-19. The Hub points acquisition using CMM.	62
Figure 3-20. Planar curves on the repaired mesh.	63
Figure 3-21. Final obtained surfaces of Sail Rib.	64
Figure 3-22. The Sail Rib solid 3D model using Part Design in CATIA.....	65
Figure 3-23. Annotation set added on Deviation Result Distribution of the Sail.....	65
Figure 3-24. Various snapshots of the Sail Rib according to the CATIA report.	66
Figure 3-25. A snapshot of Sail Deviation Analysis.	68
Figure 3-26. A snapshot of Sail Tie Deviation Analysis.	69
Figure 3-27. A snapshot of Sail Rib Deviation Analysis.	71
Figure 3-28. A snapshot of Rotor Arm Deviation Analysis.....	72
Figure 3-29. Inner and Outer Bands Deviation Analysis maps.	73
Figure 3-30. The complete Rotor 2d drawing.	75
Figure 3-31. 3D-CAD assembly model of the windmill Rotor.	75
Figure 3-32. Flow diagram for designing and manufacturing Sail's curving die.	76
Figure 3-33. (a) A single-operation die; (b) A typical die system.....	77
Figure 3-34. The Sail's sheet metal blank.	78
Figure 3-35. The 3D model of the Sails curving die.	78
Figure 3-36. The CAM process workflow diagram.	79
Figure 3-37. Preparing of 3D model & rough Stock.	80
Figure 3-38. "Z-level" milling strategy of lower Sail's die.	81
Figure 3-39. "Roughing" the milling strategy of lower Sail's die.	82
Figure 3-40. "Sweeping" milling strategy of lower Sail's die.	82
Figure 3-41. The tool path "Roughing" simulation.	83
Figure 3-42. The tool path "Z-level" machining simulation.....	84
Figure 3-43. The tool path "Sweeping" machining simulation.....	84
Figure 3-44. Screenshot during the "Sweeping" Level 1 in the video simulation.	85
Figure 3-45. Screenshot during the "Sweeping" Level 2 in the video simulation.	85
Figure 3-46. Machining analysis of upper part.....	86
Figure 3-47. "Z-level" operation of lower Sail die.	87
Figure 3-48. "Roughing" and "Sweeping" operations of lower Sail die.	87
Figure 3-49. Sails curving die installed on the bending machine.....	88

Figure 3-50. Unfolded view of the Sail.	94
Figure 3-51. Cutting the Sails using a CNC plasma machine.	94
Figure 3-52. Curving Sails die attached to the bending machine.	95
Figure 3-53. Isometric and unfolded view of the Sail Tie.	95
Figure 3-54. A picture of the Sail Tie while executing the three holes.	96
Figure 3-55. The bending process of the Sail Tie by the bending press machine.	96
Figure 3-56. Front and Unfolded view of the Sail Rib.	97
Figure 3-57. Front and unfolded view of the outer Rotor Bands.	98
Figure 3-58. Drilling passing holes of the Outer Rotor Bands.	98
Figure 3-59. Bending the outer Band by CNC rolling machine.	99
Figure 3-60. Front and unfolded view of the Rotor Inner Bands.	100
Figure 3-61. Complete Rotor Arms 2D drawing.	100
Figure 3-62. Sail section and Rotor assembly.	101
Figure 3-63. The complete Rotor Sails section assembly.	102
Figure 3-64. Installing the Rotor Arms into the Hub.	103
Figure 3-65. Installing the 4th Sails section.	103
Figure 3-66. Installing the 6th Sails section.	104
Figure 3-67. The complete windmill Rotor assembly.	105
Figure 3-68. Rotor and tower installation.	108
Figure 3-69. Extracting water from the well by the windmill system.	109

LIST OF ACRONYMS

g	Acceleration due to gravity
ρ_a	Air density
A	Approach distances
F	Bending force
CNC	Computer Numerical Control
CAD	Computer-Aided Design
CAM	Computer-Aided Manufacturing
CATIA	Computer-Aided Three-Dimensional Interactive Application
CMM	Coordinate Measuring Machine
CDF	Cumulative Distribution Function
D	Cutter diameter
f	Cutting force
V_c	Cutting speed
DMU	Digital Mock-up
DSE	Digitized Shape Editor
f_t	Feed per tooth
f_r	Feed rate
FE	Forward engineering
V_s	Geometric volume displaced by the piston
P_{hyd}	Hydraulic power required
LSQM	Least Square Method
CSERS	Libyan Center of Solar Energy Research and Studies
T_m	Machining time
R_{MR}	Material removal rate
MTD	Mold Tooling Design
n_t	Number of cutting edges of the cutter
NC	Numerical Control
D_p	Piston pump diameter
C_p	Power Coefficient
PDF	Probability Density Functions
$f(v)$	Probability of observing wind speed
QSR	Quick Surface Reconstruction
RI	Range Image
RPD	Rapid Product Development
RP	Rapid Prototyping
R_a	Reference area
RE	Reverse Engineering
N	Rotational speed
D_r	Rotor diameter

c	Scale parameter
SLS	Selective Laser Sintering
k	Shape parameter
S	Shear strength of the sheet metal
P_{wind}	Specific wind power
n	Spindle speed
t	Stock thickness
s	Stroke number
TDD	Technical Data Development
TS	Tensile strength of the sheet metal
3DP	Three-Dimensional Printing
H	Total discharge head
T.B.Co.	Truck and Buses Company
Q_p	Water demand
P_w	Water density
w	Width of part in the direction of the bend axis
W	Width of the workpiece
V	Wind velocity

CHAPTER ONE: INTRODUCTION

1 INTRODUCTION

1.1 Background

Background

In some situations, a physical part or product may be without technical details, such as drawings, bill-of-material, or engineering data. The process of duplicating an existing component without drawings, documentation, or a computer model and capturing the physical dimension of the component is known as Reverse Engineering (RE) [1,2].

RE is the opposite of Forward engineering (FE) since it takes the existing component (part) and creates a Computer-Aided Design (CAD) model to modify or reproduce the new component's design without accessing the original manufactured component design. RE may also be referred to as “the basic concept of producing a part based on an original or physical model without using an engineering drawing”. RE is a process that includes measuring or digitizing the part, analyzing, and testing to reconstruct the mirror image of the part using a CAD system [3,4]. It is a technology of reinvention, a road map leading to reconstruction and reproduction. RE is also the art of applied science to preserve the design intent of the original part [1,5].

The mechanical windmills in remote areas are a good, feasible option for pumping water. The design and evaluation of stand-alone renewable energy systems, such as windmills for pumping underground water, is a challenge and a possible alternative in many situations. Even at lower wind speeds, the wind-mechanical pumps can be sufficient to produce feasible energy for pumping water economically [6,7,8,9]. There is no way to manufacture a water-pumping windmill successfully using the RE technique if it is applied directly to a physical windmill without precisely evaluating the site's wind resources and choosing the appropriate size of the wind water pumping system. Unfortunately, there is no explicit power curve for water-pumping windmills. Since the windmill and site characteristics cannot be separated, as is usually the case with wind turbines, the output curve of the water pumping windmill depends on both the feature characteristics of the windmill and the wind system at the site chosen to install the windmill. Identifying the wind speed at a specific location or area is complex due to the random nature of the wind, which does not follow any known statistical distribution. Therefore, collecting wind data for many years and using Probability Density Functions (PDF) is best to characterize the wind speed for a specific location [10,11]. The Weibull and Rayleigh functions are the most commonly used PDFs to study wind characteristics at the target location [10,12,13]. Reverse engineering provides powerful tools

in the CATIA V5 (now referred to simply as CATIA) environment [14], enabling flexibility in manipulating point clouds and meshes to optimize them into high-end 3D surface shapes. RE Integrated in the CATIA design environment helps reduce project costs and is more efficient and effective by employing faster and simpler design iterations. One of the benefits of wind-mechanical systems is their simplicity, and for a solution to be appropriate and sustainable, it should employ local skills and enough resources [15].

One of the aims of this study is to apply the reverse engineering process using CATIA to build a 3D CAD model of the water pumping windmill Rotor based on the site wind characteristics. This model was adopted for the design, development, and manufacturing prototype of the windmill Rotor components locally as a pilot project to pave the way for the manufacture of the many windmills systems to provide water for irrigation, farms, homes, and community in remote areas of the State of Libya, commensurate with the local manufacturing capabilities. CATIA offers die and tool makers powerful virtualized functions to better suit the design and construction of dies and powerful automation capabilities to reduce Numerical Control (NC) programming and processing time. CATIA was used as an integrated CAD/CAM system for designing and developing the die and simulating the operation through graphic models in 3D. The NC codes can be generated using a CAD/CAM program and a virtual model of the piece [16,17,18,19]. Process planning is a function in a series of manufacturing activities that define the production process and its parameters to transform material from its initial form into a shape according to the desired design [20,21,22]. In the ideal CAD/CAM system, the product design specification in the CAD database is automatically converted into a process plan for making the product. As one of the RE applications, this thesis also applies an integrated practical example for designing a bending die for curving water pumping windmill Sails using simulation programming Computer Numerical Control (CNC) machines utilizing CAD and Computer-Aided Manufacturing (CAM). The RE approach was chosen to measure the dimensions and reconstruction CAD model of the physical Sail. That was used to design a suitable die, a CAM model was prepared, and a CNC machine programmed for machining the die for curving the Sails was requested to produce the windmill Rotor prototype. The components selected for this study are essential for the windmill. To obtain all the relevant dimensional data necessary to create a design drawing or CAD model, digitizing or scanning is needed. The precision and tolerances required to reverse engineer a component (part) are often determined by the criticality of the component.

Precision measurement devices, advanced software, and modern RE technologies have made the reinvention of mechanical parts feasible with tight tolerances and high fidelity [23]. Figure 1-1 illustrates the RE concept.

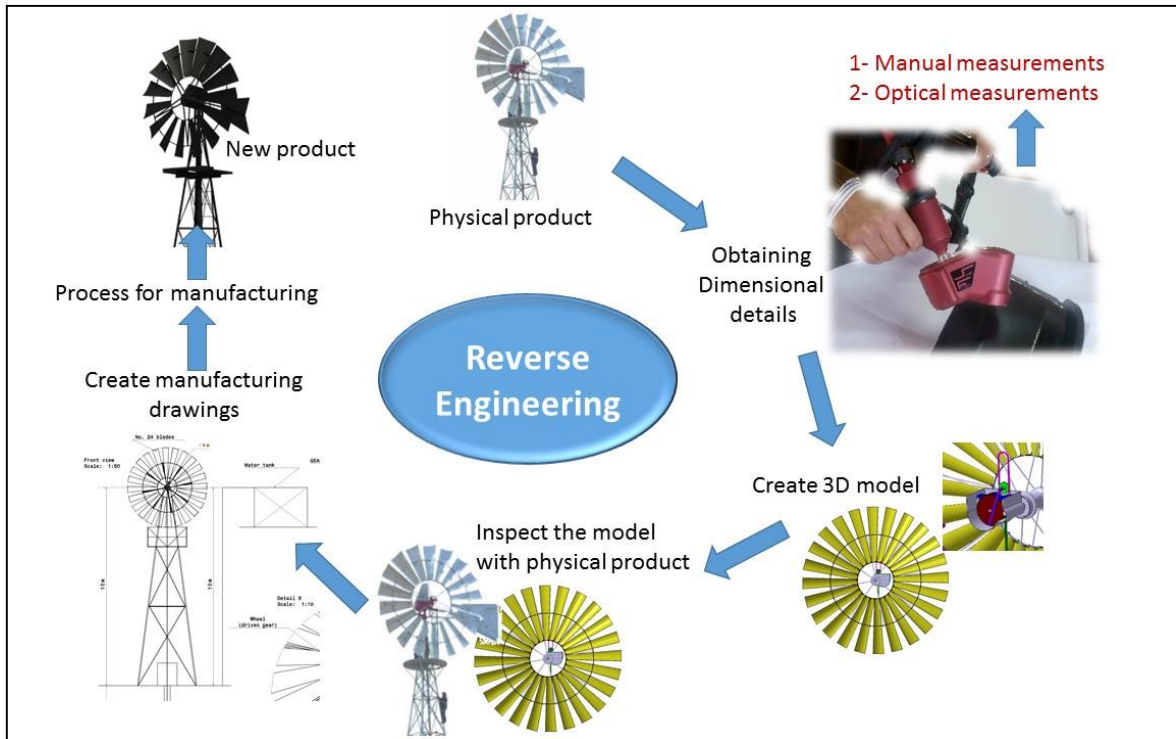


Figure 1-1. RE Concept.

1.2 Problem Statement

In 2004, Al-Inma Company for Engineering Industries located in Tajoura purchased some subassemblies (powertrain and brakes group) for 20 water pumping windmills. Some other components were provided as samples to manufacture all the components locally.

Due to the company's circumstances, the project stopped at that time and has not been completed. As part of a program to develop the company, the top management decided to complete the project, but for the extended long downtime, the company lost most of the requirements of the manufacturing process, such as executive and assembly drawings and work steps for the rest of the components targeted to be manufactured locally.

In this research study and based on some of the technical specifications and the samples currently available in the company, the researcher applied the RE process using the CATIA in manufacturing the prototype of the windmill Rotor components on one of the 20 subassemblies of the powertrain and brakes group.

1.3 Research Objectives

Due to the large number of components needed to manufacture the water pumping windmill and the limited resources and time required to complete this research study, only the Rotor components were designed and manufactured using the RE process.

The objectives of this study can be summarized as follows:

- To participate in introducing alternative clean energy for groundwater extraction to meet the selected site's water needs without using an electricity grid.
- To determine the amount of wind energy available at the site, chosen to operate a wind water pump and provide water requirements. Therefore, it is essential to assess the site's wind power resources for pumping water with windmills, at least an estimation.
- To choose the size of the water pumping system according to the amount of wind energy available at the site.
- To build a 3D CAD model of the Rotor component of a wind water pumping system using CATIA by applying Reverse Engineering to an existing classic commercial windmill, according to the size selected based on the available wind energy.
- To manufacture a prototype of the components of a Rotor for water pumping windmill in order to pave the way for the manufacturing of the entire model designed to pump water in Libyan rural (i.e., Tajoura), commensurate with local manufacturing capabilities.
- An attempt was made to manufacture a die for curving the Rotor Sails of the windmill, starting with digitizing the component and rebuilding the CAD model to CNC machining.

1.4 Research Limitations

- **Spatial limitation:** the study is confined to spatial limitation, which involves the Tajoura area.
- **Time limitation:** the study is confined to a specific period of time.

1.5 Expected Scientific Contributions

The expected scientific contributions can be summarized as follows:

- To Introduce the RE as a novel process to shorten the design, development, and manufacturing cycle time.

- Due to the lack of such research studies in Libya, the researcher expects that this study will assist the Solar Energy Research and Studies Center and other Research Centers, Universities, Colleges, and Institutes in raising awareness and knowledge of the RE process.
- To enrich the academic libraries locally and internationally by the findings of this study.
- If this research study succeeds in manufacturing the prototype, it would be useful to complete the manufacture of the remaining components of the water pump windmill locally in collaboration with other institutions.

1.6 Methodology

In this study, the researcher applied the RE process to develop and manufacture components of a Rotor of a water pumping windmill. The RE process can principally be viewed as a process chain that is composed of the following primary operations; namely: (i) selecting the optimum size of the water pumping windmill for the selected site that is intended for the RE process, (ii) digitizing the components, (iii) processing the measured data, (iv) creating a CAD model, and finally (v) manufacturing the prototype.

In more detail, the methodology involves applying the Reverse Engineering (RE) approach and some activities usually used as a prerequisite when designing windmills to obtain the Rotor 3D CAD model and the Rotor prototype of a water pumping windmill system. Both activities were carried out:

(a) Activities before applying RE:

These activities related to the use of the wind data collected over several years (2005-2016) at CSERS for:

- Fitting the wind data using the Weibull distribution to characterize the wind speed and evaluation of wind resources.
- Determining the monthly and hourly average wind speed values during the day (Diurnal wind pattern).
- Selecting the site and sizing the windmill according to the amount of wind energy available at the site.

(b) Reverse Engineering (RE) activities:

The various activities of the RE process in designing and constructing a CAD model of an existing classic commercial windmill were carried out as follows:

- Digitizing the Rotor components using the Baces3D portable laser scanning system to obtain dimensional data.
- Processing the measured data and creating the final surfaces by overlapping the point cloud with the mesh was done by performing several operations using the CATIA's Digitized Shape Editor (DSE).
- The surface models of the scanned components were created by the Quick Surface Reconstruction workbench (QSR) in CATIA.
- The solid 3D model of the Rotor Sail was created by the Part Design workbench (PD) in CATIA.

In addition to being used to create manufacturing drawings, the generated Rotor Sail 3D model was the basis for designing and manufacturing the Sails curving die as a final RE application:

- Die design was done using the CATIA die tooling design (DTD).
- The manufacturing process simulation was defined for the CNC machine in CATIA's advanced machining workbench (AMG).

1.7 Potential Contributors to the Research and their Contribution

- Solar Energy Research and Studies Center, Tajoura. (Climate Data).
- Al-Inma Company for Engineering Industries, Tajoura. (Manufacture and assembly of prototype components).
- Higher Technical Center for Training and Production, Janzur. (CNC Machining).
- Truck and Buses Company (T.B.Co.), Tajoura. (Measurements and manufacturing some components).
- Advanced Center of Technology, Abusaleem. (Measurements and CNC Machining).

**CHAPTER TWO:
LITERATURE REVIEW**

2 LITERATURE REVIEW

2.1 Wind Energy Technology

Energy is inevitable for human life, and a secure, accessible supply of energy is essential for the sustainability of modern global societies [24]. Energy sources are conventional (nonclean), such as coal, petroleum, & natural gas; and nonconventional (clean) sources, such as biomass energy, solar energy, wind energy, geothermal energy, and many other renewable energy sources. Shortage of conventional sources is unavoidable in the coming future, as was reported in the literature, and at the same time, it causes pollution and global warming problems. However, renewable energy is environment-friendly, and plenty of renewable fuel sources from the atmosphere are available [25].

Wind energy is a promising source in the power generation sector due to pollution-free power production and wind resources' sufficiency worldwide [24,25,26]. Wind energy can be generated through various windmills; the basic and cheapest are mechanical windmills. Many research studies have demonstrated the economic feasibility of using windmill-powered water pumps to pump water mechanically. This wind energy technology is more affordable than other technologies, including conventional pumps that operate with electricity or diesel fuel.

Odesola and Adinoyi [27] in the study they conducted, a model was designed and implemented for pumping water using a Rotor diameter of 2.14m and a solidity area of 3.733m², at a location where the wind speed was 2.5m/s, at the height of 16m from the ground. The performance tests for this windmill showed that the water pumping rate for irrigation might range from 3.4 to 6.44L/min. As a guideline, effective electricity generation from wind energy requires an average wind speed greater than 5m/s [28]. However, lower wind speeds can be sufficient for mechanical wind pumps [6]. Wind-mechanical pumping can still be economically feasible even at an average wind speed of 2.5m/s [8]. The proven reliability of classical wind pumps can be important, especially for pumping from deep wells [7]. The cost of water from a windmill water pumping system is susceptible to the monthly average wind speed.

2.2 Reverse Engineering Technology

Reverse engineering is the reconstruction of digital geometric models of physical objects in the computer-aided design (CAD) field [29]. It is a process that includes measuring, analyzing, and testing to reconstruct the mirror image of an object or retrieve a past event.

RE is a technology of reinvention, a road map leading to reconstruction and reproduction. Reverse engineering focuses not only on the reconstruction of the shape and fit but also on rebuilding the physical properties of materials and manufacturing processes [30]. RE is considered essential in transferring, localizing, and generating technology in developing countries. Reverse engineering has been extensively studied in recent years due to the development and spreading of 3D scanning technologies and the increase in the number of potential applications [31].

The RE of mechanical parts requires extracting information about an instance of a particular detail about a part sufficient to replicate it using appropriate manufacturing techniques [32,33]. Technical data is critical to the smooth and continuous operation of any production or manufacturing facility. Often unavailable technical data needed to maintain and repair equipment was never furnished or purchased [33,34].

2.3 Overview of RE Technology

RE is the opposite of forward engineering. It takes an existing product that is often a free-form surface and creates a CAD model, using a software system for modification to the design aspect of the product.

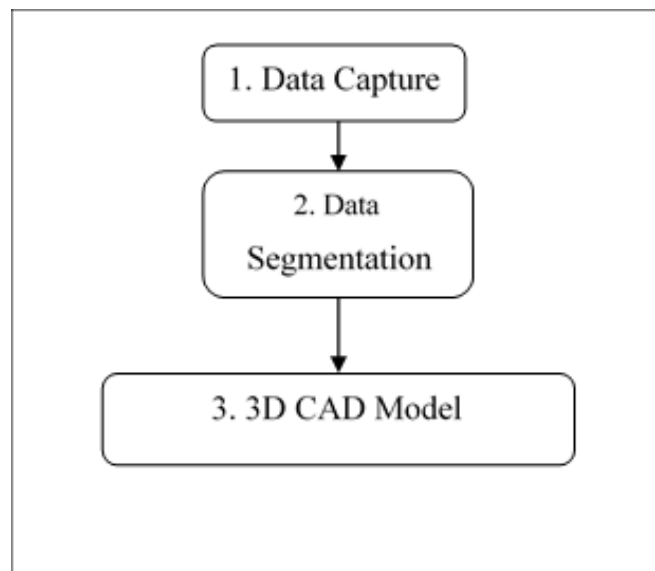


Figure 2-1. Steps of the RE process.

RE is usually undertaken to redesign the system for better maintainability or to produce a copy without access to the original design from which it was created [35]. Reverse engineering has two key technologies, i.e., digitization of the original model and creation of its CAD model [3,4]. The objective of the RE process is to generate a 3D CAD model of an

original part that can be used for future modeling of components where no CAD model exists. The steps of RE are presented in Figure 2-1 [35].

2.4 Applications of RE Process

It is often necessary to produce a copy of a component (when no original drawing or documentation is available) or re-engineer an existing part, when analysis and modification are needed to construct a new, improved one. Some of the application avenues of the RE are [36,37]:

- RE is used when documentation of a particular device has been lost.
- RE is used to bring existing physical geometry into digital product development environments to make a digital 3D.
- RE is used in rapid product development (RPD), using 3D scanning to generate a surface model or create a CAD model, and manufacturing the component to get a good product in terms of accuracy and surface finish faster and cheaper.
- RE is used to produce complex prototypes, such as blades in gas turbines and compressors.
- RE is used to produce prostheses in medical applications.

2.5 Rapid Prototyping

Rapid Prototyping (RP) includes various automated manufacturing techniques such as selective laser sintering (SLS), stereolithography, and three-dimensional printing (3DP), which use virtual 3D data sets to fabricate solid forms in a layer-by-layer technique [38]. RE and RP have been widely used as two advanced integrated techniques. Where reverse engineering technology enables the creation of CAD models of existing objects by capturing their surface data, rapid prototyping is another emerging technology that allows promptly fabricating a product's physical prototype using an adaptive manufacturing technique [39]. In rapid prototyping, a faceted model called STL (Stereolithography) file has been the industry standard for providing the CAD input to RP machines. It approximates the CAD model of a part using many planar triangular patches and has drawbacks. Integrating RE with RP will facilitate reverse-engineered geometric data for rapid prototyping, thereby reducing the product development time [40].

2.6 Technical Data Development

Accurate Technical Data Development (TDD) is the core and keystone of reverse engineering. This data can be in the form of engineering drawings, equipment specifications, performance characteristics, special tooling, or any other information critical to the ongoing performance of the manufacturing capability.

Background information can be found in the technical manuals, repair data records, performance criteria, and other vital information that can augment the engineering drawings [33].

2.7 Preparation for RE Process

This preparation should consist of the following [33]:

2.7.1 Reverse engineering teams

RE is a multidisciplinary collaboration that requires the talents of many engineers, technicians, drafts people, and shop personnel.

2.7.2 Communication with system users

Many design questions arise during the course of a RE project. The available data is often insufficient, which leaves room for many assumptions, and additional data must be obtained to make the decision as rational and scientific as possible.

Developing a good bond with the system users is crucial to resolving many thorny design issues and aids in making many decisions wisely.

2.7.3 Data collection

All available data must be collected before the pre-screen recommendation sheet is completed. Data collection may be as difficult as any research task, but thorough data collection will reduce the overall project costs. Any available operational parameters are helpful but not necessary.

2.7.4 Technical data and manuals

Valuable technical data includes all drawings and technical manuals. Engineering drawings include layout, detail assembly, installation, arrangement, control drawings, schematics, and wiring diagrams.

2.7.5 Data evaluation

The raw data that should be fed into the data collection must be processed to make the best evaluation decisions.

2.8 Reverse Engineering Cost

The RE project cost estimate reflects a more accurate cost through a detailed breakdown of the project's steps. In calculations, this quantity is identified as "RE cost"; (i) a projected cost to RE from pre-screen, or (ii) a cost estimate to reverse engineering for steps needed to complete the project [33].

2.9 Determination of Project Type

Determining project type is part of the pre-screening process, which accounts for both the type and account of available data.

Data availability directly influences the cost and risk factors; Figure 2-2 shows this relationship graphically [33]. It shows that the more data available, the less risk and the lower the cost.

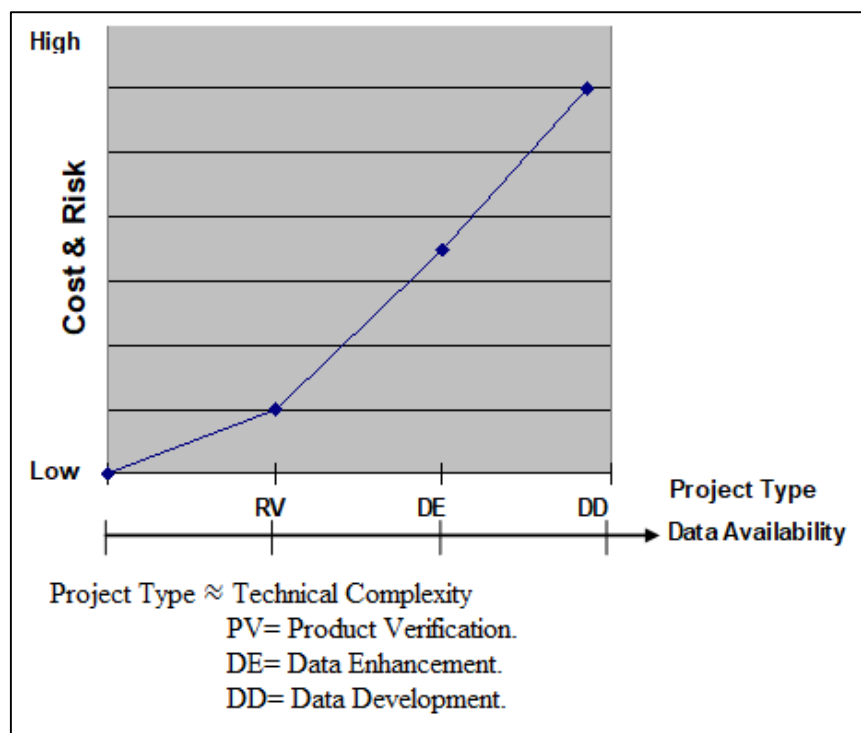


Figure 2-2. Relationship of cost and risk to data availability.

There is product verification when the technical data appears complete, but there is some doubt about its usefulness.

If some of the required technical data is available, then the project requires data enhancement, and data enhancement is performed whenever there is incomplete or missing data. If no technical data is available, the project requires full data development [33].

2.10 Comparison with the Available Data

After all measurements are taken, they must be compared with the dimensions shown in the available technical data. All differences between the stated parameters and the actual dimensions must be noted and recorded.

2.11 Reverse Engineering Process

A process consists of a series of actions conducted to achieve an end. As mentioned in the definitions, reverse engineering means obtaining a geometric CAD model from 3D points acquired by scanning (digitizing) the existing products [41]. It is an intensive process that enables designer interaction to capture design intents and integrate digital data from previous products in a new product life cycle [42]. Success for an entire RE program is achieved one project at a time through clear thinking, good judgment, and hard work [43]. Reverse engineering can be accomplished by using the following steps [44,45,46].

2.11.1 Digitization of the object:

Digitization is the process of acquiring point coordinates from component surfaces. The result of the digitization process is a cloud of 2D or 3D data points stored as an image.

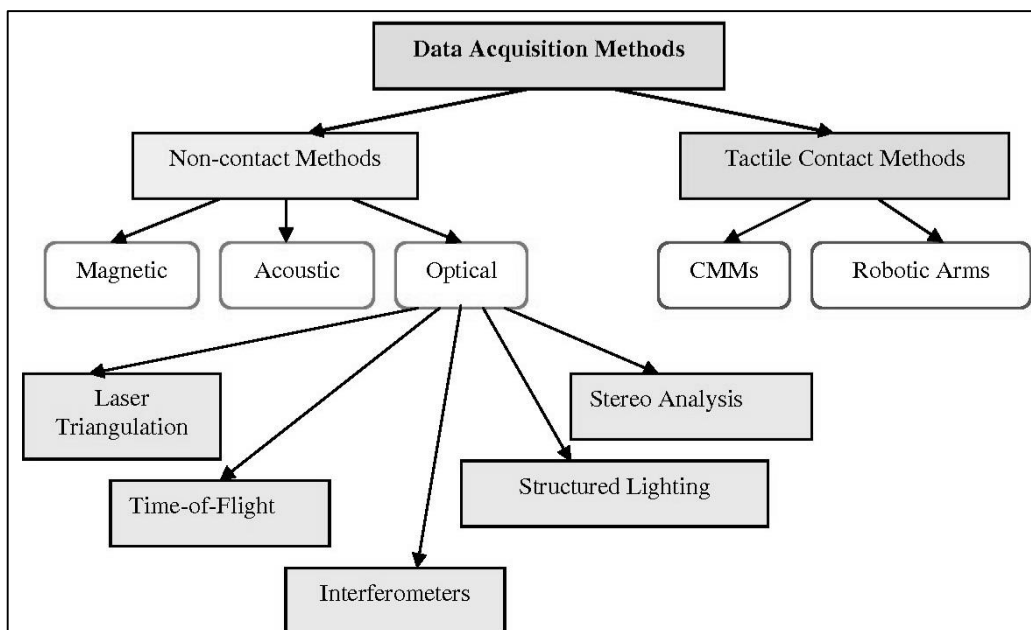


Figure 2-3. Classification of data acquisition methods.

A 3D image, called a range image (RI), is a map of depth information at different points on a scene. RI data can be acquired using available contact (tactile) or non-contact techniques. These techniques are classified in Figure 2-3 [47].

A Coordinate Measuring Machine (CMM) is the commonly used contact device for extracting 3D coordinates (X, Y, and Z) from the part surface. Ultrasonic imaging is also a contact technique; a "gun" whose tip emits ultrasonic signal contacts a point on the part. A series of sensors that form a reference coordinate system can identify the location of the tip, the gun, and thus the coordinate of the point on the part surface [44,48,49].

2.11.2 Data segmentation

Identifying surface features from the cloud of points acquired by digitization is crucial to model a component surface in CAD. These features include boundaries and surface segments. The segmentation of 3D digitizer data algorithms is based on the assumption that the image exhibits surface coherence. An algorithm is used for segmenting the images. The first stage of the algorithm divides the image into eight different primitive surfaces: peak, pit, ridge, saddle ridge, valley, saddle valley, flat, and minimal. These primitives are assumed to have invariant characteristics, which can break down any given surface. The output of this stage is a labeled image. By using the labeled image, a seed region is extracted and used for region growing in the second stage. The second stage is an interactive region growing process. In this stage, the seed region is approximated by a bivariate polynomial (degree less than 5) [50].

2.11.3 Creation of CAD model:

The output of the surface segmentation process consists of labeled points belonging to a particular region. In geometric modeling, surfaces are presented by either polyhedral or curved approximation [51].

Algebraic surfaces are the ones where they are approximated using a polynomial equation in the form $f(x, y, z) = 0$. Generally, algebraic surfaces have an infinite domain while parametric surfaces are bounded.

Dual representation of surfaces includes both algebraic and parametric surfaces.

There are two approaches for algebraic surface fitting, one by interpolation and the other by approximation. Interpolation schemes result in surfaces that interpolate the measured data at each point. Interpolation is used when the function values at the measured points are known to be high precision. In approximation methods, the least square method (linear and

nonlinear) is used to find the coefficient of the polynomial function. The polynomial function takes the algebraic quadratic form to represent standard surfaces [42,52].

2.12 Physical Mock-Up and Digital Mock-Up

A physical mock-up is a tangible, 3D prototype or model of a physical device or product, often one that can be held and often crafted rapidly out of materials at hand, used during exploration and evaluation to at least simulate physical interaction [53].

The Digital Mock-up (DMU) is a computer-based product definition of a real product. It consists of documents, attributes, and structures. 3D CAD design and Digital Mock-ups (DMU) have emerged as one of the major pillars of what became to be called "Virtual Product Development".

The DMU, in particular, has revealed itself as an excellent means of anticipating many more questions during development than ever before, at lower costs, in a shorter time, and with higher quality output [54]. The best-known RE process is the correlation between Physical Mock-Up and Digital Mock-Up. The evolution processes have been improved, and the Digital mockup is now the reference for product validation.

Thanks to advanced tools such as realistic rendering, it is possible to check the shape quality on the screen [55]. In a study, the development stages to produce a new variable geometry saddle (VGS) were described to clarify the correlation between Physical Mock-Up and Digital Mock-Up [56].

2.13 Background of the Windmill

The classic multi-bladed windmill is still being manufactured in industrialized countries, and probably about a million are in use today, particularly in the U.S., Argentina, Australia, and South Africa. They provide water for households, for livestock, and sometimes for irrigation. As new and more efficient windmill designs are developed and production costs are lowered through the use of materials obtained locally, the costs of pumping water with wind pumps should go down. It is expected that they will reduce by a factor of 2 to 4 in the foreseeable future. The trend in this direction has already begun in evidence [7].

The amount of water needed influences the size of the Rotor one must select, influencing the windmill's cost. The cost of water storage must be included in the costs of the system since the wind pump, unlike engine-driven pumps, electric pumps, or even hand pumps, cannot be counted on the provided water on demand [7].

Windmills (multi-blade wind turbines) have a high starting torque, making them suitable for driving mechanical water pumps. The number of rotations is low, and the blades are made from simple sheets with an easy geometry [57]. Windmills were developed in the mid-1900 century mainly to provide drinking water to people and cattle in North America. Moreover, it was used to ensure the water supply for the steam locomotives of the new railways expanding into the West of America. The most important component of this windmill is the Rotor, also called the "Rotor rosette" because of its structural design. Its diameter varies between 3m and 5m and has more than 20 metal sheet blades. So the Western windmill is still a "modern" machine of which tens of thousands are installed with a nearly unchanged design in Australia, Argentina, and the USA [58]. Figure 2-4 shows the main classifications of wind turbines and their different types [57].

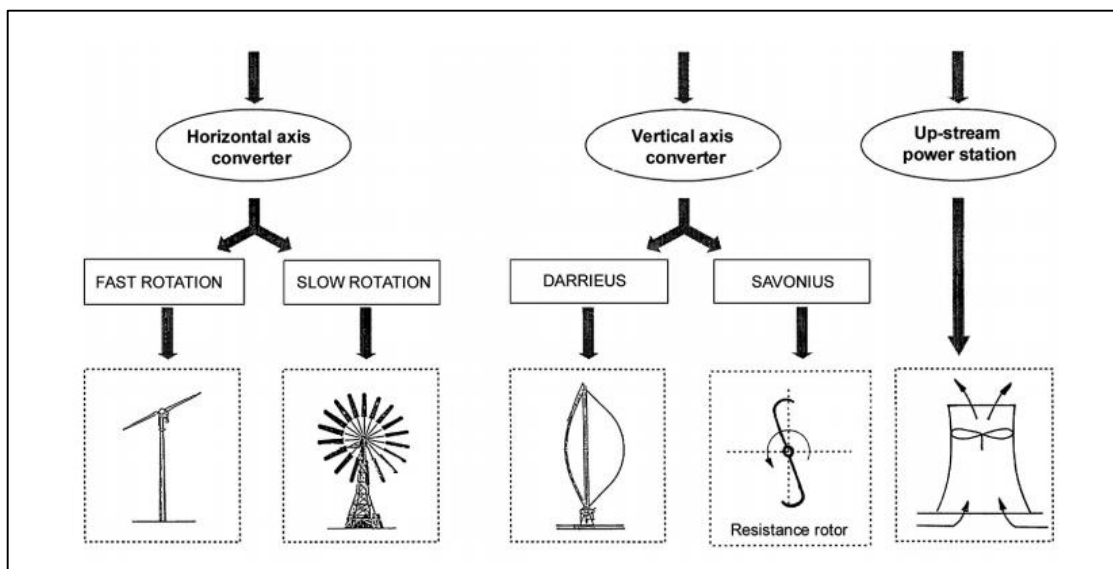


Figure 2-4. The main classification of various types of wind turbines.

Turbines can deliver power ranging from 10 kW to some MW. The largest turbine on the European market has a power of 7.6MW; bigger machines are being tested. The efficiency of these types of turbines is very high. Therefore, it is solely used for electricity generation, which needs "high-speed engines" to keep the gear transmission and the generator small and cheap [57]. It's increasingly common to see wind farms on ridges, open pastures, plains, and offshore wind farms in the ocean.

2.14 Manufacturing Processes Classification

A manufacturing process is a designed procedure that results in physical and/or chemical changes to a starting work material to increase the value of that material [56,57]. A manufacturing process is usually carried out as a unit operation. It is a single step in the

series of steps required to transform the starting material into a final product [59]. The classification of manufacturing processes has been divided into six subsections: casting, machining & finishing, joining, sheet metal, polymer processing, and bulk deformation [60]. The most important processes related to the experimental procedure of this thesis are discussed in the following sections.

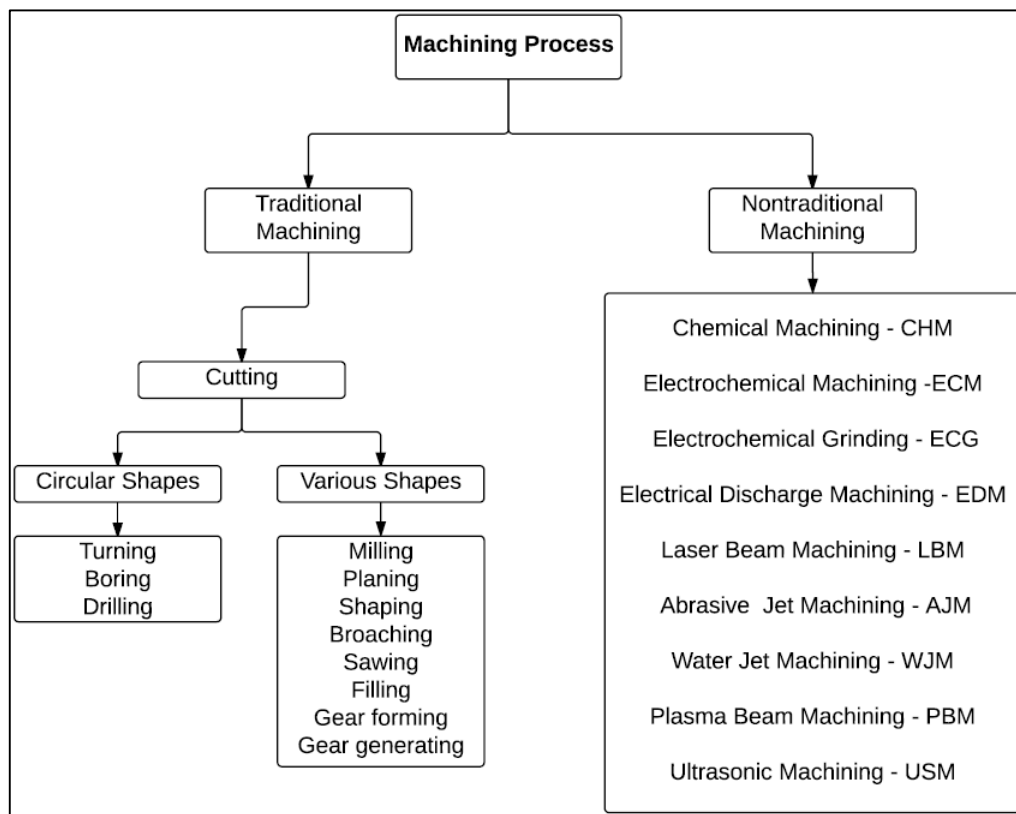


Figure 2-5. Classification of machining processes.

2.15 Machining Process

Machining is a manufacturing process in which a sharp cutting tool is traditionally used to cut away material to leave the desired part shape [59].

Machining or (material removal processes) can be divided into traditional (conventional) and nontraditional (nonconventional) machining. Figure 2-5 shows the classification of machining processes [61]. In this thesis, only traditional machining is discussed in the following sections.

2.16 Traditional Machining Processes

They are generally used for the execution of various processes on metallic materials through the use of cutting and chip removal operations; among them:

2.16.1 Turning

Turning is a machining process in which a single-point tool removes material from the surface of a rotating workpiece. The tool is fed linearly in a direction parallel to the axis of rotation to generate a cylindrical geometry [59]. A variety of other machining operations can be performed on a lathe in addition to turning; these include the facing, chamfering, threading, etc., and are illustrated in Figure 2-6 [59]: (a) facing, (b) taper turning, (c) contour turning, (d) form turning, (e) chamfering, (f) cutoff, (g) threading, (h) boring, (i) drilling, and (j) knurling.

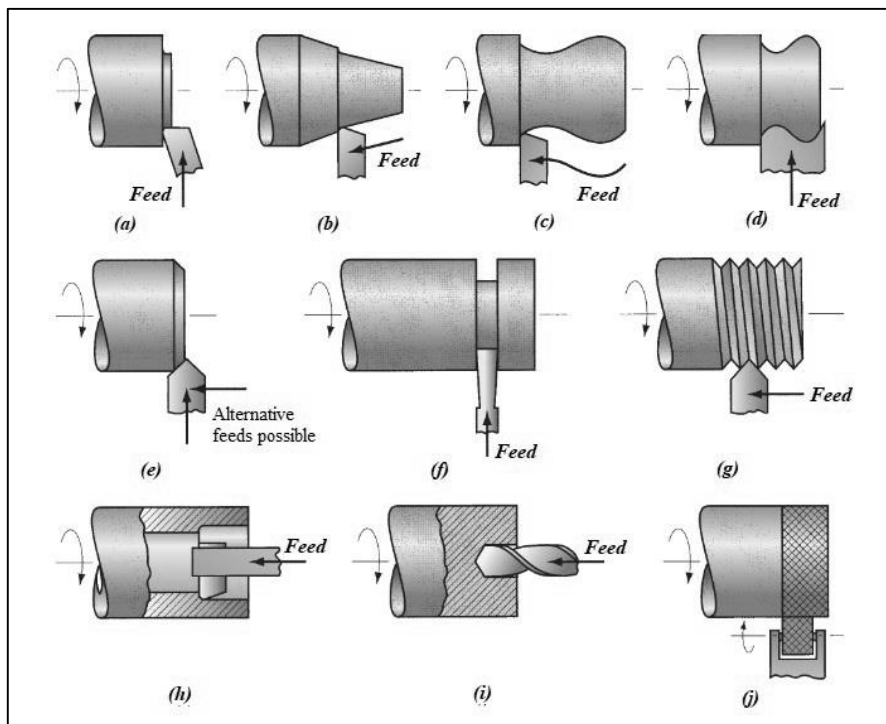


Figure 2-6. Turning operations that are performed on a lathe

2.16.2 Milling

Milling is a machining operation in which a part (workpiece) is fed past a rotating cylindrical tool with multiple cutting edges, and the axis of rotation of the cutting tool is perpendicular to the feed direction [59]. Milling operations may be classified as peripheral (plain) milling or face (end) milling, as shown in Figure 2-7 [62].

2.16.2.1 Peripheral milling

In peripheral milling, as shown in Figure 2-7 (a), the cutting occurs by the teeth arranged on the periphery of the milling cutter, and the generated surface is a plane parallel to the cutter axis. Two types of peripheral milling are differentiable, namely, up-milling (conventional cut) and down-milling (climb cut) [62,63].

2.16.2.2 Face milling

The rotation axis is normal to the machined surface; with specific machine tools, both millings can be done with the same machine. When using cutters of large diameters, it is good to tilt the spindle head slightly at an angle of 1–3° to provide some clearance, which leads to an improved surface finish and eliminates tool blunting, as shown in Figure 2-7 (b).

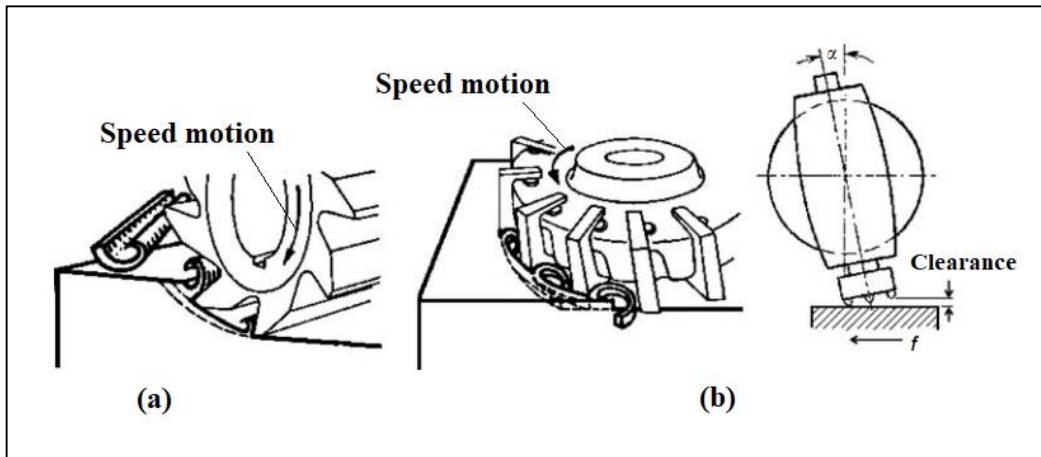


Figure 2-7. peripheral and face milling cutters.

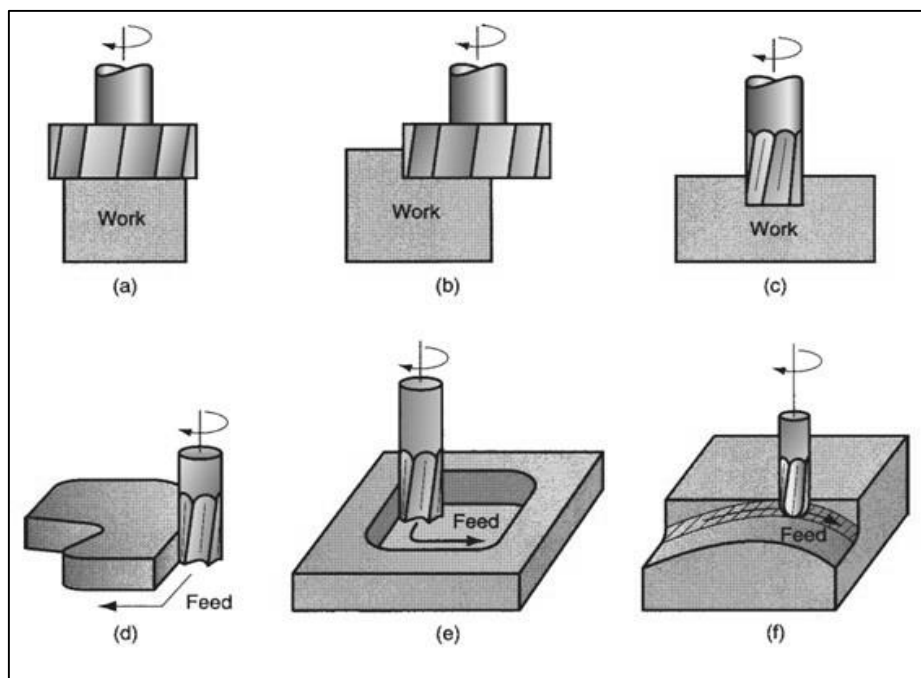


Figure 2-8. Face milling.

Various forms of face milling exist [59], several of which are shown in Figure 2-8:

(a) conventional face milling; (b) partial face milling; (c) end milling; (d) profile (contour) milling, a form of end milling in which the outside periphery of a flat part is cut; (e) pocket milling; (f) surface contouring, in which a ball-nose cutter (rather than square-end cutter) is

fed back and forth across the work along a curvilinear path at close intervals to create a three-dimensional surface form.

The same basic cutter control is required to machine the contours of mold and die cavities, in which case the operation is called die sinking.

Figure 2-9 represents milling with reference to a contouring machining with an integral end milling as shown in Figure 2-9 (a), and a case of face milling is represented in Figure 2-9 (b).

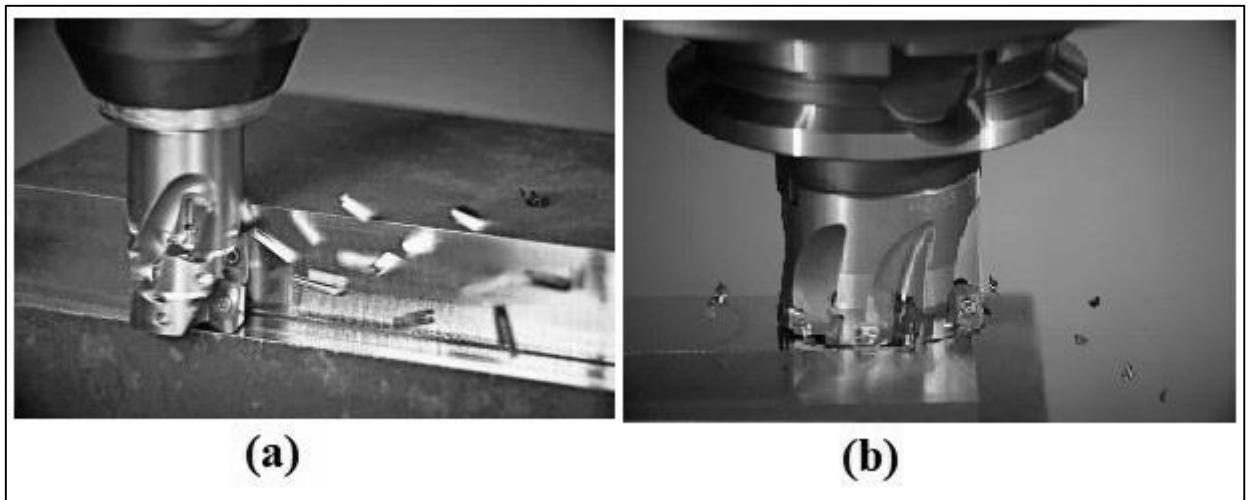


Figure 2-9. Profile or contouring milling and partial face milling

2.16.2.3 Cutting conditions in milling:

A. **Cutting speed (V_c):** the V_c indicates the relative speed between tool and material to be removed; generally, it is expressed in meters per minute [m/min]. It is calculated using the following equation [51, 52]:

$$N = \frac{1000 \cdot V_c}{\pi \cdot D} \quad (1)$$

Where: N = the rotational speed, rev/min; D = the cutter diameter, mm.

B. **Feed:** the feed per tooth (f_t); called the chip load, which can be converted into feed rate (f_r) taking into account the spindle speed and the number of cutting edges of the cutter (n_t) as follows:

$$f_r = N \cdot n_t \cdot f_t \quad (2)$$

where f_r = feed rate, mm/min; N = spindle speed, rev/min; n_t = number of teeth on the cutter; and f_t = chip load, mm/rev.tooth.

C. **Material removal rate (R_{MR}):** In milling, R_{MR} is determined using the product of the cross-sectional area of the cut and the feed rate. If a slab-milling operation is cutting a workpiece with width W at a depth d , the material removal rate is:

$$R_{MR} = W \cdot d \cdot f_r \quad (3)$$

D. **Machining time (T_m):** The time required to mill a workpiece of length L must account for the approach distance needed to engage the cutter fully. The time T_m in which the cutter is engaged milling, the workpiece is therefore [59] :

$$T_m = \frac{L+A}{f_r} \quad (4)$$

For face milling, the possible two cases are presented in Figure 2-10:

Case (1): when the cutter is centered over a rectangular workpiece; Figure 2-10 (a), the approach distances (A) are given by:

$$A = 0.5(D - \sqrt{D^2 - W^2}) \quad (5)$$

where D cutter diameter, in (mm) and W width of the workpiece, in (mm).

If $D=W$, the above equation can be reduced to $A = 0.5D$.

And if $D < w$, then a slot is cut into the workpiece and $A = 0.5D$.

Case (2): when the cutter is offset to one side of the workpiece, as shown in Figure 2-10 (b), the approach distance is given by:

$$A = \sqrt{W(D - W)} \quad (6)$$

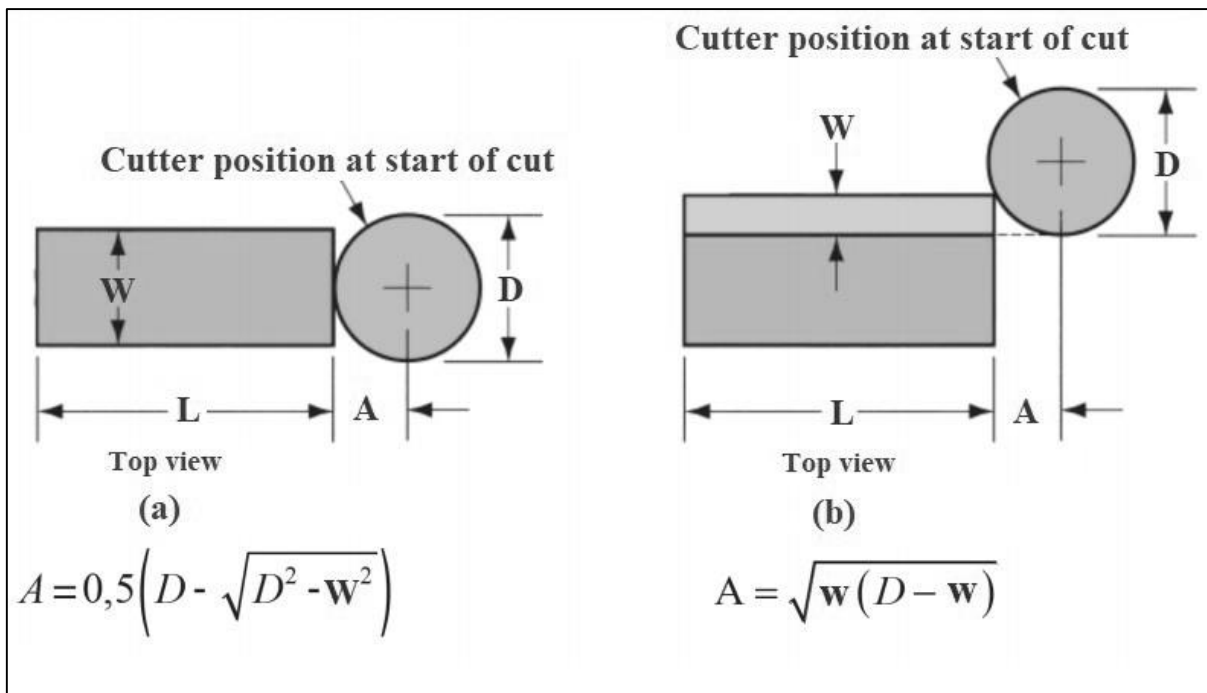


Figure 2-10. Face milling showing approach and overtravel distances.

2.16.3 Roughing and finishing operations

Roughing operations are those parts of cutting processes mainly concerned with removing a high volume of material and using maximum machine power [64]. Original methods developed by [65] typically incorporate roughing and finishing operations in one orientation. Within the orientation, roughing operations will be performed first, followed by finishing operations. The quality of a mold and machined parts is primarily dependent on surface roughness and part accuracy [66]. Therefore, suitable cutting parameters and tool selections need to be prioritized in planning machining operations.

In machining, surface finish is a prominent factor to be considered to ensure the product's final desired quality [67]. Therefore, proper control of cutting parameters and tool selection can help attain a good surface finish and accuracy.

Because of this capability, CNC machining meets the requirement for producing high-specification parts such as tools and dies.

2.17 CNC Machining Process

In CNC machining, the development of cutting tool paths is carried out by a CAD/CAM system. These systems are capable of assisting in toolpath generation, but the task of determining the type and size of the cutting tool is usually overlooked [68].

Roughing operations are performed in CNC machining to remove the bulk of material from the workpiece and generate the part's profile. In the metal cutting industry, roughing operations are considered time-consuming processes. They can take up to 50% of the total machining time depending on the size of the workpiece and part [69].

Since roughing and finishing operations are directly correlated, removing the bulk of the material in the first place will assist the rest of the cutting processes in finishing operations. A CNC milling machine can be a reliable alternative for rapid manufacturing (RM) applications. It employs a subtractive process, shaping a block of material by cutting off chips until the entire shape of the model is formed [70].

The 3D model is transferred to a CAM system, where the cutting tool paths are developed to achieve the desired accuracy and surface finish. Prior to that, several cutting parameters and strategies need to be defined, and these closely rely on the skill of CAM operators to produce optimum cutting operations. The process flow shown in Figure 2-11 [71] illustrates the typical steps employed to execute machining processes.

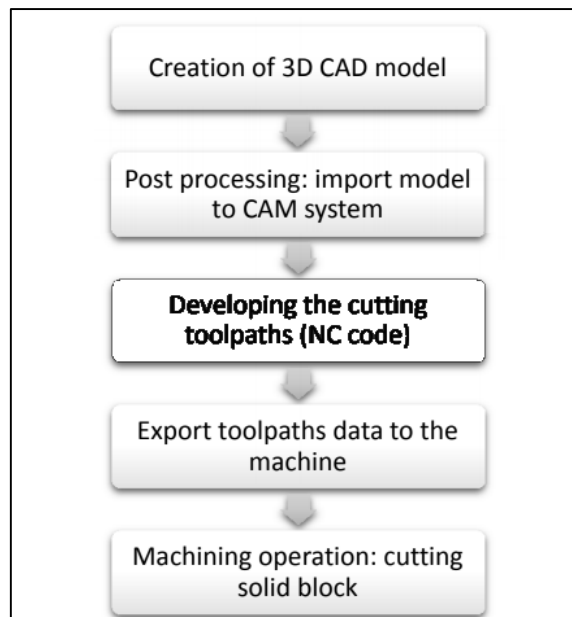


Figure 2-11. CNC machining process flow.

The third block represents a critical stage of the planning process in machining. Other factors influencing machining quality include cutting strategies, process parameters, tool positioning, and networking communication [72].

2.18 CAD and Engineering

CAD involves the use of computers to create design drawings and product models. CAD is usually associated with interactive computer graphics, known as a CAD system. Several powerful commercially available programs aid designers in geometry description and engineering analysis, such as SolidWorks, ProEngineer, CATIA, AutoCAD, Solid Edge, and Unigraphics NX (also known as Siemens NX). CAE allows several applications to share the information in the database. These applications include, for example, finite element analysis of stresses, strains, deflections, and temperature distribution in structures and load-bearing members [73].

2.19 CAD and Manufacturing Combination

The integrated CAD/CAM approach prepares the part program directly from the CAD part geometry, either by using NC programming commands called in the CAD/CAM system or passing the CAD geometry into a dedicated CAM program. By using CAD/CAM systems, the CAD drawings can therefore be changed to CNC programs [62]. The programming steps for CAD/CAM approach are as follows:

- Obtaining the 3D model applying the forward engineering or RE approach for machining purposes within the CAM software environment.

- Defining the tool geometry by selecting tools from the software library.
- The operator will decide which operations and which paths the tools the machine is equipped with must follow to create the designed object.
- Displaying the tool motion may be modified to improve the tool motion, or other details may be added for particular machining cycles or operations.
- The designer will send this information to the controller that manages the CNC machine. To make sure that the CNC machine controller reads the information defined in the CAM software, it is necessary to perform a post-processing operation.

The postprocessor created for the specific machine translates the path of the machine tool defined in the CAM into the programming language that the machine will understand, called G-CODE or, more commonly ISO. The program can be written and tested before it is run, and jigs, fixtures, and clamping can be shown during simulation to determine any potential problems. Operations can then be adjusted to optimize production offline, which keeps the machine operating [62]. Prototype work, CAD/CAM has made possible significantly reduced manufacturing costs and improved productivity [73].

2.20 Sheet Metal Cutting and Forming Processes

Metal forming includes a large group of manufacturing processes in which plastic deformation is used to change the shape of a metal workpiece. Deformation results from using a tool usually called a die in metal forming.

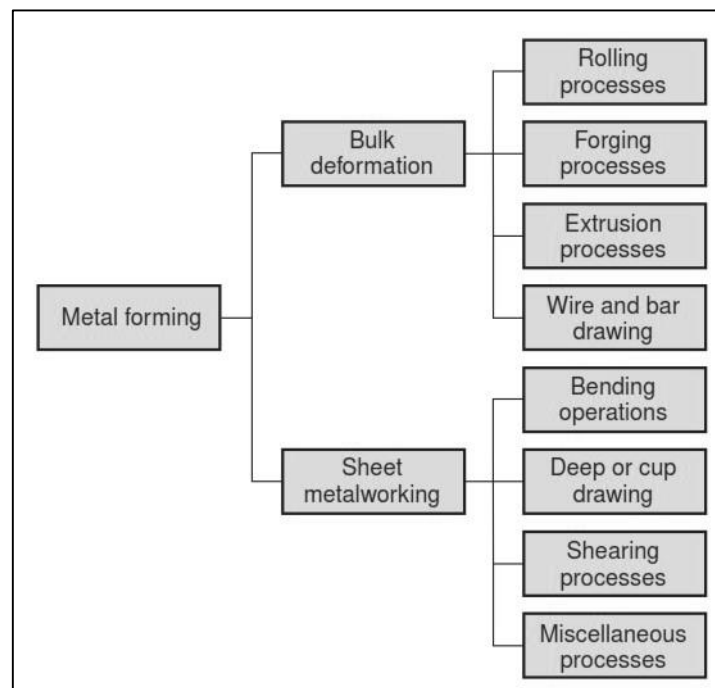


Figure 2-12. Classification of metal forming processes.

Metal forming processes can be classified into two basic categories: bulk deformation processes and sheet metalworking. Figure 2-12 shows the general classification of metal forming operations [61]. This chapter focuses on some of the sheet metal forming processes due to their importance in manufacturing the Rotor prototype intended to be manufactured within this thesis.

2.20.1 Cutting operations

Cutting sheet metal is accomplished by a shearing action between two sharp cutting edges. The shearing action is depicted in the three phases [74], as shown in Figure 2-13:

Phase I. Initially, the upper blade compresses the material, thus giving rise to elastic deformation of the material. To prevent the movement of material during the cutting operation, the material is held by the material holder.

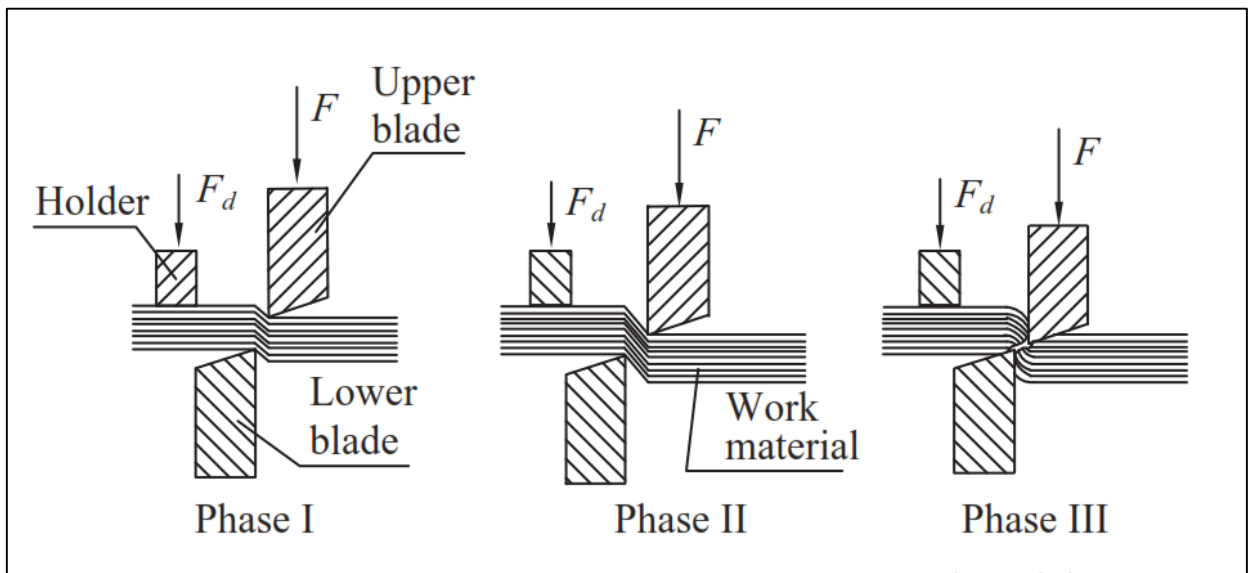


Figure 2-13. Schematic illustration of the shearing process.

Phase II- The descent of the upper blade continues until the compressive stress becomes higher than the plastic deformation yield.

Phase III- The upper blade continues descending until the compressive stress becomes equal to the material's shear strength: here, a crack or breakage allows the piece to detach from the rest of the sheet. Some of the factors determining the characteristics of the shearing are: (i) the thickness of the sheet, (ii) the quality of the material, (iii) the size of the tools, (iv) the clearance between the upper blade (punch) and the lower blade (die), and (v) the conditions of the cutting edges.

2.20.2 Cutting forces

Cutting force F in sheet metalworking can be determined by:

$$F = S \cdot t \cdot L \quad (7)$$

Where: S = shear strength of the sheet metal, MPa; t = stock thickness, mm, and L = length of the cut edge, mm. As in Figure 2-14: (a) side view of the shearing operation; (b) front view of power shears equipped with inclined upper cutting blade (Symbol v indicates motion). If shear strength is unknown, an alternative way of estimating the cutting force is to use the tensile strength [59] :

$$F = 0.7(TS) \cdot t \cdot L \quad (8)$$

where TS = ultimate tensile strength MPa.

The equations for estimating cutting force assume that the entire cut along the sheared edge length L is made at the same time. In this case, the cutting force will be a maximum. It is possible to reduce the maximum force by using an angled cutting edge on the punch or die [59].

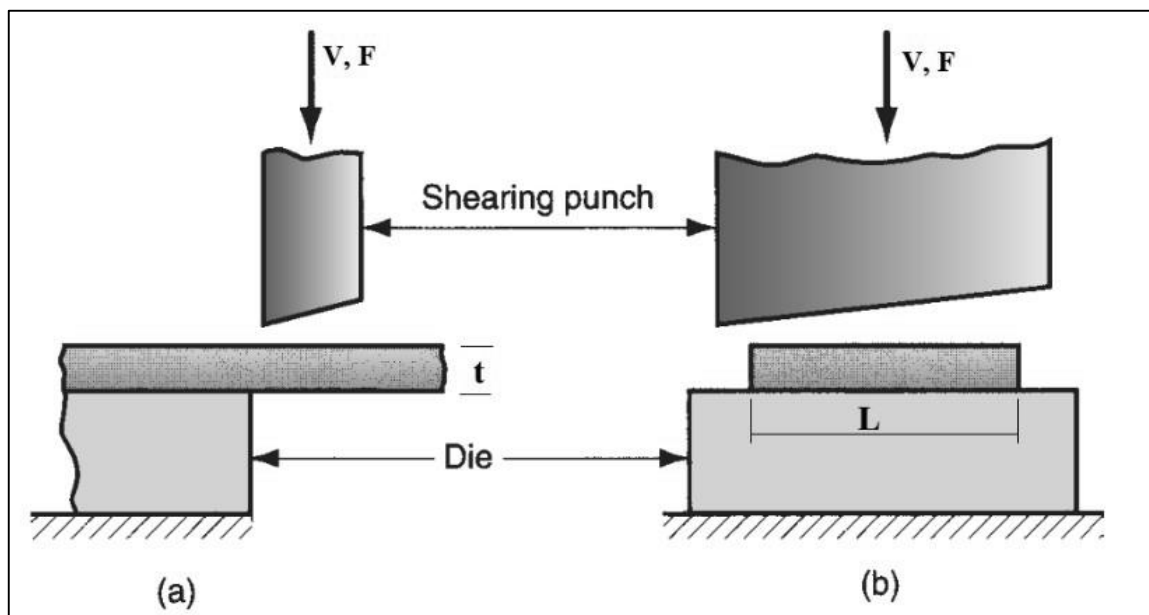


Figure 2-14. Shearing operation.

2.20.3 Bending operations

Bending can be defined as the operation that changes the element's shape by bending the edges and walls at an angle from 0° up to 180° [74]. Before carrying out a bending, two factors must be taken into consideration:

(A) Minimum bend radius: The bending radius affects the performance of the component subjected to mechanical stress: if the radius is small, cracks form, which reduces the

piece's strength. The minimum permissible radius depends on the material and the thickness of the sheet: it is greater for hard materials and must be greater than the thickness of the sheet.

(B) The elastic return of the material: when making a die, the bending angle must be accentuated in such a way as to make the workpiece takes on the desired angle once the punch pressure has stopped.

Radius (R_{min}) to which a workpiece can be bent safely, is normally expressed in terms of material thickness (T) and is given by the following formula:

$$R_{min} = c.T \quad (9)$$

The coefficient c for various materials has been determined experimentally, and some typical results are given in some handbooks [74].

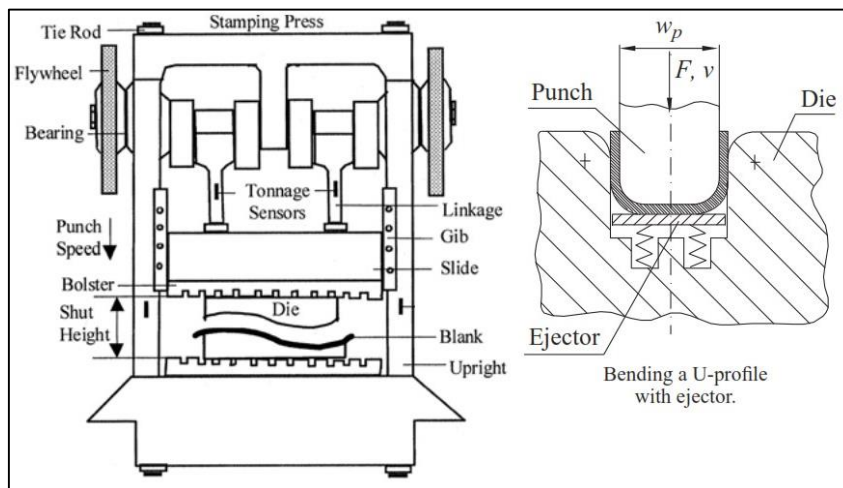


Figure 2-15. Sheet metal bending using dies mounted on presses.

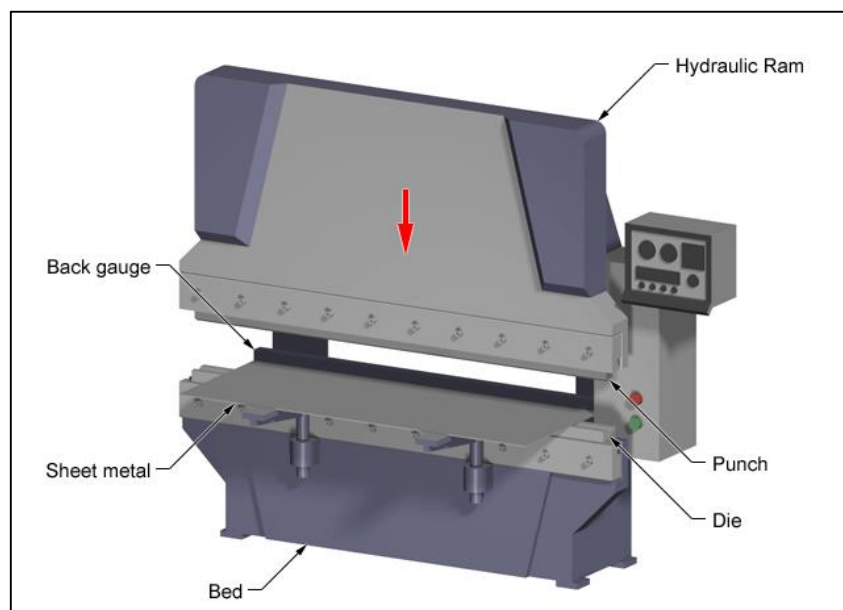


Figure 2-16. A bending press is used to create sheet metal bends.

The bending can be carried out through dies mounted on presses as in Figure 2-15 [75] or through bending presses as shown in Figure 2-16 [76]; either choice depends on the quantity and size of the component to be made. Obviously, dies are used for short and small pieces.

2.20.4 Bending force

The bending force for sheets and plates is estimated by assuming that the process is one of simple bending of a beam [59].

The maximum bending force is obtained from the following formula [63]:

$$F = \frac{K_{bf} \cdot (TS) \cdot w \cdot t^2}{D} \quad (10)$$

where F = bending force, N; TS = tensile strength of the sheet metal, MPa; w = width of part in the direction of the bend axis, mm; t = stock thickness, mm (in); and D = die opening dimension as defined in mm as in Figure 2-17 [59]; the factor K_{bf} ranges from about 0.3 for a Wiping die, to about 0.7 for a U-die, to about 1.3 for a V-die.

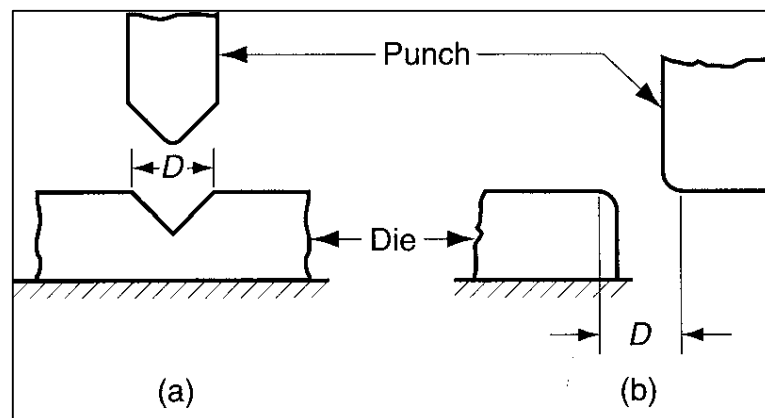


Figure 2-17. Die opening dimension D : (a) V-die, (b) wiping die.

For a V-die, equation (10) is often modified as [63]:

$$F = \frac{(TS) \cdot w \cdot t^2}{D} \quad (11)$$

Where: TS is the ultimate tensile strength of the material.

This equation applies well to situations where the punch-tip radius and the sheet thickness are relatively small compared to the die opening, D .

2.20.5 Cold stamping operations

Cold stamping of sheet metal means the set of operations that make it possible to obtain objects of the desired shape and size without removing material. A sheet metal part produced in presses is called a stamping [63].

This technique allows the rapid production of many identical pieces, of large, medium, or small dimensions, even with irregular and complex shapes.

2.20.6 Die classifications depending on the production quantity of parts

Depending on the production, stamping dies can be classified [74], (i) Class A (for high production only), (ii) Class B (for medium production quantities), and (iii) Class C (for the cheapest usable tools that can be built and are suitable for low-volume production of parts).

2.20.7 Dies types

There are various classifications of dies, such as: (i) Dies for cutting, (ii) Dies for bending and curving, and (iii) Dies for drawing.

2.20.8 Die design: general criteria

When designing and manufacturing a die, many different factors must always be considered, such as (i) the characteristics of the object (shape, dimensions, material), (ii) the characteristics of the machines available (stroke, size, tonnage, etc.) pieces to be made.

Material for tools (punch and die) are chosen based on the characteristics of the object to be stamped.

2.20.8.1 Use of the die according to the cost

Most pieces deriving from sheet metal processing can be made by hand using antiquated and rudimentary systems and means. This method, however, is in contrast with the needs of mass production, which requires less time and minimum costs. Hence, an optimal design of a die and an excellent drawing up of the operating cycle are of considerable importance.

CHAPTER THREE:
EXPERIMENTAL PROCEDURE AND
ANALYSIS

3 EXPERIMENTAL PROCEDURE AND ANALYSIS

3.1 Windmills Water Pumping Rotor Components

One of the main objectives of this thesis is to apply the RE process for manufacturing a prototype of the components of a Rotor for a water pumping windmill to pave the way for manufacturing the entire model designed to pump water in Libyan rural (i.e., Tajoura), commensurate with local manufacturing capabilities. Emphasis will be placed on implementing the approach adopted in this chapter to applying RE to manufacture the windmill Rotor and its main components shown in Figure 3-1, which is described as follows:

Rotor or Wheel: converts wind energy into rotary motion.

The Sail or Blade: the wind's power is extracted by decelerating it. However, there is a limit on how much power can be extracted from the wind.

The Sail Ribs: fixing the Sails on the outer Bands and helping to fix the attack angle of the Sails.

The Sail Ties: The first function controls the attack angle of the Sails, and the other function is to fix the blade to the inner Bands.

The Inner and Outer Rotor Bands: are sheet plates that form the outer and inner circles for fixing the Rotor blades.

The Rotor Arms: (ASTM A36, 0.25 wt.% carbon steel) rods with a circular cross-section to secure fixing the Sails sections on the Hub; the Rotor assembly is attached to a Hub assembly by these long Arms.

The Cross Ties: are Fixed on the Rotor Arms to fasten the inner Bands to these Arms.

Table 3-1 describes the Rotor's main parts shown in Figure 3-1. These parts were targeted for applying the RE.

Table 3-1. Windmill Rotor Components Description.

Part No.	Description	Part No.	Description
Win 001	Outer Rotor Bands	Win 005	Sail Ribs
Win 002	Inner Rotor Bands	Win 006	Cross Ties
Win 003	Sail Ties	Win 007	Rotor Arms
Win 004	Sails	Win 008	The Hub

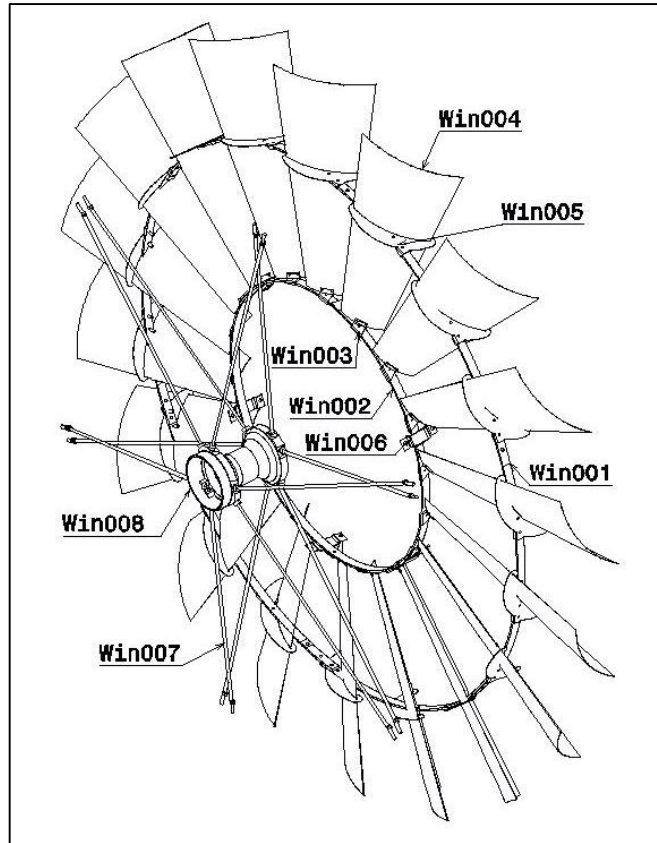


Figure 3-1. The main components of the windmill Rotor.

3.2 Data Presentation

Wind speed data were collected from CSERS located in Tajoura. These data were organized to investigate the wind conditions in Tajoura and select the appropriate commercial windmill to apply the RE approach. This area has enough wind availability per day and some underground water reserves. Being located near agricultural or pastoral areas, the windmill water pumping finds excellent opportunities for its use in these areas. Reliability, accuracy, and calculating wind speed averages of the site data are a prerequisite for the success of the windmill since a small error in the wind speed can cause a much larger error in the calculated power because the power in the wind is proportional to the cube of the wind speed. For the calculations and analysis, wind speed data for the selected location were prepared based on the monthly and daily averages for 11 years from 2005 to 2016 at CSERS.

3.3 Viability of Wind Pumping

The quantity of wind available at a site (location) is affected by the overall wind patterns, the general characteristics of the land's topography surrounding the site, and whether the location is open or has obstacles such as trees or buildings [77]. While the data available for a region are helpful for the first impression of wind resources, accurate calculations and

analysis are inevitable. In addition to the monthly average values shown in Figure 3-2, the hourly average wind speed values during the day were considered for the collected data at the CSERS Climate Station in 2017, as shown in Figure 3-3. On most days of the year, the wind speed exceeds the annual average from midday until 04:00 pm. In general, the wind speed begins to rise from 9:00 am and continues to increase until it reaches its highest levels and then decreases at 6:00 pm. That means the windmill will often be standing still during the late night and early morning but will mostly run during the rest of the day. The windpump design should satisfy the daily pumping requirements during those hours of strong winds a day.

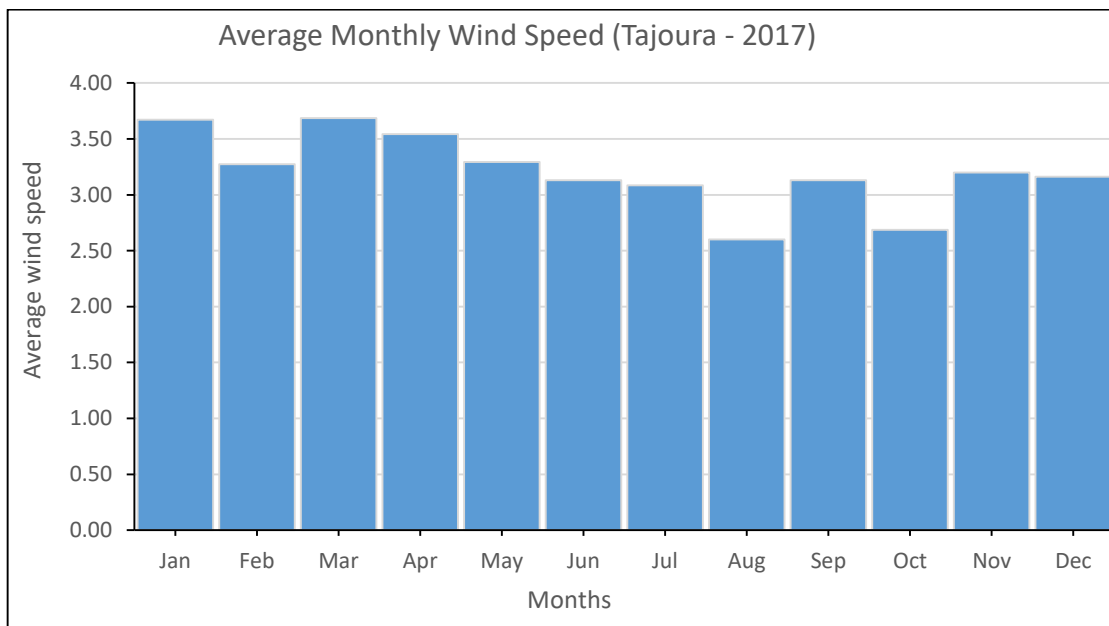


Figure 3-2. Monthly variations of wind speed, Tajoura (2017).

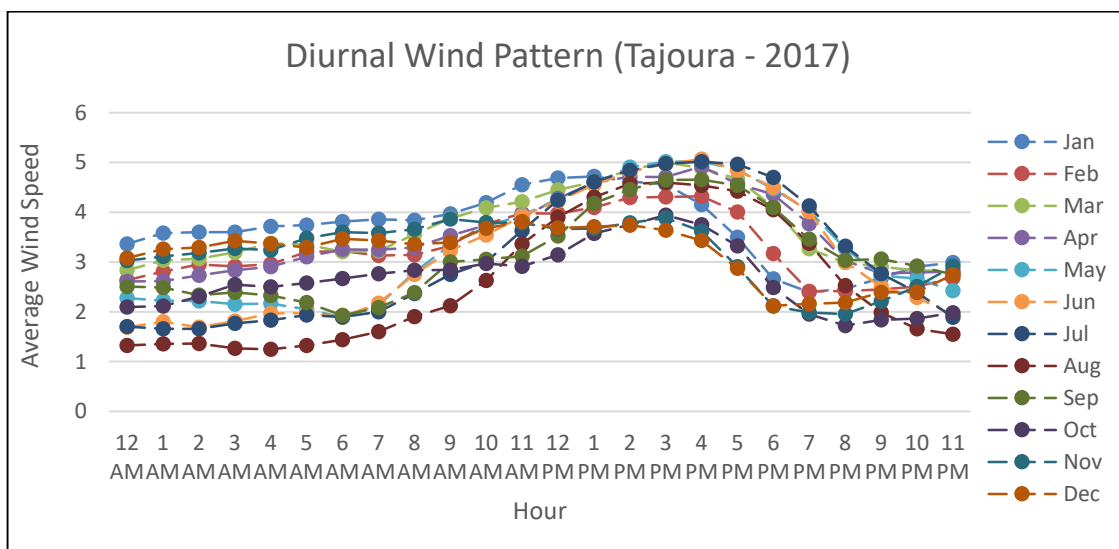


Figure 3-3. Hourly wind speed variations (Diurnal wind pattern), Tajoura (2017).

From what was mentioned earlier, one can deduce that the hours during which the wind speed approaches the annual average during the day are 8 to 9 hours. So to improve the starting behavior, it is very important to reduce the time that the Rotor starts to rotate by balancing the weight of the pump rod or sacrificing some water output to reduce the time to start running the windmill using a starting nozzle in the piston pump. Eventually, the water displaced in the discharge pipe will leak through the nozzle.

3.4 Wind Speed Distribution

The most widely used PDF to fit wind data is the Weibull distribution [10,78,79,80], which is defined as:

$$f(v) = \frac{k}{c} \left(\frac{v}{c}\right)^{k-1} e^{-\left(\frac{v}{c}\right)^k} \quad (12)$$

for ($v > 0$, $k > 0$ and $c > 0$).

where $f(v)$ is the probability of observing wind speed (v), the scalar quantity (k) is the shape parameter, and (c) is the scale parameter in m/s. A special case of Weibull distribution when $k=2$ is called the Rayleigh distribution. Weibull distribution function fits the wind speed variation better than the Rayleigh distribution function [81]. In this study, the selected method of estimating Weibull parameters is the least square method (LSQM) [82,83]. The LSQM, also known as the graphical method, is based on logarithmic transformations applied to the Weibull cumulative distribution function (CDF) and, thus, can be represented by a straight line:

$$y = Mx + Y_0 \quad (13)$$

and:

$$y = \ln[-\ln[1 - F(v)]]; x = \ln v \quad (14)$$

The Weibull parameters can be calculated by:

$$k = M; c = e^{-Y_0/M} \quad (15)$$

and:

$$M = \frac{\sum_{i=1}^n (x_i - x_m)(y_i - y_m)}{\sum_{i=1}^n (x_i - x_m)^2};$$

$$Y_0 = y_m - Ax_m \quad (16)$$

Where: x_m and y_m are the mean values of x & y , respectively. Where x_i & y_i are the values obtained using Equation (13) with each wind speed data set.

By applying the least squares (the graphical method), as shown in Figure 3-4 for CSERS wind speed data in 2017, the Equation of the line is:

$$y = 1.99x - 2.53 \quad (17)$$

Thus, and based on Equation (15), Weibull parameters can be calculated as $k=1.99$ and $c=3.4$.

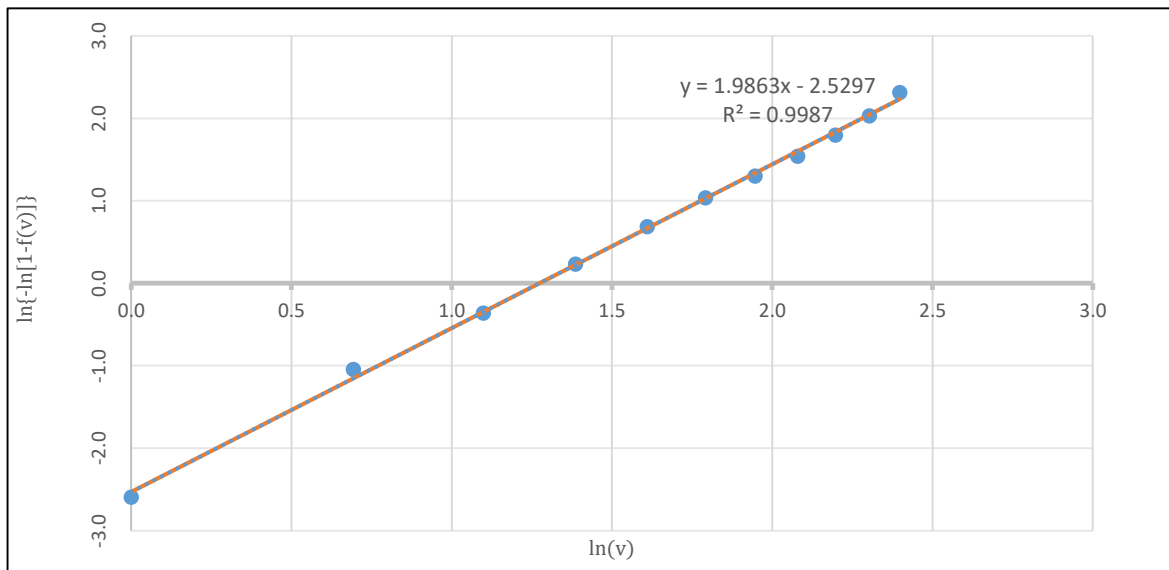


Figure 3-4. Graphical method of determining Weibull parameters.

The wind distribution function at Tajoura for Weibull parameters is shown in Figure 3-5.

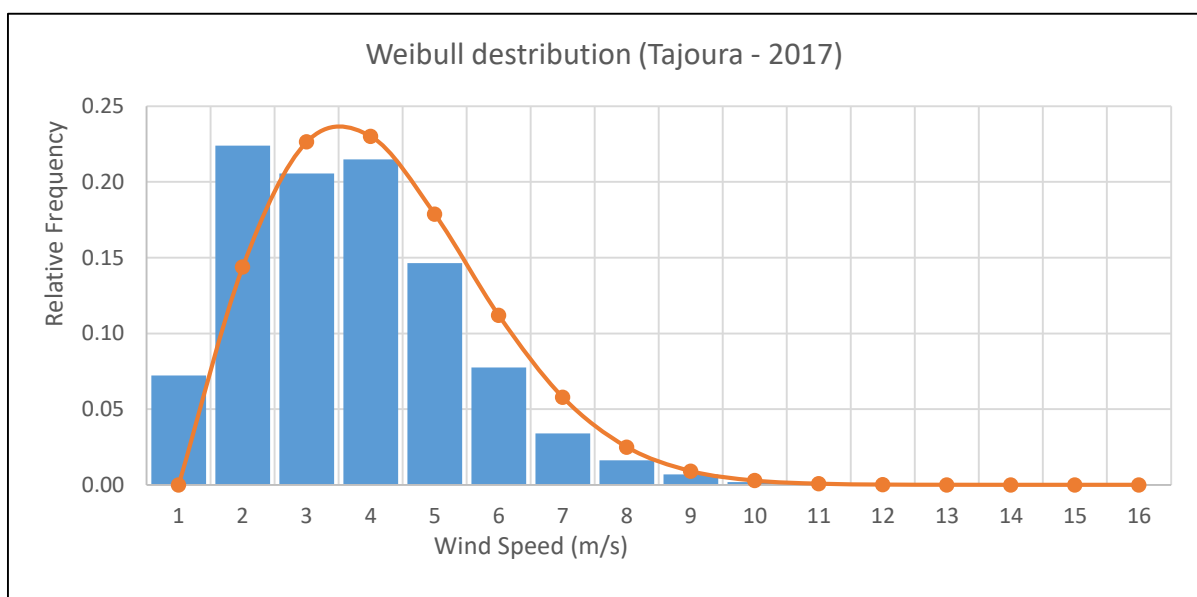


Figure 3-5. Weibull distribution to Tajoura (2017) for $k=1.99$, and $c=3.4$.

3.5 Selecting the Site and Size of the Windmill

In this study, simple calculations were made to determine the proper Rotor size for the site where the windmill will be installed. The calculations used in the design of the windmill were made to examine whether the size of the Rotor to which the RE was applied is appropriate for the site. The steps that were followed in selecting the optimum size of a water pumping windmill for the site are:

3.5.1 Site selection:

The feasibility of a windmill is largely affected by its site. The site must have enough wind power to move the windmill and be away from any obstruction that might cause turbulence. The climatic condition of the site should be examined for over a year and recorded on a wind map which is then used to analyze the site's suitability [84,85,86]. The Rotor should be tall enough to ensure it's far above the obstacles. Identifying and determining the site of the windmill understudy was done. The analysis of the site to assess its suitability and the findings are as follows:

- The wind speed of Tajoura varies from 2.35m/s to 4.69m/s, and these were the minimum and maximum daily average wind speeds recorded from January to December for eleven years, with an annual average wind speed of 3.24 m/s.
- The site (location) of the windmill is strategically away from tall buildings and trees; therefore, minimal obstruction of the wind. The selected standard tower height of 12m is sufficient to lift the Rotor over the surrounding isolated trees.

3.5.2 Determining the water demand

The determination of the water demand (Q_p) depends on the total number of site beneficiaries and the daily per capita water. Water consumption at the Center for Solar Energy Research and Studies is constant. The water pumping requirements are estimated as 5m³/day, which satisfies human uses and garden irrigation needs.

3.5.3 Determination of the hydraulic power

The hydraulic power required (P_{hyd}) to lift water from the source to the storage tank is calculated based on Equation (18)[86]:

$$P_{hyd} = Q_p \cdot \rho_w \cdot g \cdot H \quad (18)$$

Where:

Q_p = the water demand (m³/s).

ρ_w = water density (1000kg/m³).

g = acceleration due to gravity (9.81m/s²).

H = the total discharge head (m).

The total discharge head is found by adding the depth of the water level in the well and the height of the tank (93m).

The delivery pipe length is (96m), and the pressure loss in the pipes is about 10% of the total head [7]. The head loss in the delivery pipe is 9m, and the total discharge head (H). The average hydraulic power requirement (P_{hyd}) is 57.8W calculated based on Equation (18).

Table 3-2 shows various losses that have to be considered for determining the average hydraulic power requirement [7,87,88].

Table 3-2. Power Losses in the Windmill.

Factor	Typical Efficiency
Rotor to shaft	92-97%
Shaft to gearbox	93-96%
Gearbox	99%
Pump	60-75%

The average efficiency of the pump is 70%. The average efficiency of the shaft from the gearbox to the pump is 95%. The gearbox's average efficiency is 99%, which is the actual efficiency of the gears. The efficiency of the horizontal shaft between the Rotor and gearbox is 95%. The amount of the average hydraulic power requirement from the wind (P_{hyd}) is 92.4W.

3.5.4 Wind power potential determination

The wind power potential is given as the specific wind power (P_{wind}) or power per unit area[86,87,89]. It is calculated by using Equation (19):

$$P_{wind} = \frac{1}{2} \cdot \rho_a \cdot V^3 \cdot C_p \quad (19)$$

Where:

ρ_a = air density(1.207kg/m³).

V = the wind velocity, C_p = Power Coefficient.

The roughness of the terrain (isolated buildings, small trees) is estimated to be 0.25m taken from the Davenport classification of effective terrain roughness [90,91,92,93]. By using Equation (20), the data for 10m above terrain height are converted into 12m, as the standard tower height (12m) chosen.

$$\frac{V_z}{V_{zr}} = \frac{\ln(z/z_0)}{\ln(z_r/z_0)} \quad (20)$$

Where:

z = height above the ground surface (m); z_r = reference height (m); z₀ = surface roughness length (m); V_{zr} = the wind speed at the reference height z_r and V_z = wind speed at any height z. Table 3-3 shows the results for the understudy windmill system.

Table 3-3. Determination of Specific Wind Power.

DETERMINATION OF SPECIFIC WIND POWER (P_{wind})				
Location : <u>Tajoura</u>			Height above sea level: 50m	
Hub height: 12m			Terrain roughness: 0.25m	
Combined correction factor for Hub height and roughness: 1.05				
Month	Average wind speed at 10m (m/s)	Average wind speed at Hub height (m/s)	Density of air (kg/m ³)	Specific wind power (W/m ²)
Jan	3.5	3.7	1.2	8.9
Feb	3.53	3.7	1.2	9.2
March	3.47	3.6	1.2	8.7
April	3.55	3.7	1.2	9.3
May	3.42	3.6	1.2	8.3
June	3.34	3.5	1.2	7.8
July	2.99	3.1	1.2	5.6
Aug	2.97	3.1	1.2	5.4
Sept	3.06	3.2	1.2	6.0
Oct	2.97	3.1	1.2	5.4
Nov	3.03	3.2	1.2	5.8
Dec	3.12	3.3	1.2	6.3

The site is practically at sea level, and the air density is assumed to be 1.2kg/m³. In the last column, the specific wind power is calculated using Equation (19) multiplied by the Power Coefficient, assuming the maximum practical value of the Power Coefficient (C_p) is 0.3.

3.5.5 Reference area and size of the windmill

The ratio of the hydraulic power of each month [86] divided by specific wind power potential for the same month has the dimension of the area and is referred to as the reference area (R_a):

$$R_a = \frac{P_{hyd}}{P_{wind}} \quad (21)$$

The Rotor diameter (D_r) is given in Equation:

$$(D_r) = \sqrt{\frac{4R_a}{\pi}} \quad (22)$$

3.5.6 Determination of the design month

The design month is found by calculating the ratio of the hydraulic power requirement to the wind power resource for each month. The month in which this ratio is a maximum is the design month. The monthly averages of wind speed Table 3-4 were recorded at the height of 10m and converted into 12m (at the Hub height) from the earth's surface at the Libyan Center for Solar Energy Research and Studies in Tajoura. From Table 3-4, August and October are the design months with $R_a = 17m^2$.

Table 3-4. Sheet for Identification of Design Month.

DESIGN MONTH					
Location : Tajoura (CSERS)					
Month	Average hydraulic power (P_{hydr}) (W)	Average wind speed at Hub height (m/s)	Specific wind power (P_{wind}) (W/m^2)	Reference area (P_{hydr}/P_{wind}) (m^2)	Design month
Jan	92.4	3.7	8.9	10.4	
Feb	92.4	3.7	9.2	10.1	
March	92.4	3.6	8.7	10.6	
April	92.4	3.7	9.3	9.9	
May	92.4	3.6	8.3	11.1	
June	92.4	3.5	7.8	11.9	
July	92.4	3.1	5.6	16.6	
Aug	92.4	3.1	5.4	17.0	←
Sept	92.4	3.2	6.0	15.5	
Oct	92.4	3.1	5.4	17.0	←
Nov	92.4	3.2	5.8	16.0	
Dec	92.4	3.3	6.3	14.6	

Hence, by using Equation (22), the Rotor diameter is:

$$(D_r) = \sqrt{\frac{4 * 17}{\pi}} = 4.7m$$

The nearest standard Rotor diameter is 4.88m (16ft), as reported by [94] and Aermotor windmill company. This diameter was selected for the RE process in the present study, which would be suitable for the site where the windmill will be installed [95,96].

3.5.7 Pump selection

The choice of a small pump enhances availability but reduces output. In matching a pump to a windmill, one must establish the best possible compromise between output production and availability [97]. Referring to some diagrams and tables found in reference [7] to determine the volume of water pump suitable for a classical back-gearred windmill with a deep well pump, in this case of a Rotor diameter of 4.88m (16ft); wind speed average of the critical month of 3.1m/s:

- The effective stroke volume of 0.755L.
- Assuming a volumetric efficiency of 90%, the geometric stroke volume is 0.84L.
- The maximum stroke available for the 16ft windmill is 288,93mm ($11\frac{3}{8}$ in).
- Through all of this, it is possible finding the right pump with a diameter of 56mm; this is close to one of the pumps of the standard range in use, 2.5in (63.5mm).

To check the suitability of the pump to the water requirements for 9 hours/day when the windmill is running with 11 strokes/min, the water requirements =

$$0.84 \times 11 \times 60 \times 9 = 4989.6 \text{L/day.}$$

These large quantities of water will be in the critical months of August and October, which are appropriate quantities, and expected to be an excessive water production in the remaining months that will return to the well through a pipe designated [86]. Equation (23) can be used to find the geometric volume displaced by the piston (V_s) of a piston pump diameter (D_p) in each stroke (s).

$$\text{Stroke volume} = V_s = \frac{1}{4} \cdot \pi \cdot D_p^2 \cdot s \quad (23)$$

Since the flow rate provided by the wind is irregular, water is usually required at a relatively high flow rate during short periods of the day. The storage and distribution of water is an important part of pumping systems; the main purpose of a storage tank is to store surplus water during days of strong wind for later use when there is less wind. A tank with a capacity equivalent to 3 days of water requirement is available on site (about 15m³) and will be used within the system.

3.6 Acquisition Tools and Equipment

One important endpoint of this thesis is the application of techniques and methodologies typical of "RE" to manufacture a windmill that was mentioned earlier. It starts with the 3D scanning techniques, where two different types of scanning techniques were selected to carry out the dimensional acquisition operations for all Rotor components.

3.6.1 Hardware with non-contact techniques

The experimental work in this thesis for obtaining dimensional data of all the Rotor components was carried out with the BacesSCAN portable laser scanning system at T.B.Co. It comprises a Baces3D three-coordinate measuring arm (7 axis M100) and BacesSCAN V2 Scanner. Figure 3-6 shows the Baces3D measuring arm and the captions relating to its characteristics [98].

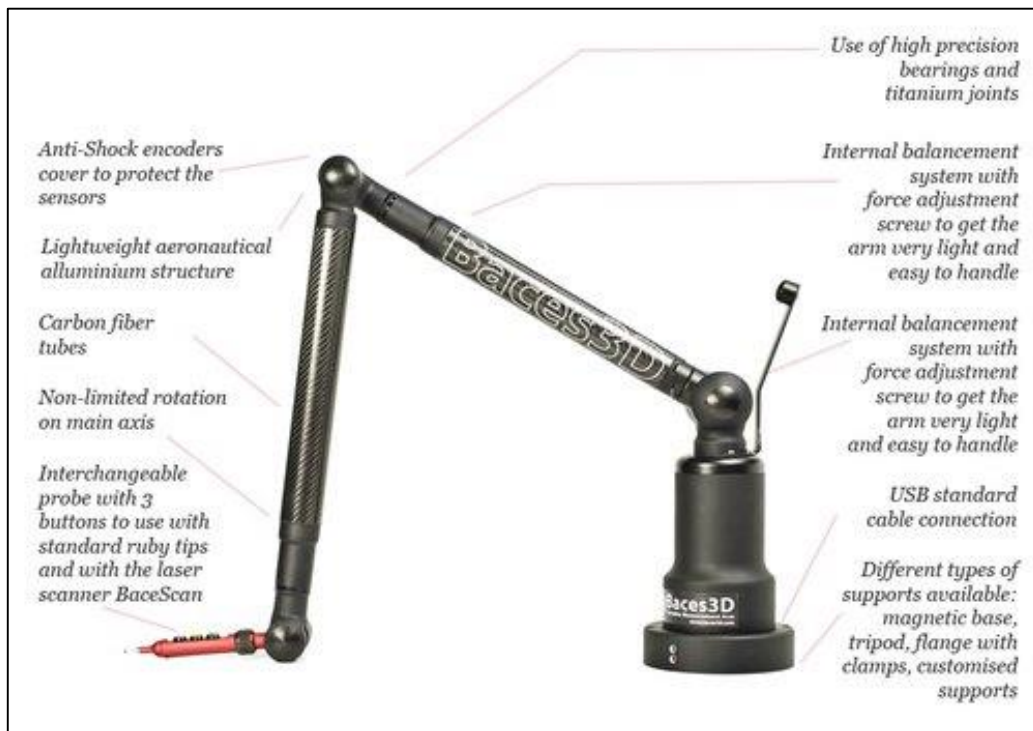


Figure 3-6. Baces3D three-coordinate measuring arm.

The Baces3D is a portable measurement arm designed to acquire 3-dimensional measures points and surfaces within its work-space with a simple manual movement of the user with contact technique, or non-contact technique for acquisition, using the BacesSCAN laser scanner. The Base3D shown in Figure 3-7 is an ideal instrument for digitization for the understudy Rotor components (parts) as a powerful reverse-engineering and metrology tool.

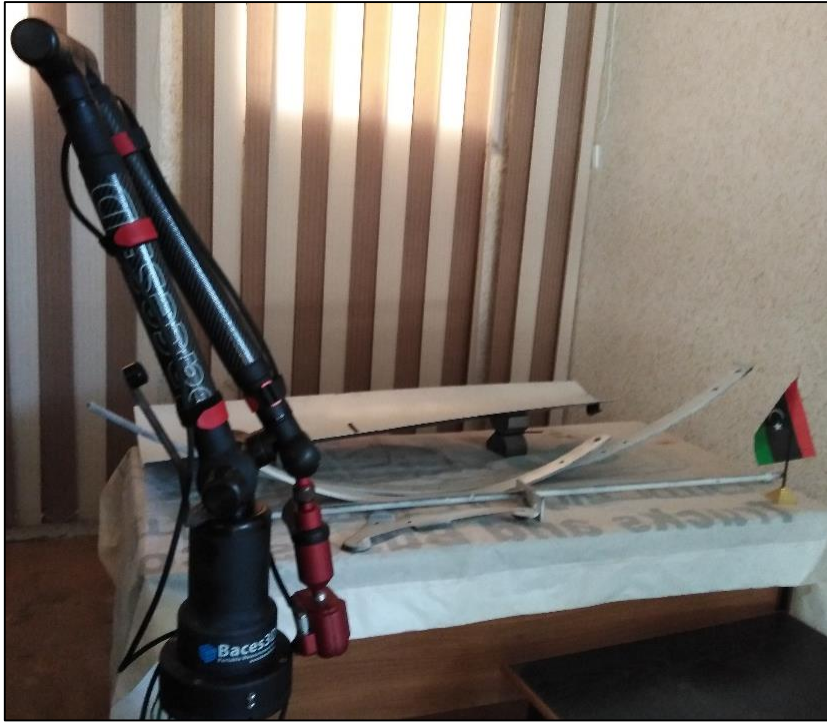


Figure 3-7. BacesSCAN portable laser scanning system.

The scanner's output is the 3D scan data as a point cloud or dense triangle mesh. This data serves as a visual sketch and requires manipulation before it becomes a final CAD file.

In Figure 3-8, the BacesSCAN portable laser scanning system is shown in a moment of its use during scanning the Sail Rotor.



Figure 3-8. The BacesSCAN laser scanning system is shown in a moment of its use.

3.6.2 Hardware with contact techniques

One of the dimensional acquisition techniques was also done in this work using the CMM. This machine is located at the Technical Research Center of Abusaleem with measuring ranges X (650mm), Y (500mm), and Z (400mm). In Figure 3-9, the picture of the CMM was taken while making some measurements of the Hub.

All the machine elements making up the main parts of the slides are in black granite, the workpiece support surface is provided with threaded holes within a distance of 200mm for the clamping of the pieces to be measured, and the mechanical balancing of the "z" axis guarantees the extreme sensitivity of the machine.



Figure 3-9. CMM during some measurements of the Hub.

The "Poli" measuring machine gives the following advantages in 3D control:

- Self-alignment of the piece to be controlled thanks to a specific software function.

- Measurement of the workpiece on all faces except for the support face.
- Extreme ease of use.
- The slides made on pneumatic guides guarantee the high precision of the equipment.

3.7 Reverse Engineering Software

Nowadays, there are many software products dedicated to geometric RE, often integrated into high-end CAD systems, for example, Cloud to Geometry in CATIA V4, Digitized Shape Editor and Quick Surface Reconstruction in CATIA V5, Pro / Scan in PRO-ENGINEER, Surface and Verdict in IMAGEWARE, Surface Reconstruction in STRIM100 by CISIGRAPH, and CopyCAD in DELCAM, etc. They can read digitized point files, sorted in scans according to various formats (ISO_G code, ASCII, proprietary formats of the various manufacturers of digitizing machines), and create a corresponding point cloud CAD model [99].

The starting point for further modifications of scanned surfaces and the creation of a 3D CAD model was a transformation of the point cloud from the Baces3D software into 3D software. This is realized by a universal file format for data transfer between various 3D software solutions (IGES).

The advantage of this file format is an option of significant size data transfer. To create the final surface by overlaying the point cloud with a mesh, a number of operations must be made using CATIA's Digitized Shape Editor (DSE) to achieve these operations.

3.8 Digitization of the Component

To begin the work of geometric modeling of the workpiece (component) subjected to RE, it is necessary to obtain the "cloud of points" in the three-dimensional space that forms the geometric representation of the digitized points.

The file containing the information obtained from the acquisition device must be preliminarily optimized through appropriate filters; only subsequently can the point cloud be converted into a neutral format (IGES, VDA, STEP, etc.) or imported directly into the software used for modeling.

Figure 3-10 illustrates the general process flow diagram for applying RE in this thesis. This flow diagram demonstrates some of the possible applications of the generated 3D CAD model obtained from the RE process.

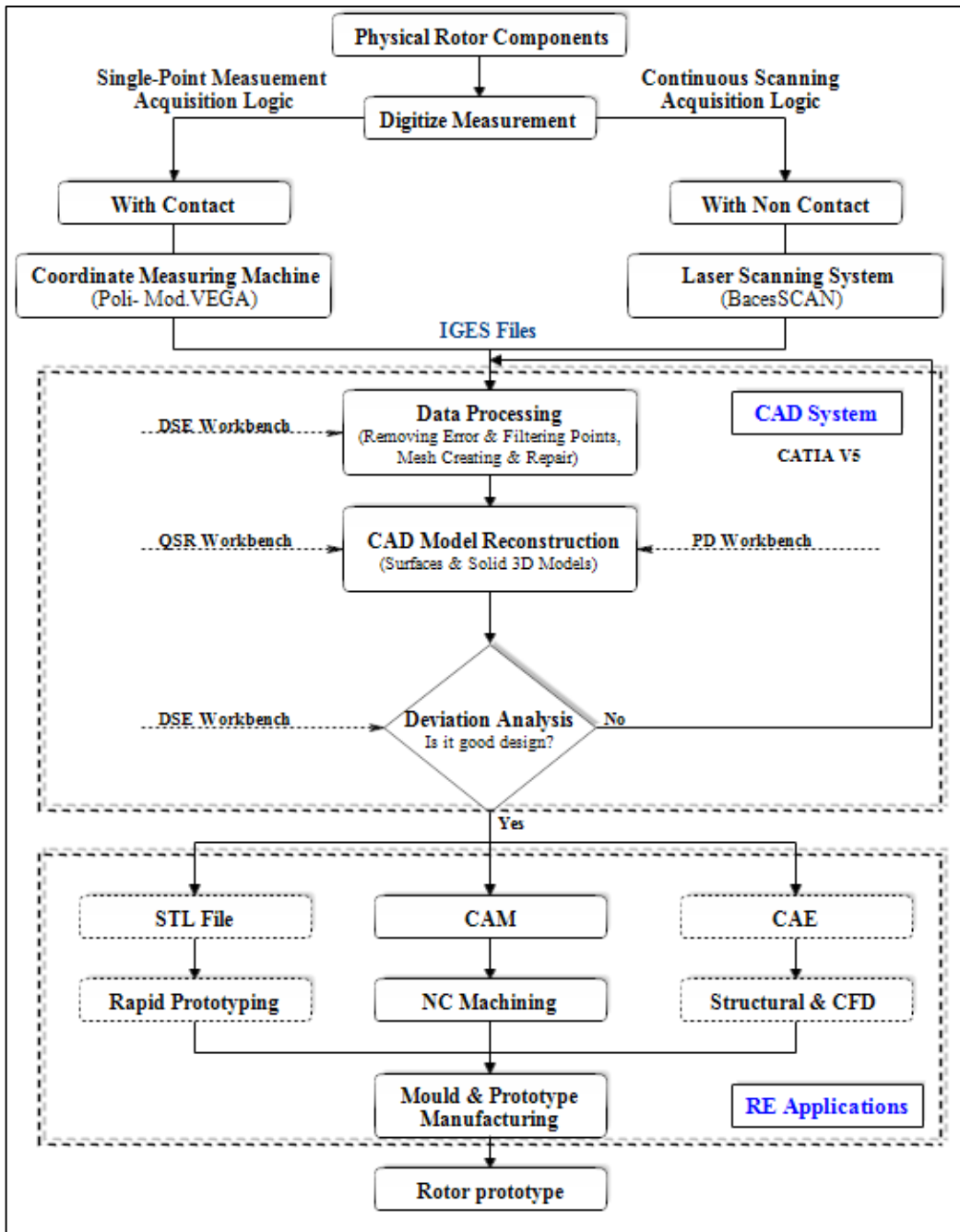


Figure 3-10. Thesis's RE Process Flow Chart.

3.8.1 Preparation of the components for scanning

The high shine of surfaces is one problem of optical scanning systems, such as chrome-plated surfaces or black surfaces that don't reflect laser rays. One viable solution to avoid this problem is to spray the component with a temporary matte powder (coat) to improve scanning accuracy.

Even slightly glossy surfaces degrade scan quality, while reflective and transparent surfaces cannot be scanned without a matte coating. In this research study, the surface color of the Rotor Sail is theoretically proper for 3D scanning; however, it is expected that there will be

a problem with point cloud by scanning unadjusted surfaces because of the uncontrolled laser ray scattering. That causes incorrect scanning, where this problem looks like points in space which doesn't exist in reality, as shown in Figure 3-11. These incorrect points cause a serious problem with CAD modification, especially for rapid prototyping processes and manufacturing with NC machining.



Figure 3-11. Surface color cause incorrect scanning.

The surface color of the tested parts (components) was changed to white, as shown in Figure 3-12, which allows for scanning the surface more precisely.

3.8.2 Scanning of the physical rotor components

All components are precautionary painted white, as mentioned in the previous paragraph. The parts have been well fixed one after the other on the prepared measuring table to prevent any movement of the measured piece during the scanning process.

The examination room is also dimmed to reduce errors. Scanning of all components was performed without fragmentation (one scan or one patch) of the scanning process.

In Figure 3-13, the BacesSCAN is shown in a moment of its use during scanning the Sail Rib. The IGES format was chosen to transfer the point cloud files obtained from the Baces3D software digitizing machine to the CATIA used to perform the point processing operations and the CAD model reconstruction.

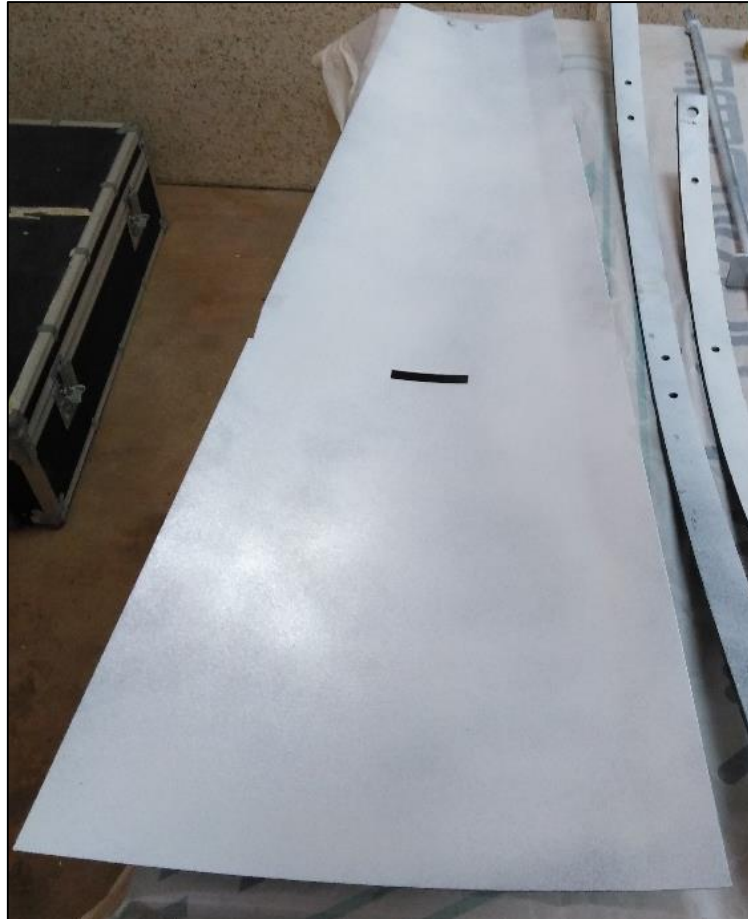


Figure 3-12. The parts of the Rotor were painted white.



Figure 3-13. The Baces3D arm during scanning of the Sail Rib.

3.9 Processing the Measured Data

The first two problems that arise in the 3D rendering (on the CAD software) of a physical object being scanned are the enormous number of digitized points and the errors that any scanning operation affects. Therefore, on these points, appropriate preprocessing work must be carried out to ensure that they can be profitably used for the subsequent phase of geometric modeling. Although they are all imported into the CAD model, only a small part of them is utilized directly to obtain the geometric model of the piece in question. The excluded points are used indirectly to control the trend of the model surfaces. Furthermore, measurement errors must be corrected as much as possible, and any points that may have an error greater than a pre-established threshold must be discarded. After getting the detailed dimensions of the Rotor parts from the scan files, they can be refined into a final part. This process varies based on the software program used.

It combines automated technology inside the software and human manipulation to complete the CAD model. They turn the point cloud or mesh that was received from the scanner into a polygonal model. The resulting mesh is cleaned up, smoothed, and sculpted to retain its required shape and accuracy.

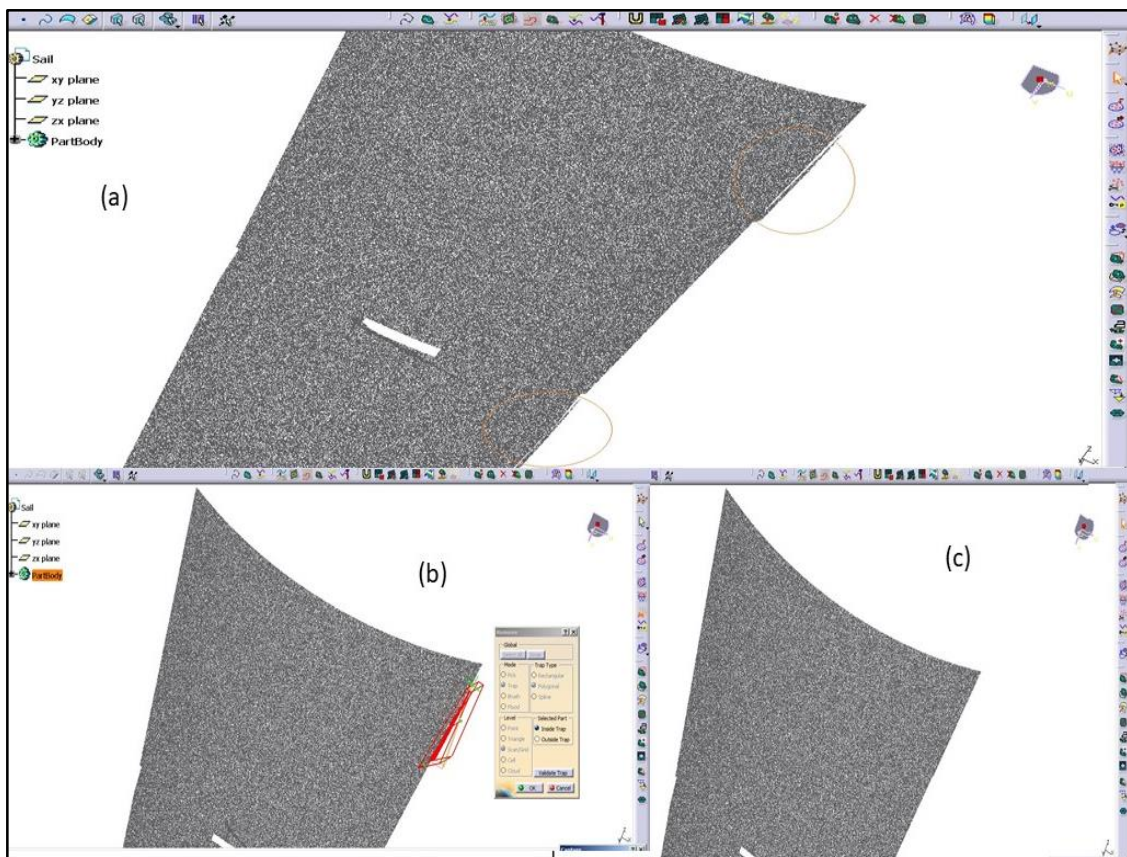


Figure 3-14. Applying Remove Command in DSE.

3.9.1 Removing error points

During the operation; clamps, fixtures, and other unwanted points would come into the measurement area (error points), which makes up the boundary buffer.

All of these error points must be manually removed by the Remove command in DSE CATIA. Figure 3-14 shows (a) the gathered point cloud data of the Sail before removing error points; (b) the point cloud data are practicing the Remove command, and (c) the point cloud data without error points.

3.9.2 Filtering points

Currently, the commonly used methods of filtering points include the adaptive method, octree structure method, proportional method, average distance method, minimum distance method, etc. [100,101].

The homogeneous method provided in CATIA is suitable for processing the point cloud data of the model with the regular curved surface as all surfaces on the Rotor components. Various display filters can be applied to the point cloud by reducing the visible amount in order to lighten the cloud from a graphic point of view without losing the essential information for the geometric reconstruction of the object.

Figure 3-15 (a) shows the cloud relating to a Sail, consisting of 9,999,96 digitized points, which has been reduced to 140,83 points shown in Figure 3-15 (b) by applying the Filter command in DSE CATIA, which displays only enough points that determine the curvature of the Sail.

3.9.3 Creating mesh

Mesh is the triangle image of the point cloud. It's not a real surface, but it can improve the visibility of the point cloud and the efficiency of surface molding.

The modern procedures start from the recorded and edited cloud, which is subjected to an algorithm for creating meshes, representing the starting numerical model.

This is characterized by a polygonal mesh of points, from which the mathematical surfaces can be reconstructed following different paths to find the best result. Mesh is created by the command of Mesh Creation of DSE CATIA with the radius of the little sphere set to 10mm. Once the point cloud has been created, a 3D mesh is generated, as shown in Figure 3-16.

3.9.4 Mesh repair

The obtained mesh had discontinuity and large holes. The holes in the mesh were repaired with the Fill Holes, Mesh Smoothing, and Mesh Cleaning commands under the DES workbench in the CATIA. Figure 3-17 shows (a) point cloud before applying Filter Command; (b) point cloud after applying Filter Command. Finally, the repaired meshes were used to develop a solid CAD model. Generally, mesh provides a guide for placing lines and surfaces, and at the end of the process, the final structure of the part becomes similar to the mesh.

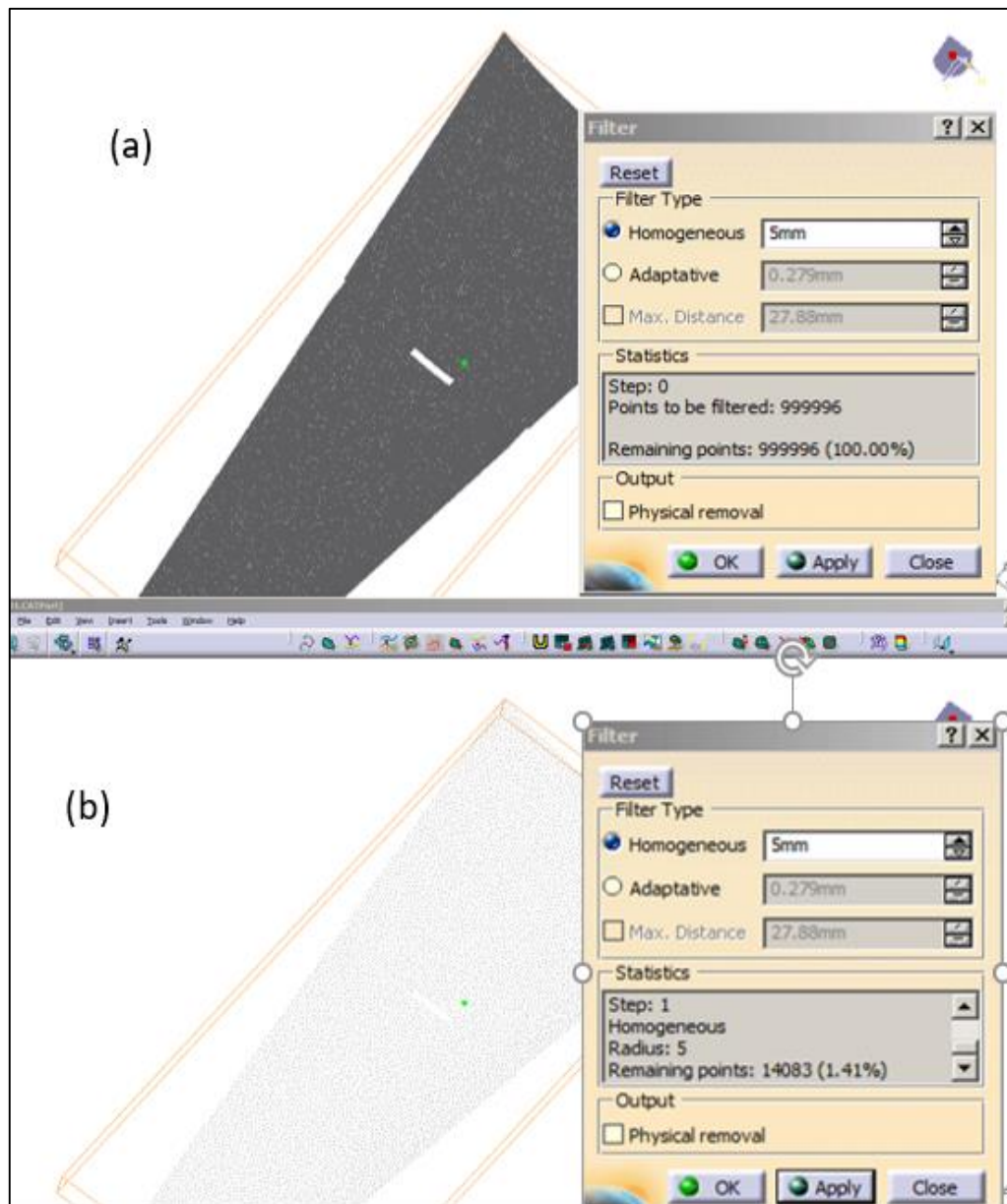


Figure 3-15. Mesh repairing

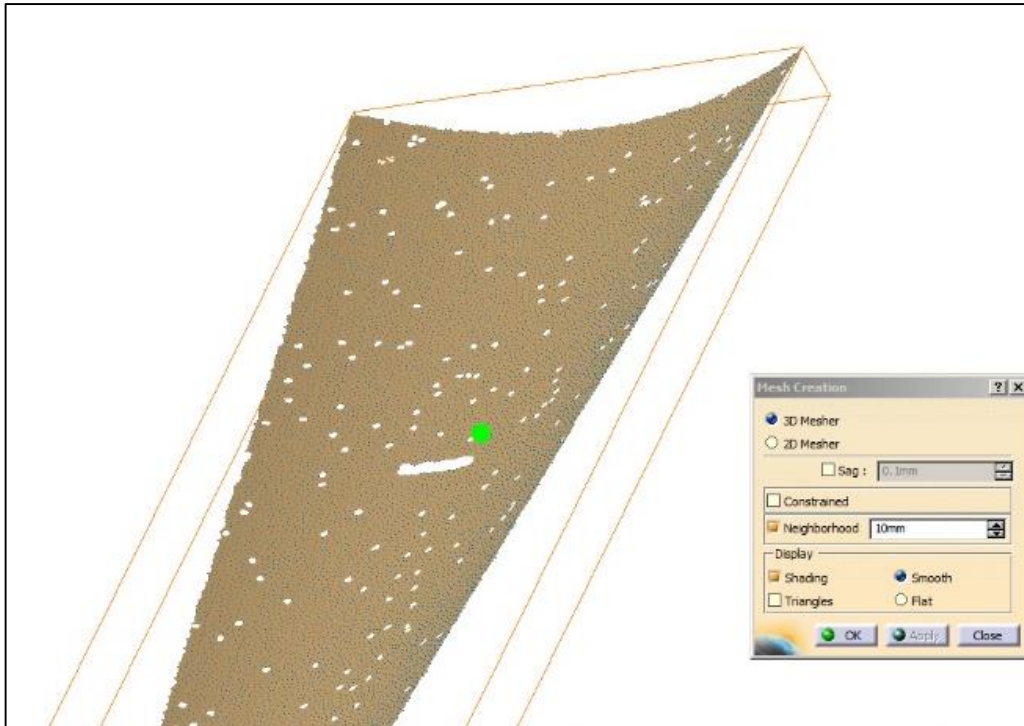


Figure 3-16. Mesh is created by the command of Mesh Creation of DSE CATIA.

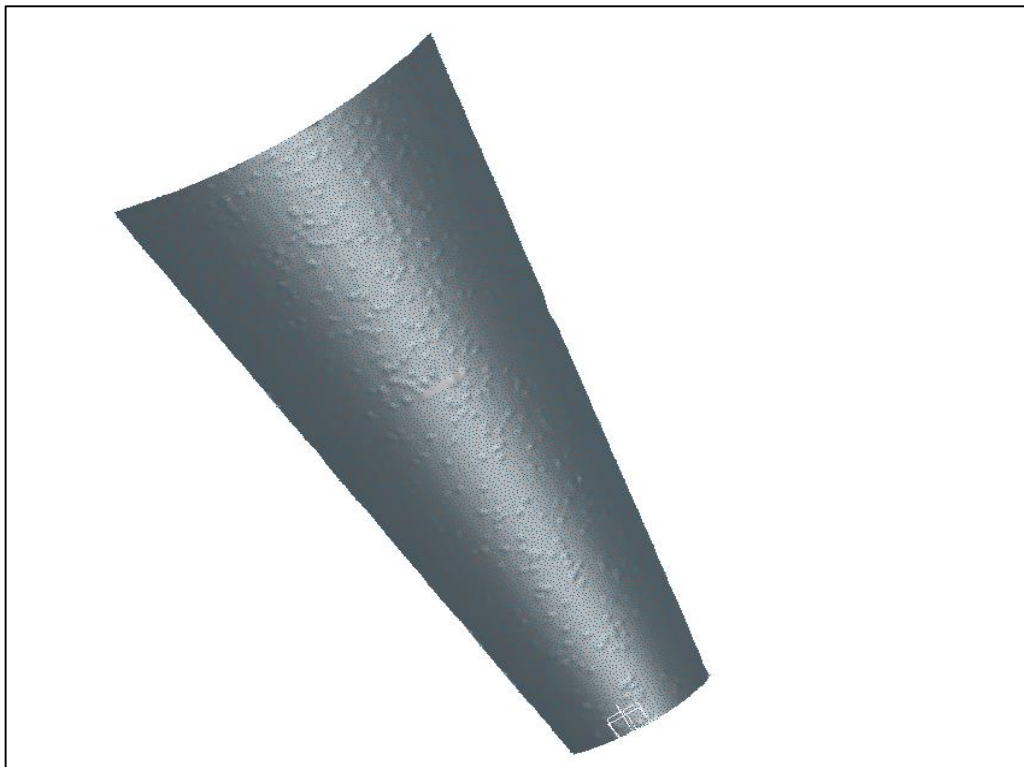


Figure 3-17. The repaired mesh of the Sail.

3.10 The Hub RE Work

The Hub is included with the water pumping windmill's physical powertrain and brakes group. All the powertrain and brakes group components have been disassembled as shown

in Figure 3-18 to obtain the Hub separately so that measurement can be done using the CMM previously mentioned located at the Advanced Center of Technology.



Figure 3-18. Disassembled components of the powertrain and brakes group.

The single-point measurement acquisition logic was adapted. The measurement focused on the anchor places of the Rotor on the Hub, particularly the holes attached to the Rotor Arms. Figure 3-19 shows the Hub during the acquisition of the points from CMM.



Figure 3-19. The Hub points acquisition using CMM.

Based on these points and other measurements taken manually (since the Hub is not intended to be manufactured), a Hub CAD model is constructed so that a CAD model for the complete Rotor assembly can be implemented.

3.11 The CAD Model Construction

After repairing the digitized points, the next step is creating (on these points) the curves on which the surfaces that form the geometric model of the piece were built. In fact, the surfaces cannot be obtained by directly interpolating the digitized points, but it is first necessary to build on these curves that constitute their support. It is often necessary to create curves that follow the object's contours or delimit particular areas. It may also be useful to create curves corresponding to appropriate sections of the point cloud. In all cases, it is always convenient, when possible, to make planar curves, as they are more easily editable. Planar curves were created with Planar Sections command under the DES workbench in the CATIA. Figure 3-20 shows planar curves that constitute the surface support on the repaired mesh. At this point, the fundamental problem is the choice of surfaces to interpolate the curves obtained to replicate the geometry of the physical component as closely as possible.

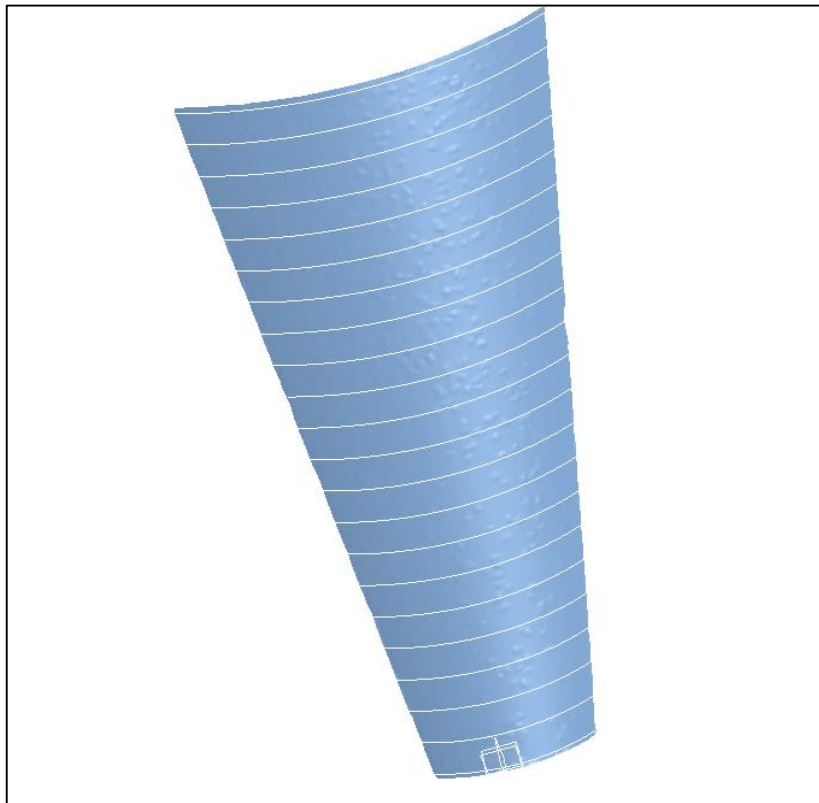


Figure 3-20. Planar curves on the repaired mesh.

All the surfaces of the Rotor parts were created by Quick Surface Reconstruction (QSR) in CATIA. This choice was selected because the characteristics of QSR are perfect in this case.

These characteristics are:

- Creation of surfaces by Powerfit or canonic shape recognition;
- Efficient for quality surface creation (if no strict accuracy is expected);
- The quality of surfaces relies on the quality of input curves.

Where the drawbacks are:

- Not efficient for high-quality design such as class A design.

From these obtained surfaces in Figure 3-21, a solid model was formed using the Part Design in CATIA, and Figure 3-22 shows a solid 3D model of the Sail Rib as an example of one of the Rotor parts executed in this thesis.

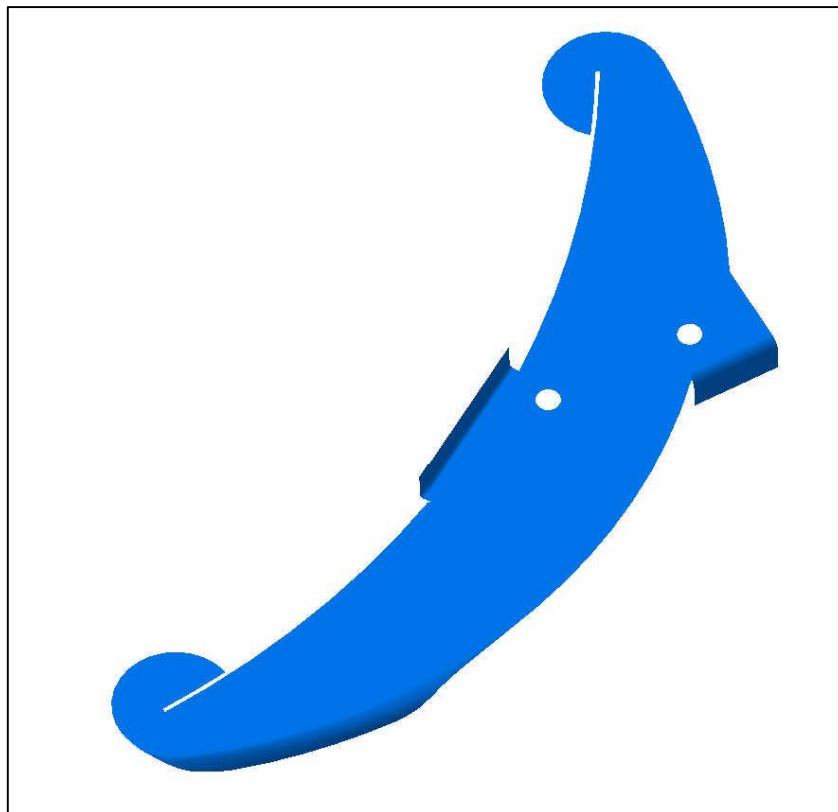


Figure 3-21. Final obtained surfaces of Sail Rib.

Thus all the components were ready to perform assembly operations using the Assembly Design in CATIA and test their ability to assemble them before starting the prototype manufacture phase. The final solid 3D model of the Rotor assembly is executed in this thesis. Various engineering applications such as structural analysis and airflow can be performed using one of the CAE software or CAM software to manufacture the dies of the parts or the prototypes.

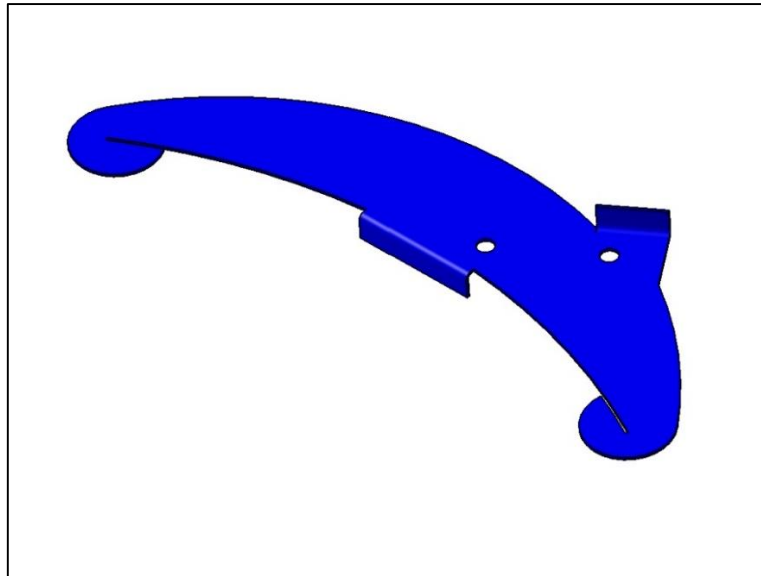


Figure 3-22. The Sail Rib solid 3D model using Part Design in CATIA.

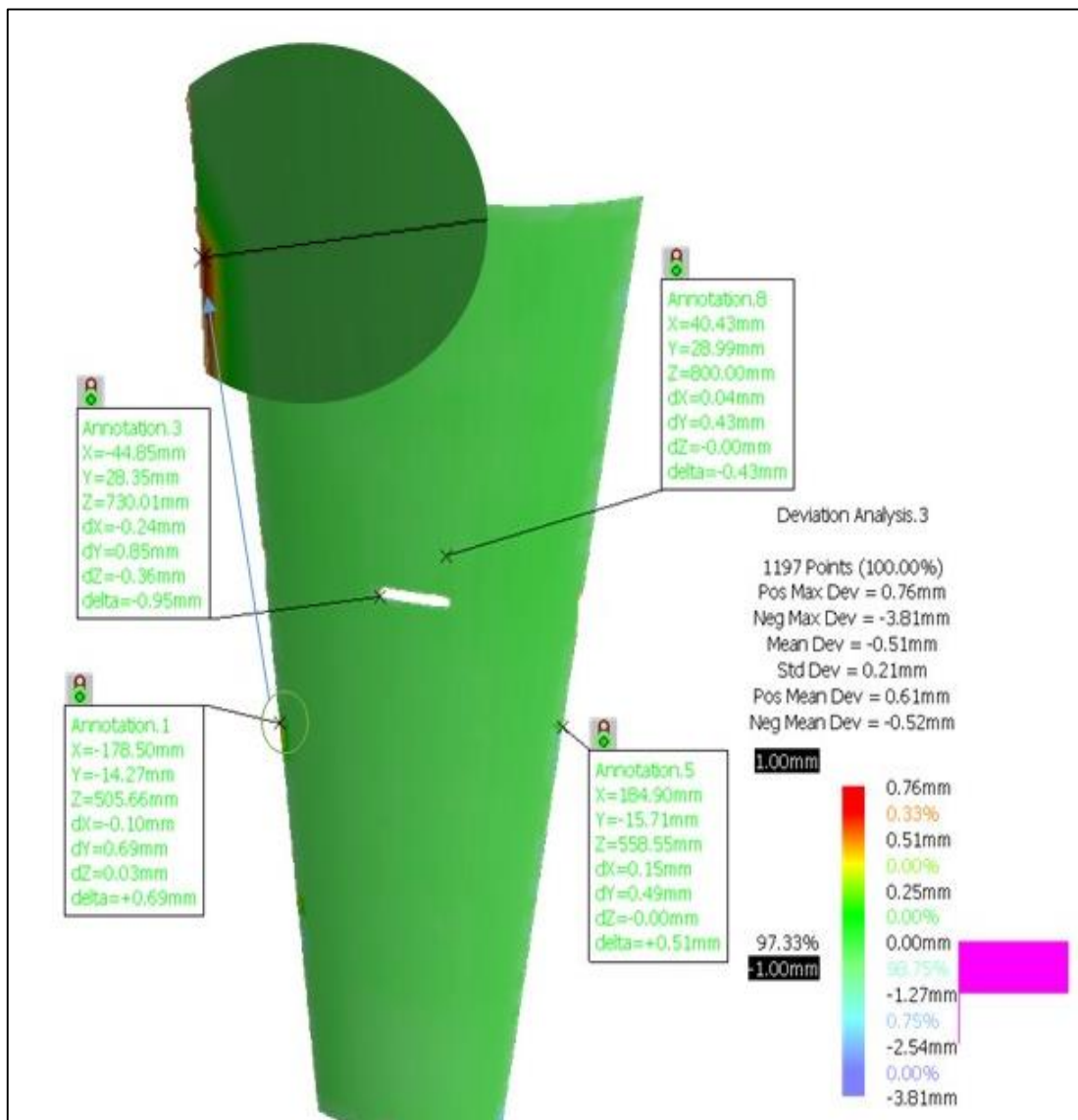


Figure 3-23. Annotation set added on Deviation Result Distribution of the Sail.

3.12 Deviation Analysis Results

The Deviation Analysis command in DSE of CATIA was used to perform the deviation analysis of all CAD models for the Rotor components by comparing the point cloud data (gathered from scanning the part) with the final CAD model.

After performing the deviation analysis, more may be needed to highlight some peculiar places and add comments. So with Annotation Set and Annotation commands in CATIA, annotations in a deviation analysis can be created and organized into annotation sets, as shown in Figure 3-23. The finished part model is compared to the original scan data in CATIA software that gives a detailed 3D Deviation Report (html file). It gives indications of the maximum and minimum values of the accepted tolerance, maximum and minimum values of deviation, various annotations, some colored maps for graphically visualizing these data, user-defined views, and multiple snapshots shown in Figure 3-24.

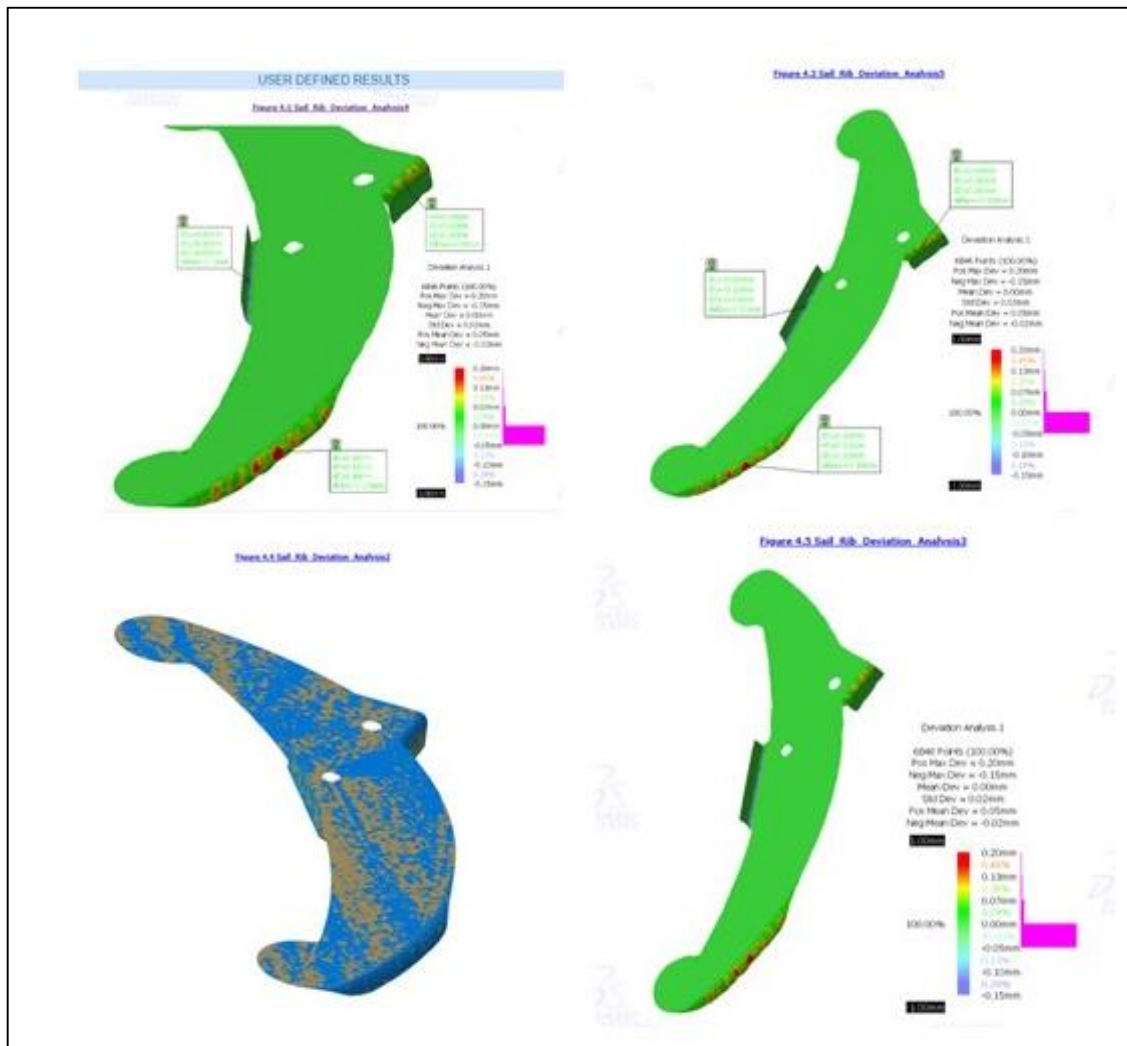


Figure 3-24. Various snapshots of the Sail Rib according to the CATIA report.

While obtaining a solid model, one may face many problems if any gap is left between the surfaces or if it is not adequately trimmed.

The deviation analysis examined all CAD models of the Rotor components. All Rotor components' scanned and CAD files were imported into the DSE CATIA software. The CAD model of the components was set as a reference, and the scan data of them as "Data to Measure". The detailed results are discussed in the following subsections:

3.12.1 Sail deviation analysis

A total of 1197 data points were tested for a 3D Deviation check. The parameters for the test are described in Table 3-5.

Table 3-5. Input Parameters of the Sail Deviation Analysis.

Reference Data	Surface.1
Data To Measure	Mesh Creation.1
Accuracy	0.010
Only Orthogonal	0
Absolute	0

The design extracted is good because around 97.33% of the points lie in the tolerance range of +/- 1mm, with a mean deviation of -0.51mm, and a standard deviation of 0.21mm. Table 3-6 gives detailed deviation distribution of the data points.

Table 3-6. Statistical Results of the Sail Deviation Analysis.

Total Number of Selected Points	1197
Number of Points Used in Computation	1197
Number of Points with Positive Deviation	5
Number of Points with Negative Deviation	1192
Positive Maximum Deviation Value	0.76mm
Negative Maximum Deviation Value	-3.81mm
Mean Deviation	-0.51mm
Standard Deviation	0.21mm
Positive Mean Deviation	0.61mm
Negative Mean Deviation	-0.52mm
Positive Tolerance	1.00mm
Negative Tolerance	-1.00mm
Percentage In Tolerance	97.33

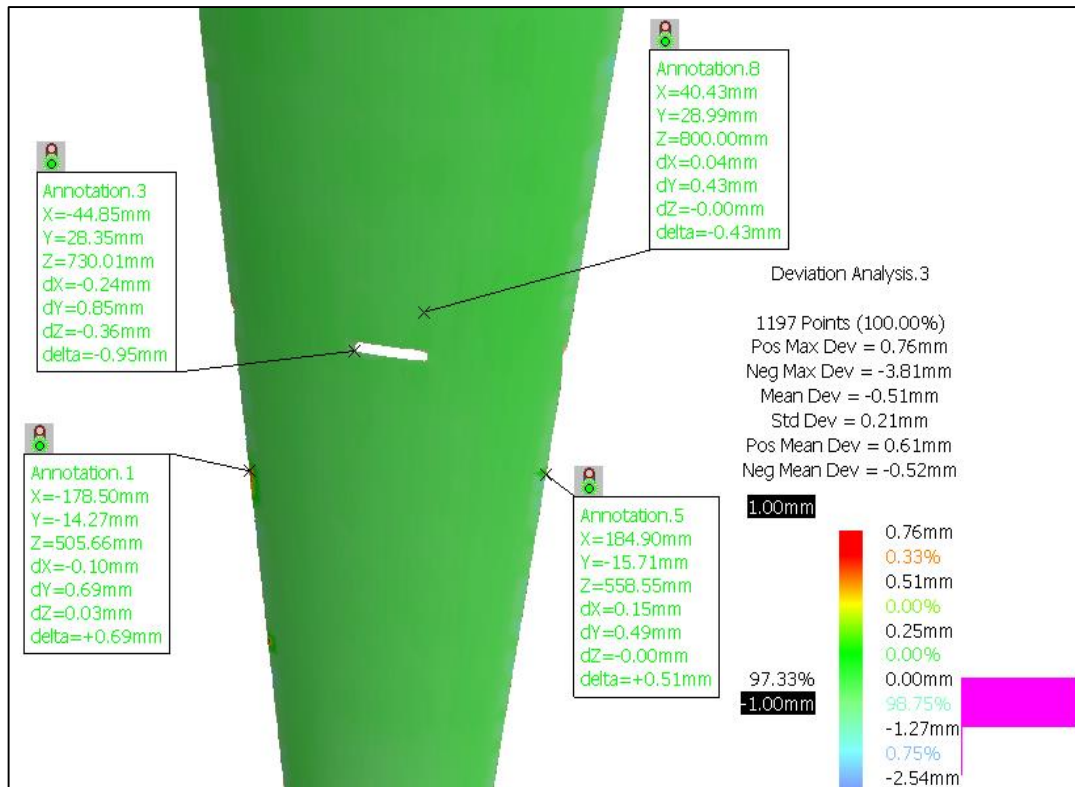


Figure 3-25. A snapshot of Sail Deviation Analysis.

Figure 3-25 shows a graphical colored map to visualize the deviation analysis data and various annotations of the Sail. These results are the best after several checks and modifications of the Sail model.

In general, it is possible for another user to obtain better or less accurate results, as modification and fitting of surfaces using CATIA software depend on the user's skills. The complete inspection reports of the Sail and the Sail tie directly produced in CATIA software are presented in Appendixes (1) and (2), respectively.

3.12.2 Sail Tie deviation analysis

A total of 3704 data points were tested for a 3D Deviation check. The parameters for the test are shown in Table 3-7.

Table 3-7. Input Parameters of the Sail Tie Deviation Analysis.

Reference Data	Surface.1
Data To Measure	Mesh Creation.1
Accuracy	0.010
Only Orthogonal	0
Absolute	0

Table 3-8. Statistical Results of the Sail Tie Deviation Analysis.

Total Number of Selected Points	3704
Number of Points Used in Computation	3704
Number of Points with Positive Deviation	614
Number of Points with Negative Deviation	397
Positive Maximum Deviation Value	0.15mm
Negative Maximum Deviation Value	-0.12mm
Mean Deviation	0.01mm
Standard Deviation	0.03mm
Positive Mean Deviation	0.05mm
Negative Mean Deviation	-0.02mm
Positive Tolerance	1.00mm
Negative Tolerance	-1.00mm
Percentage In Tolerance	100.00

As around 100% of the points lie in the tolerance range of +/- 1mm, with a mean deviation of 0.01mm, and a standard deviation of 0.03mm, the design extracted is good. Table 3-8 gives detailed deviation distribution of the data points.

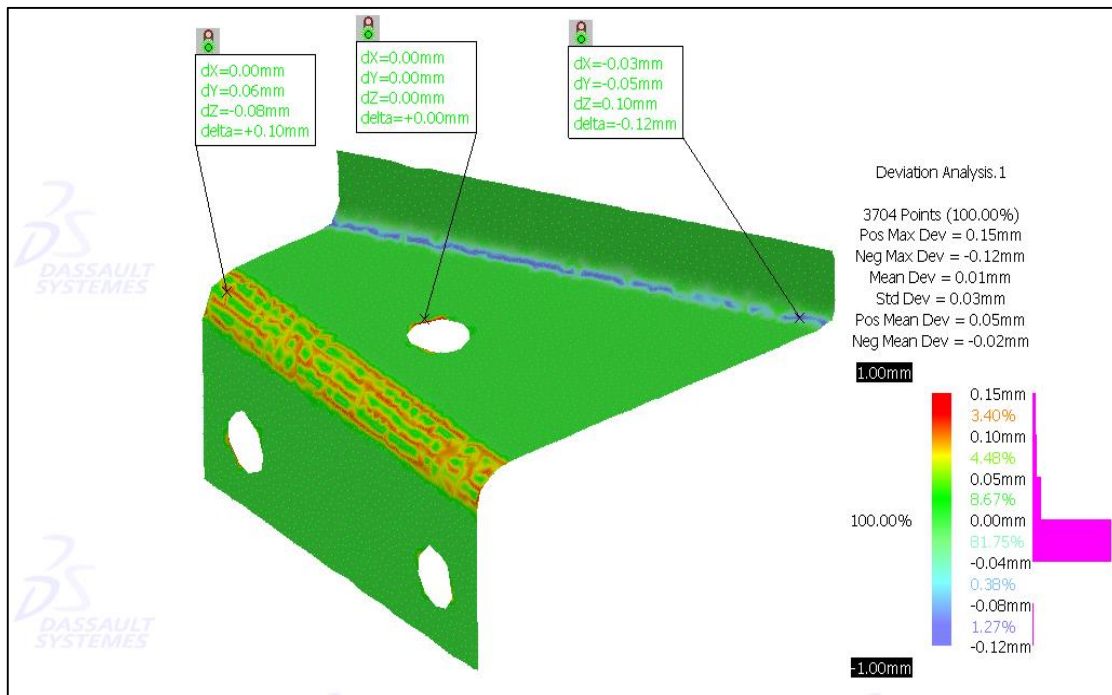


Figure 3-26. A snapshot of Sail Tie Deviation Analysis.

Figure 3-26 shows a graphical colored map to visualize the deviation analysis data and various annotations of the Sail Tie. In addition, this figure shows the histogram of the data

distribution where 81.75% of the deviation points data of the CAD surface from the original point cloud data lies between 0 and -0.04mm.

3.12.3 Sail Rib deviation analysis

A total of 6846 data points were tested for a 3D Deviation check. The parameters for the test are as shown in Table 3-9.

Table 3-9. Input Parameters of Sail Rib Deviation Analysis.

Reference Data	Surface.1
Data To Measure	Mesh Creation.1
Accuracy	0.010
Only Orthogonal	0
Absolute	0

The design extracted is good because around 100% of the points lie in the tolerance range of +/- 1mm, with a mean Deviation of 0.00mm, and a standard deviation of 0.02mm.

Table 3-10 gives detailed deviation distribution of the data points.

Table 3-10. Statistical Results of the Sail Rib Deviation Analysis.

Total Number of Selected Points	6846
Number of Points Used in Computation	6846
Number of Points with Positive Deviation	555
Number of Points with Negative Deviation	209
Positive Maximum Deviation Value	0.20mm
Negative Maximum Deviation Value	-0.15mm
Mean Deviation	0.00mm
Standard Deviation	0.02mm
Positive Mean Deviation	0.05mm
Negative Mean Deviation	-0.02mm
Positive Tolerance	1.00mm
Negative Tolerance	-1.00mm
Percentage In Tolerance	100.00

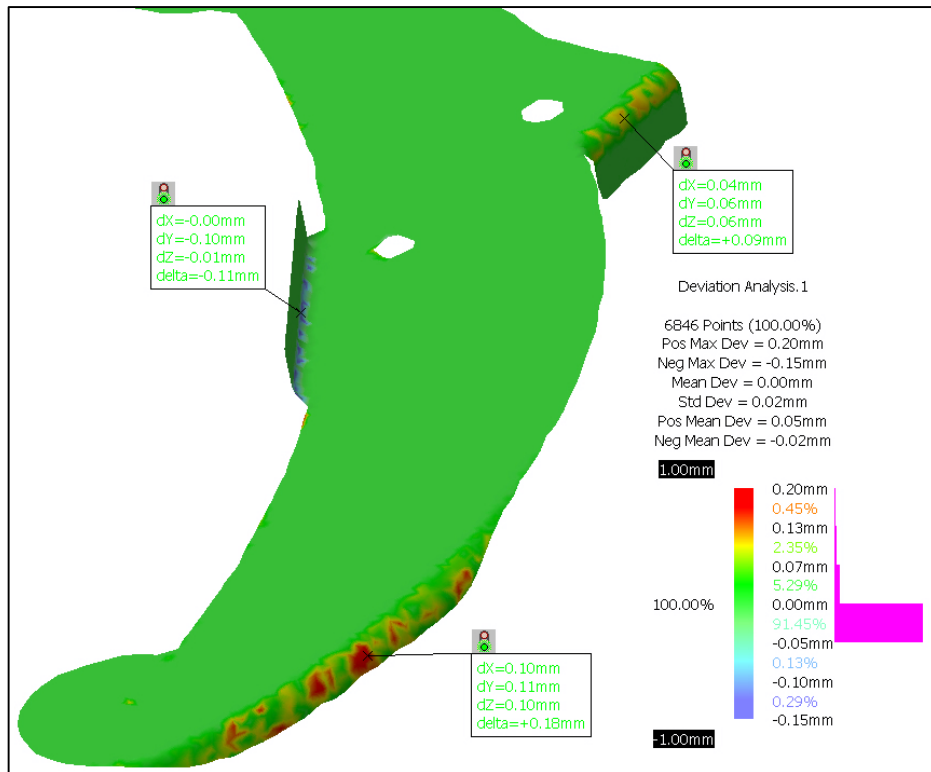


Figure 3-27. A snapshot of Sail Rib Deviation Analysis.

Figure 3-27 shows a graphical colored map to visualize the Deviation Analysis data and various annotations of the Sail Rib. In addition, this figure shows the histogram of the data distribution where 91.45% of the deviation points data of the CAD surface from the original point cloud data lies between 0 and -0.05mm.

3.12.4 Rotor Arm deviation analysis

A total of 15973 data points were tested for a 3D Deviation check. The parameters for the test are as shown in Table 3-11.

Table 3-11. Input Parameters of the Rotor Arm Deviation Analysis.

Reference Data	Surface.1
Data To Measure	Mesh Creation.1
Accuracy	0.010
Only Orthogonal	0
Absolute	0

The design extracted is good because around 100% of the points lie in the tolerance range of +/- 1mm, with a mean deviation of 0.07mm, and a standard deviation of 0.06mm. Table 3-12 gives detailed deviation distribution of the data points.

Table 3-12. Statistical Results of the Rotor Arm Deviation analysis.

Total Number of Selected Points	15973
Number of Points Used in Computation	15973
Number of Points with Positive Deviation	12888
Number of Points with Negative Deviation	593
Positive Maximum Deviation Value	0.19mm
Negative Maximum Deviation Value	-0.16mm
Mean Deviation	0.07mm
Standard Deviation	0.06mm
Positive Mean Deviation	0.09mm
Negative Mean Deviation	-0.00mm
Positive Tolerance	1.00mm
Negative Tolerance	-1.00mm
Percentage In Tolerance	100.00

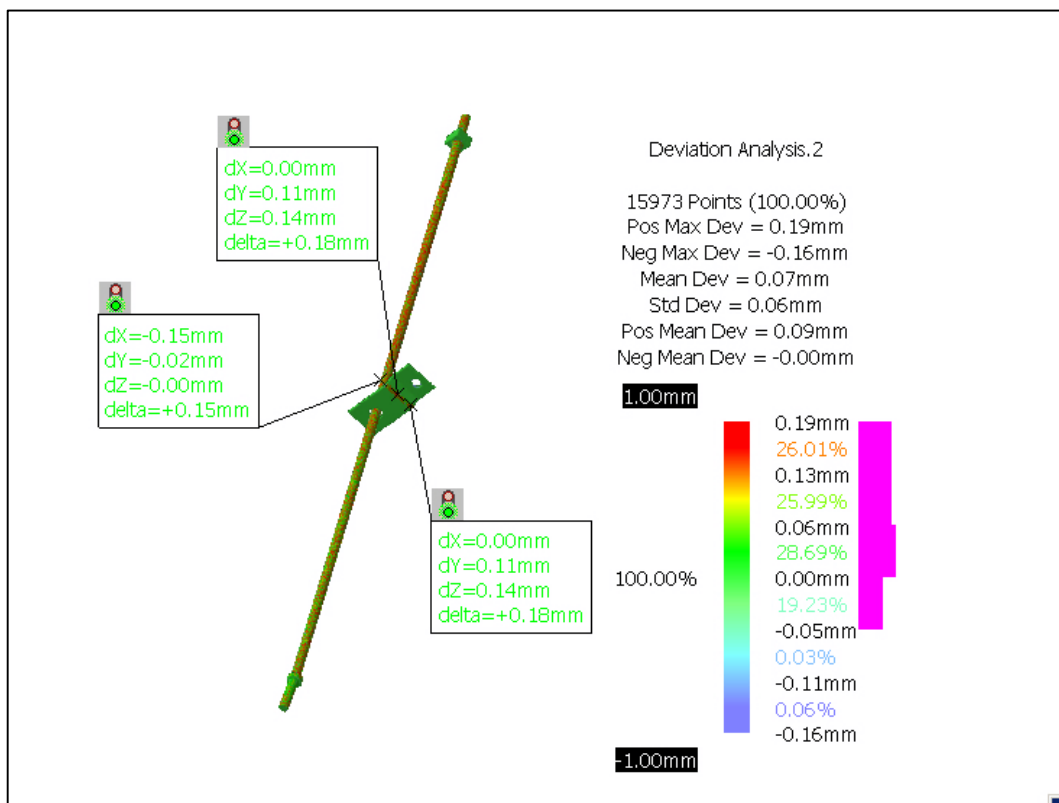


Figure 3-28. A snapshot of Rotor Arm Deviation Analysis.

Figure 3-28 shows a graphical colored map to visualize the deviation analysis data and various annotations of the complete Rotor arm. In addition, the histogram shape of the

deviation points data of the CAD surface from the original point cloud data indicates that it is very consistent.

3.12.5 Outer and Inner Rotor Bands deviation analysis

A total of 15973 data points were tested for a 3D Deviation check.

The test evidence that around 100% of the points lie in the tolerance range of +/- 1mm, with a mean deviation of -0.11mm, and a standard deviation of 0.06mm.

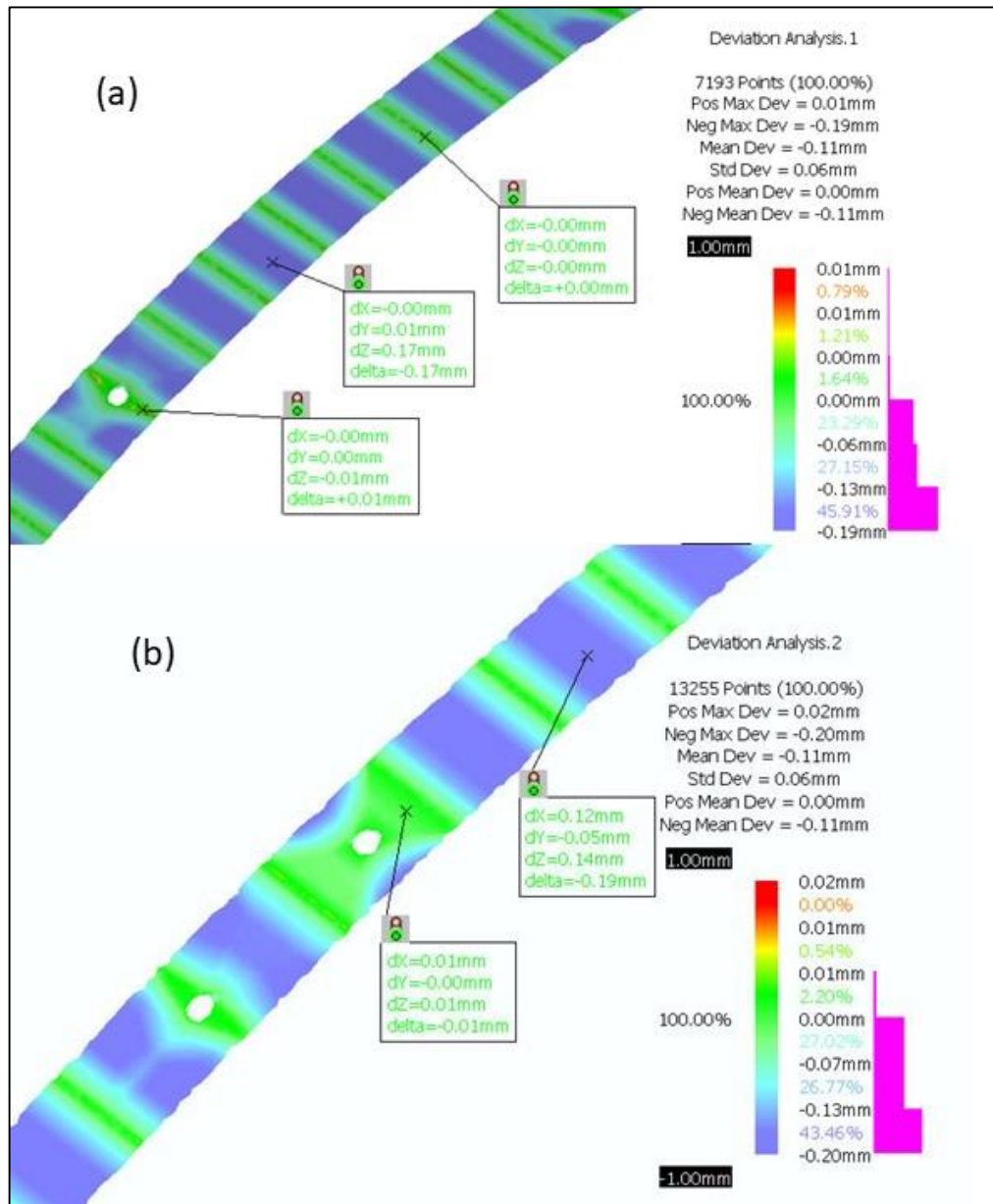


Figure 3-29. Inner and Outer Bands Deviation Analysis maps.

Regarding the Inner Band deviation analysis, the test of 7193 data points evidence that around 100% of the points lie in the tolerance range of +/- 1mm, with a mean Deviation of -0.11mm, and a standard deviation of 0.06mm. The Outer and Inner Bands design is good

and can be adopted. Figure 3-29 shows a graphical colored map to visualize the deviation Analysis data and various annotations of (a) the Inner Band and (b) the Outer Band. This figure shows the histogram of the data distribution where around 96% of the deviation points data of the CAD surface generated fall between 0 and -0.20mm.

3.12.6 Two-Dimensional manufacturing drawings

After adopting 3D models of the Rotor components as a result of the deviation mentioned in the earlier analysis, the two-dimensional manufacturing drawings in such a case are among the most important outputs obtained from applying the RE for the Rotor components.

By using these drawings, many documents are prepared for the production stage, such as the work plan, the bill of materials, and the quality inspection documents.

All drawings and documents were developed and modified upon the manufacture of the prototype and during the beginning of the pre-serial production. Figure 3-30 represents the complete Rotor 2d drawing.

3.12.7 Rotor components 3D CAD models

The final output of the digitization phase of the components in this thesis is a geometric model of the Rotor parts in CATMODEL or one of the proprietary formats such as IGES, VDA, STL, OBJ, VRML, etc. After creating manufacturing drawings, the generated 3D models were used as the basis for various engineering analyses. This can be done by using computer-aided engineering (CAE) software such as ANSYS for structural or airflow analysis, industrial applications using CAM available in CATIA for making prototypes, or manufacturing dies using NC machines or rapid prototyping technology.

Subsequently, a 3D-CAD assembly model of the Rotor components, as shown in Figure 3-31, was prepared based on the existing physical water pumping windmill. However, to validate this 3D-CAD assembly model, verification for fouling, interference in overall dimensions, etc., was carried out before the prototype was made.

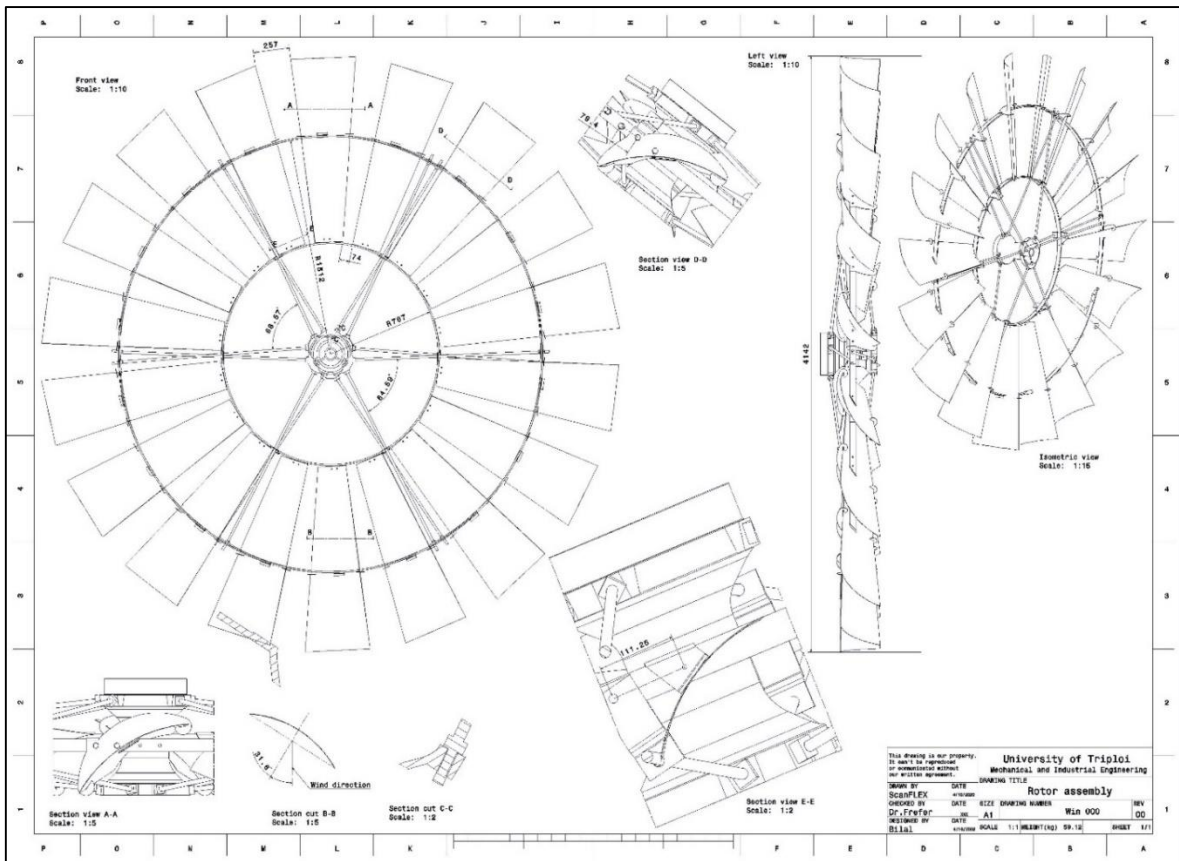


Figure 3-30. The complete Rotor 2d drawing.

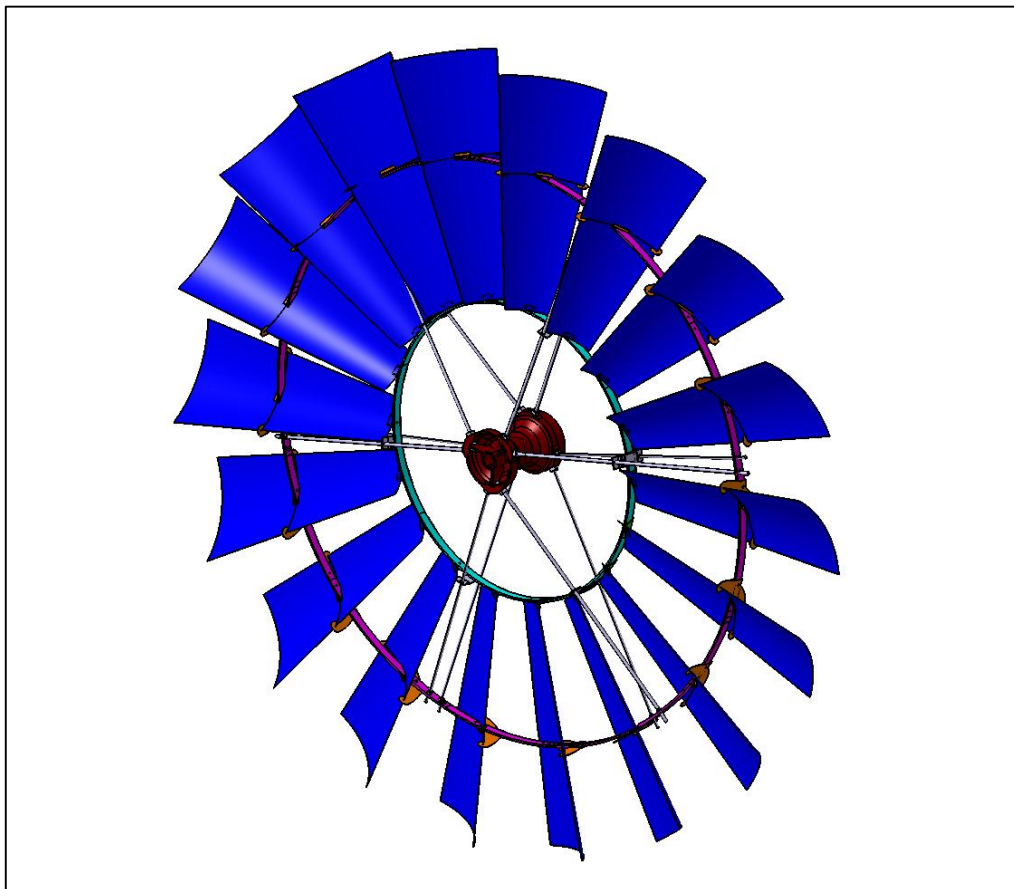


Figure 3-31. 3D-CAD assembly model of the windmill Rotor.

3.13 Die Design and Manufacturing

This thesis has used various modules CAD/CAM integrated into CATIA for the design and development of the die and the simulation of its operation through 3D graphic models and carefully followed the CNC machine's programming.

3.13.1 The Sail die design

After the 3D CAD of the Sail was approved, it was used to design, simulate the machining process, and program the specific CNC milling machine to manufacture the die for curving the Sails as the end application of the RE process. The flow diagram shown in Figure 3-32 demonstrates that the generated 3D CAD model is obtained from the RE process and used to design the Sail's die within this thesis.

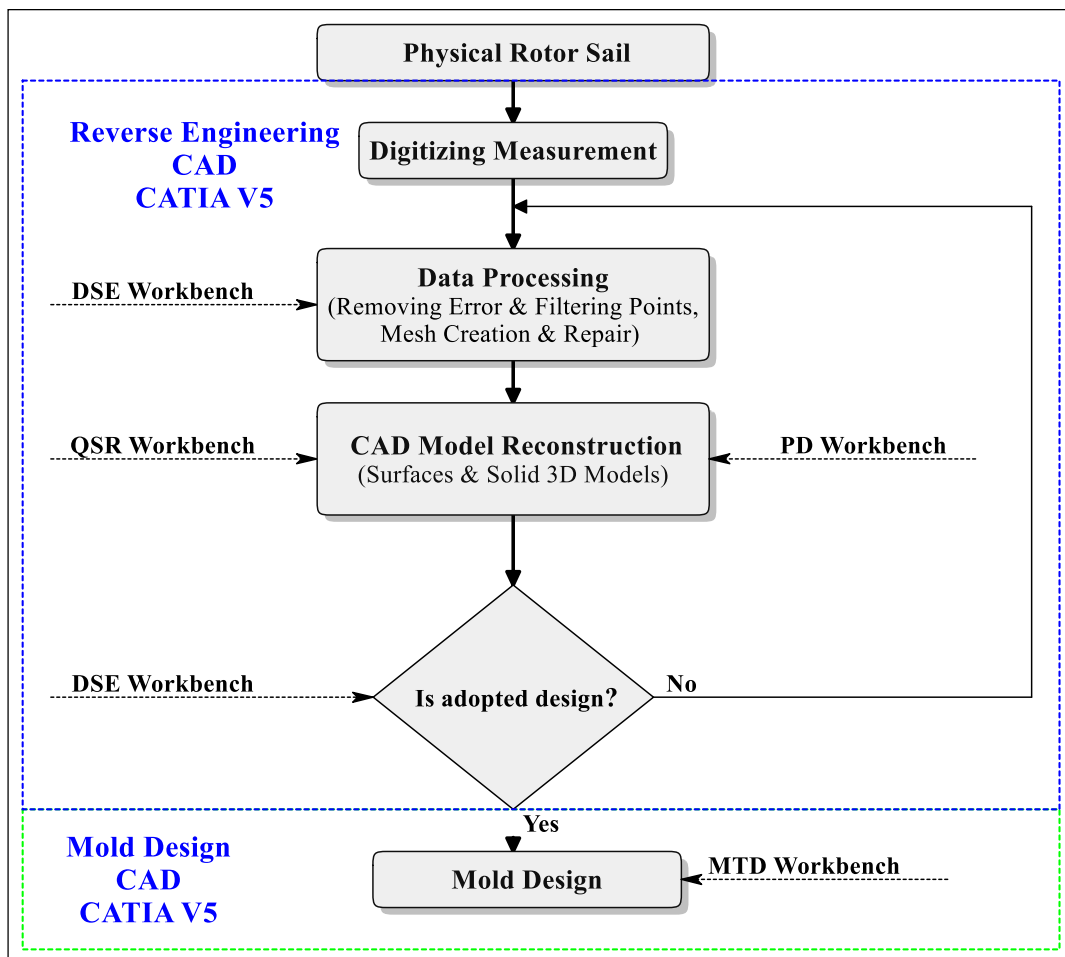


Figure 3-32. Flow diagram for designing and manufacturing Sail's curving die.

The design and development of compound die are essential phases in sheet metalworking. The minor error in the design can result in heavy manufacturing losses through die failure, part geometry distortion, and production risk [102]. When designing a die, different factors must always be taken into consideration. The choice of possible solutions to problems related

to the production of a part must be made, taking into consideration the characteristics of that part (e.g., shape, size, material), the characteristics (features) of the machines available (stroke, size, load, etc.), and the number of pieces to be manufactured [103]. Medium and large production quantities require the use of dies, while for small production, one must decide whether it is convenient to design and make the die based on the number produced. In this case, the expected production quantity is small. Nevertheless, the decision was taken according to an economic and technical point of view to design and manufacture a single-operation die, as shown in Figure 3-33 (a) for curving the Sails, instead of manufacturing a typical die system that can perform simultaneously different types of processes, such as blanking and bending to produce the Sails as shown in Figure 3-33 (b). This decision was also due to the difficulty of manually manufacturing curved Sails based on available labor, the number of Sails used to produce one unit of the windmill, and the importance of the Sails in improving the efficiency of the windmill.

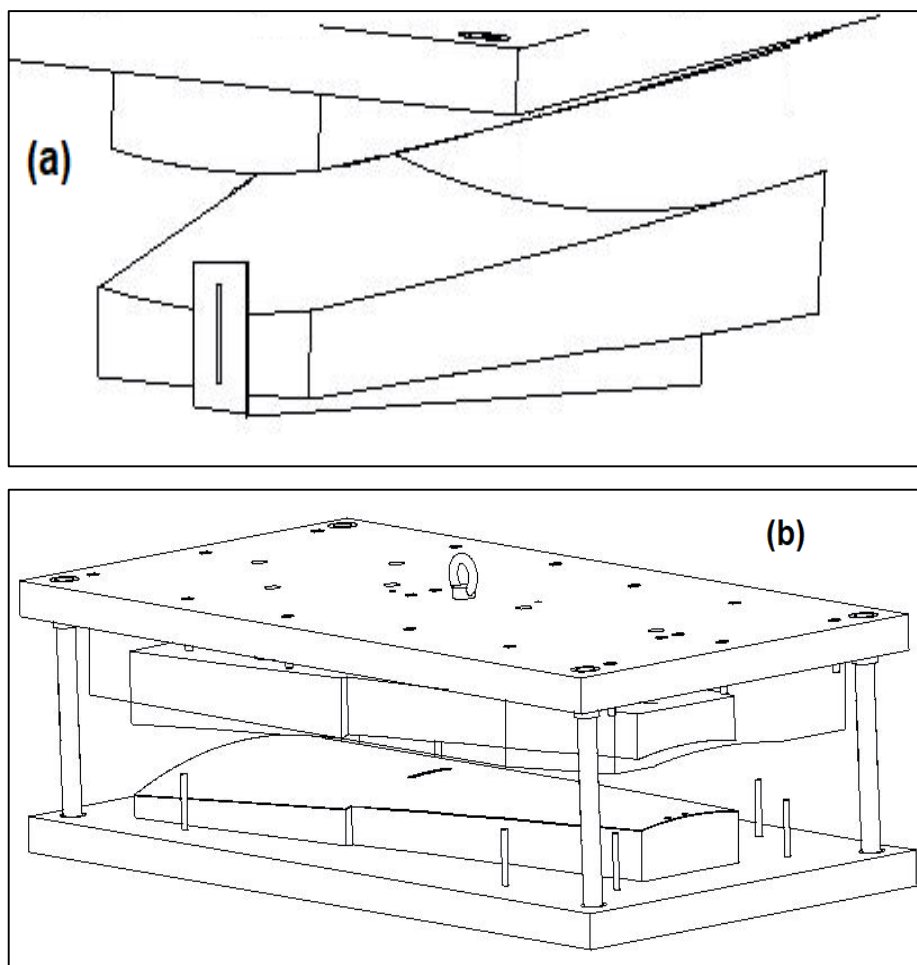


Figure 3-33. (a) A single-operation die; (b) A typical die system.

Before implementing the die design, once the operating cycle was established, it is essential to determine the development (unfolded) of the sheet metal piece to understand how much material was needed to make it. This development was determined as shown in Figure 3-34, and the sheet metal piece was manufactured using a laser cutting machine.

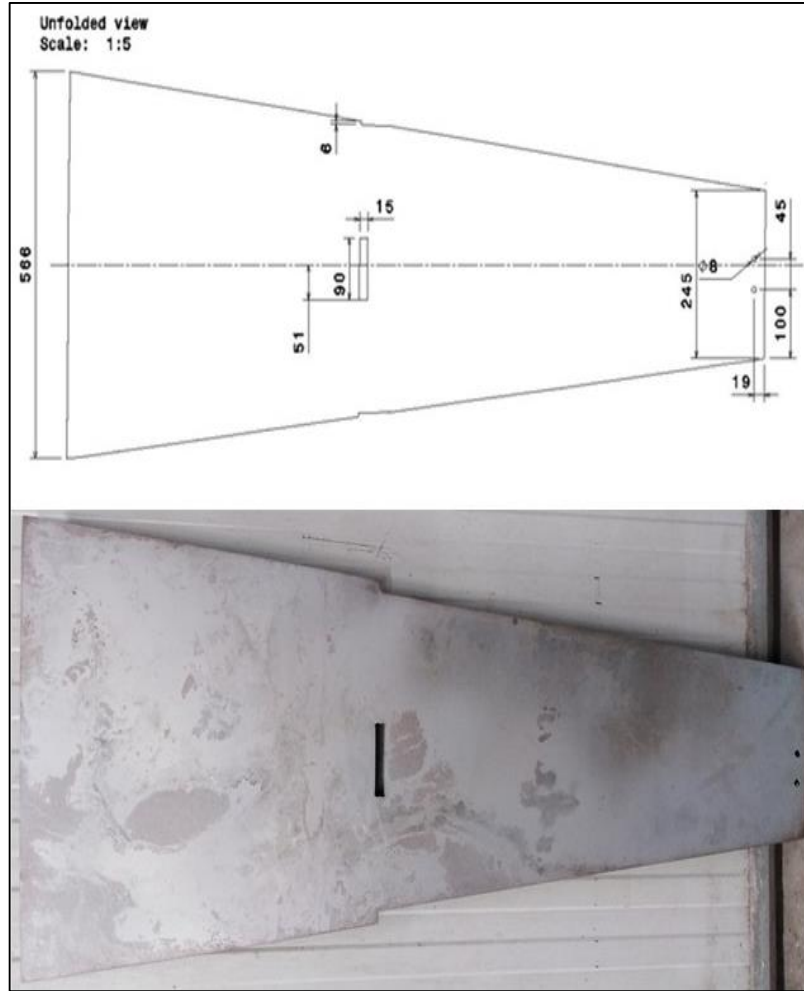


Figure 3-34. The Sail's sheet metal blank.

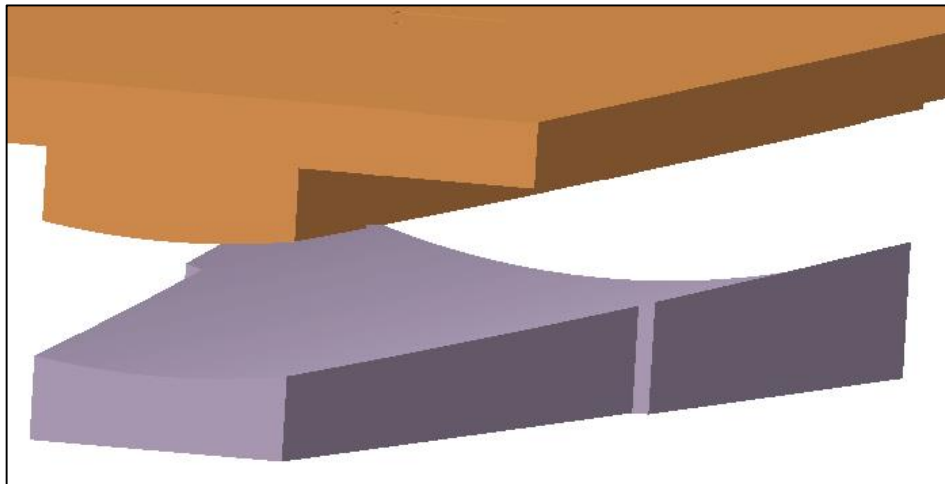


Figure 3-35. The 3D model of the Sails curving die.

The design was executed using the CATIA Mold Tooling Design (MTD), as shown in Figure 3-35, and the die is designed with four parts to suit the capacity of the CNC machine operating table.

3.13.2 The die manufacturing

CAM is a transition point from thinking like a designer to thinking like a manufacturer by applying parameters within the process that include values such as depth of cut and tool overlap. As the end goal of CNC machining, high efficiency and precision milling needs to balance many constraints for selecting the most reasonable processing parameters [104]. CATIA creates the operations and tool paths needed to mill the geometry of the Sail's die. Figure 3-36 displays the workflow diagram, starting with a 3D model of the Sail's die that was designed and approved, then the CAM processes, simulation, and manufacturing of the die parts on the CNC machine until the die testing and the beginning of the production stage.

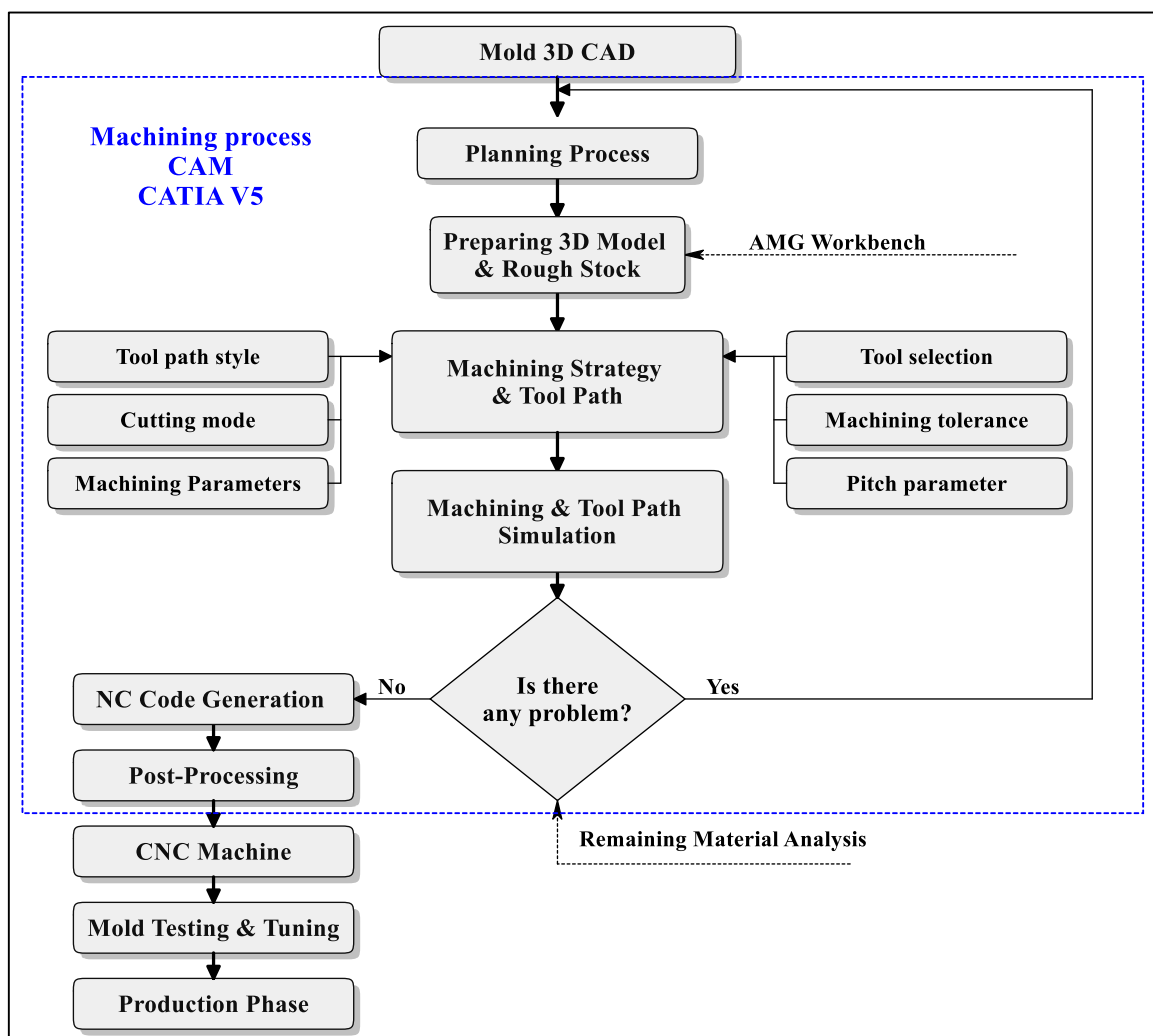


Figure 3-36. The CAM process workflow diagram.

3.13.2.1 Preparing the 3D model & rough stock.

The 3D CAD models of the two parts of the lower die with Stock dimensions of (635mmx370mmx110mm) and (465mmx498mmx110mm) were prepared within the CATIA assembly design workbench as CATproduct file.

In the same way, the two parts of the upper die with Stock dimensions of (635mmx370mmx90mm) and (465mmx498mmx90mm) were prepared as CATproduct file. After that, the CATproduct files were transferred for both the lower and upper parts to the machine mode of CATIA advanced machining workbench to generate the CATprocess files. The CATprocess file screenshot for the lower part of the die in Figure 3-37 shows the dialog box and the working tree, including the Product List (lower die Parts and Stocks) and the Process List at the top of the work tree where the production process was created. Then the workpiece coordinate system and the post-processor type of the machine are identified to generate NC code.

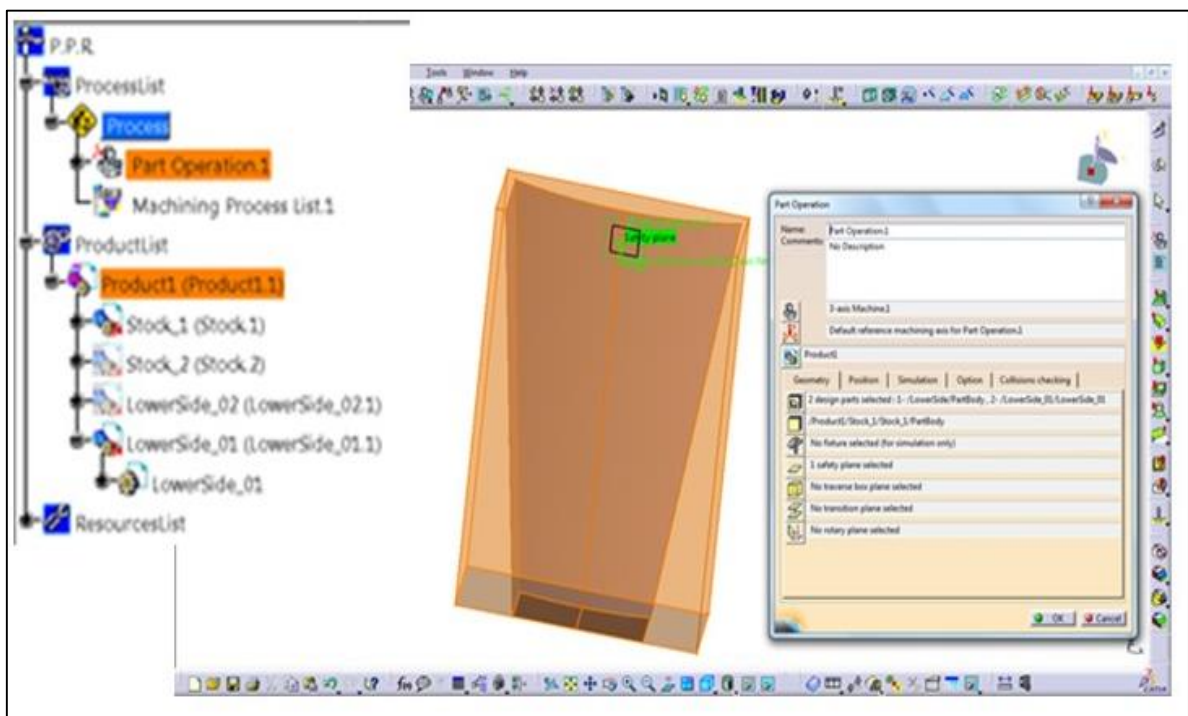


Figure 3-37. Preparing of 3D model & rough Stock.

3.13.2.2 Machining strategy

A machining strategy is a methodology used to compute an operation to carry out a geometrical entity in its final form [105,106,107]. It is vital to adopt a reasonable machining strategy and choose accurate parameters considering both the machining efficiency and quality [108,109]. Some of the CAM strategies described are used to create all parts of the

Sail's die through CATIA. The manufacturing operations strategies for the lower part of the die are displayed sequentially in the following Figures:

Figure 3-38: The first operation is to achieve external contour using Z level in AMG workbench, Z-level contouring tool path, with a flat end mill tool of diameter 20mm, the machining tolerance parameter 0.1mm, the cutting mode set to the upward mode (Climb in CATIA) because it facilitates the cutting conditions, and the constant stepover distance of 7mm. Other settings need to be set for CATIA software, also called machining parameters which are applied for the software as follows (for Mild Steel workpiece):

spindle speed (n) = 1200rev/min; feed motion (f) = 600mm/min; Offset on part = 0.0mm.

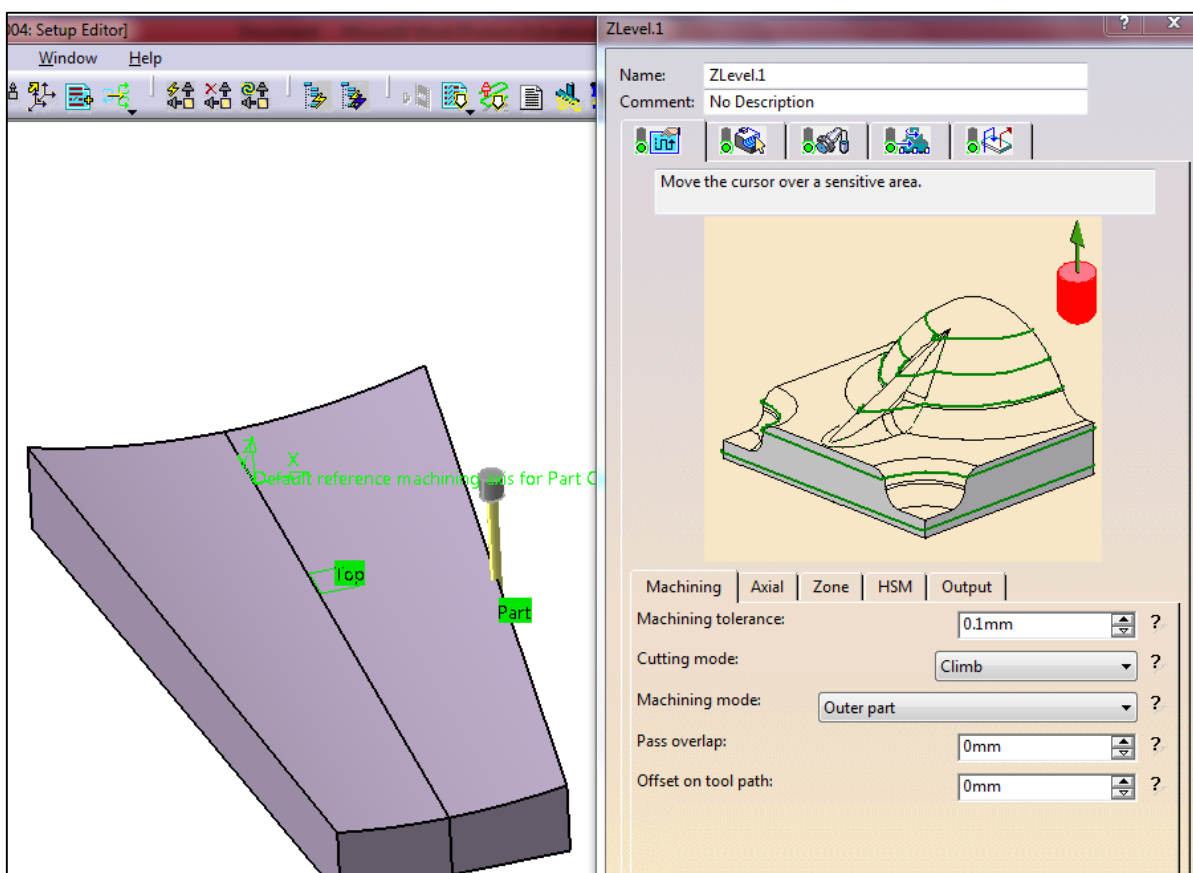


Figure 3-38. "Z-level" milling strategy of lower Sail's die.

Figure 3-39: The roughing operation is performed to reach as close as possible to the desired rough shape with a high level of cutting material flow and tool path series as smooth as possible [110]. Without the tool change, the Zig Zag tool path style, the machining tolerance parameter 0.1mm, the cutting mode set to the upward mode, and the stepover length parameter of 7mm. The other machining parameters:

spindle speed (n) = 1000rev/min; feed motion (f) = 300mm/min; Offset on part = 0.5mm.

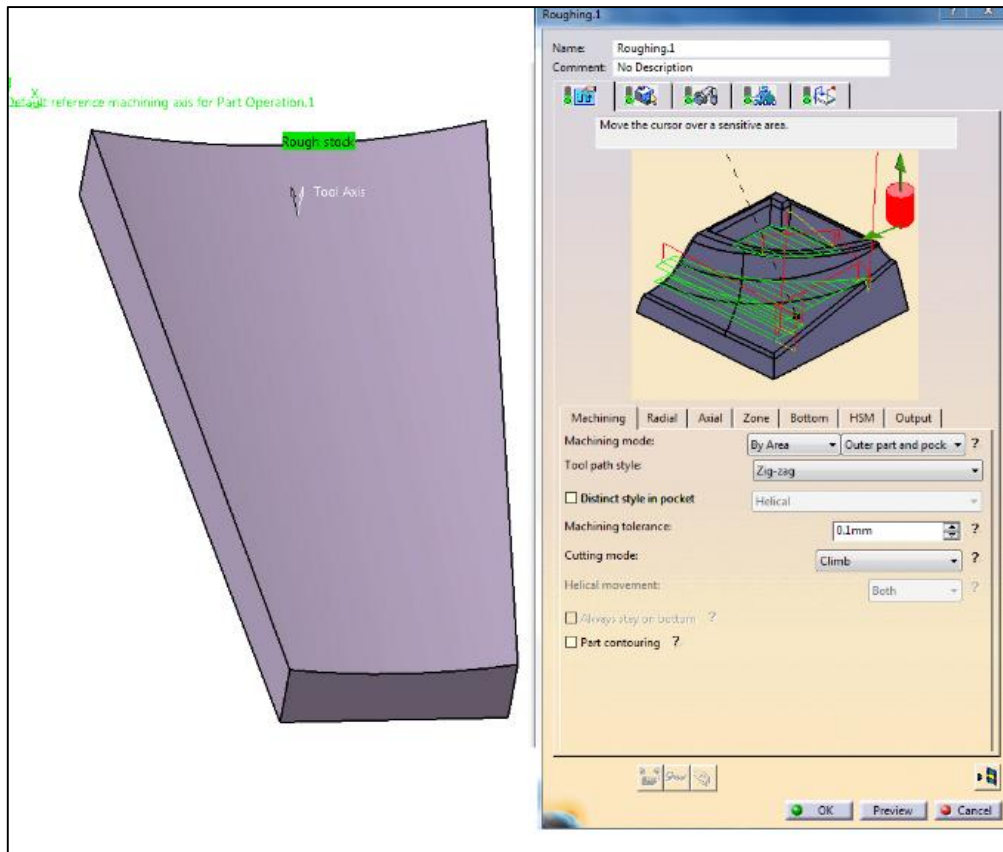


Figure 3-39. "Roughing" the milling strategy of lower Sail's die.

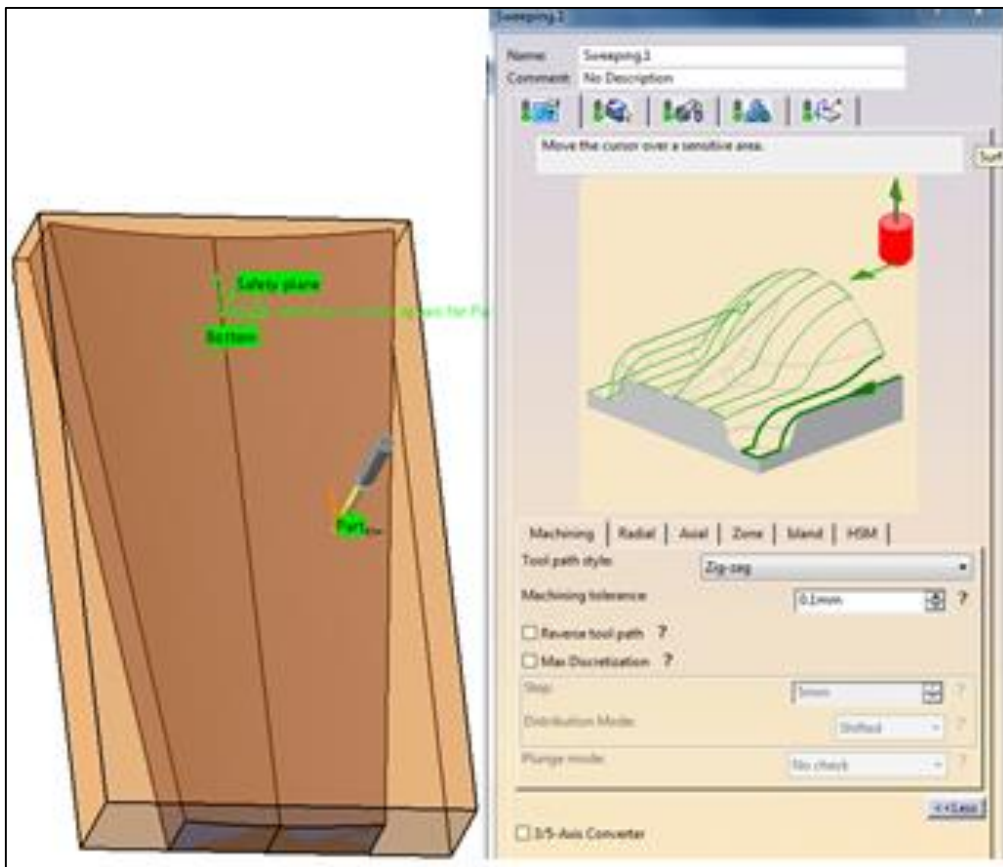


Figure 3-40. "Sweeping" milling strategy of lower Sail's die.

Figure 3-40: The Finishing operation using Sweeping Command achieves the final die shape up to the geometrical quality specified. It is done with a ball nose end mill of a diameter of 10mm, Zig Zag tool path, the machining tolerance parameter of 0.1mm, the cutting mode set to the upward mode, and the stepover length parameter of 4mm. The other machining parameters: spindle speed (n) = 1600rev/min; feed motion (f) = 300mm/min; Offset on part = 0.0mm. Table 3-13 summarizes the parameters of the CAM process of all the die parts. The generated code can be further edited on a computer or directly at the CNC machining center.

Table 3-13. Machining Parameters Applied in Preparing CAM Process of the Die Parts.

Parameter	Z-level	Roughing	Sweeping
Tool path style	Zig Zag	Zig Zag
Cutting mode	upward	upward	upward
Stepover	7	7	4
Machining tolerance	0.1 mm	0.1 mm	0.1 mm
Tool type	Flat End mill	Flat End mill	Ball Endmill
Tool diameter	20 mm	20 mm	10 mm
Offset on part	0	0.5 mm	0
Feed motion	600 mm/min	300 mm/min	300 mm/min
Spindle speed	1200 rev/min	1000 rev/min	1600 rev/min

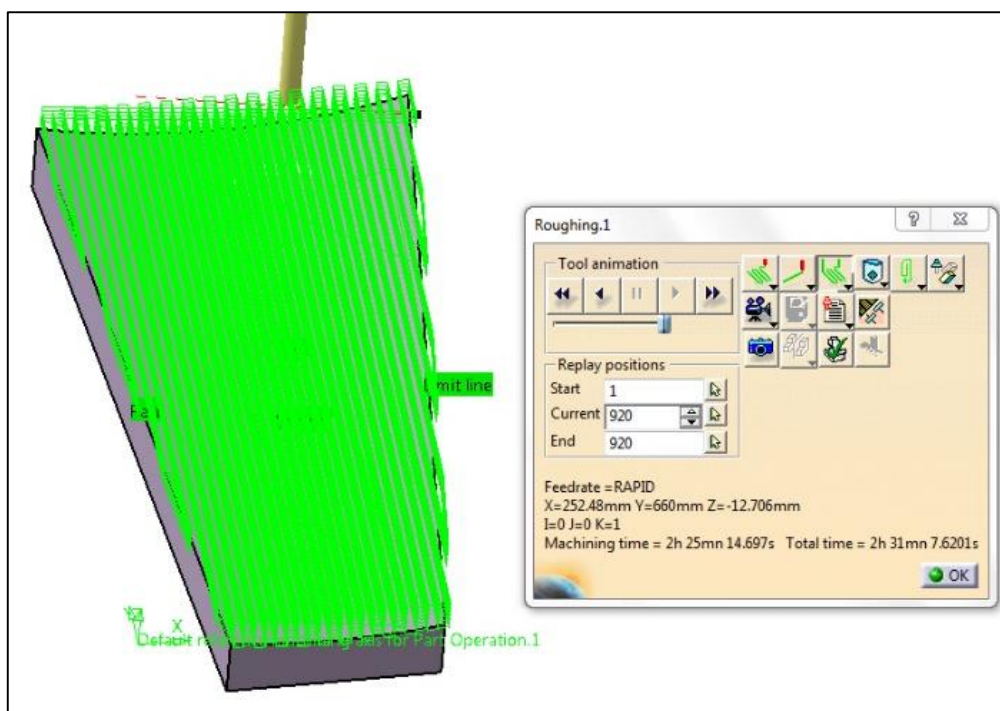


Figure 3-41. The tool path "Roughing" simulation.

3.13.2.3 Machining simulation

Once the CAM process is completed, and all the required parameters of the CATIA are set, the resulting tool path can be simulated. Figure 3-41 shows the tool path simulation of the roughing operation used to view the graphical representation of the path taken by the tool. The tool path simulation of the Z-level and the sweeping operation is shown in Figure 3-42 and Figure 3-43.

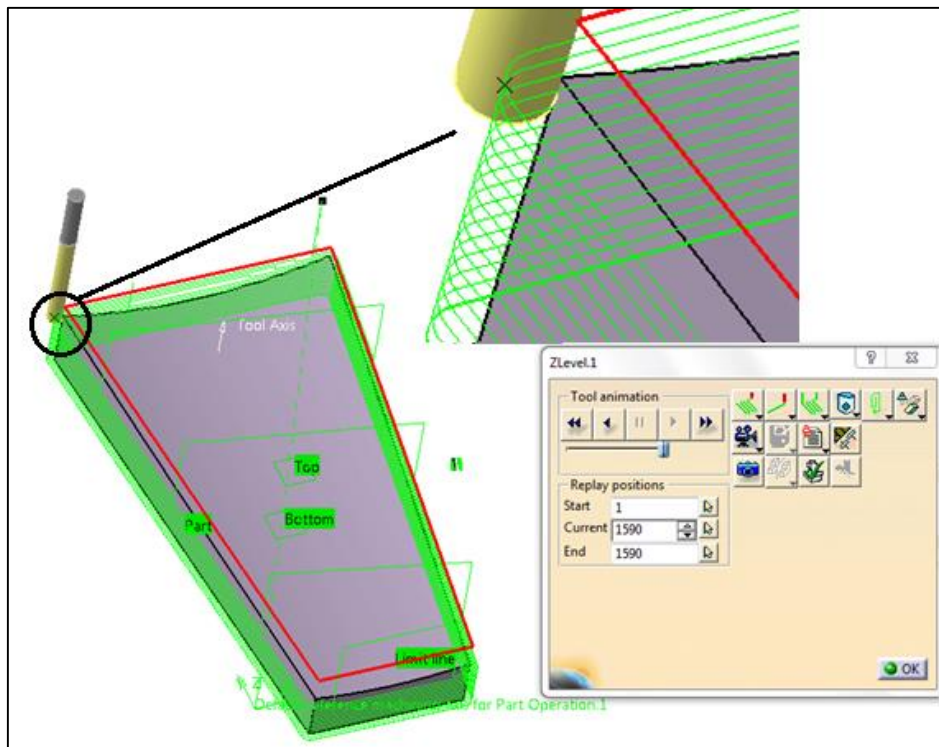


Figure 3-42. The tool path "Z-level" machining simulation.

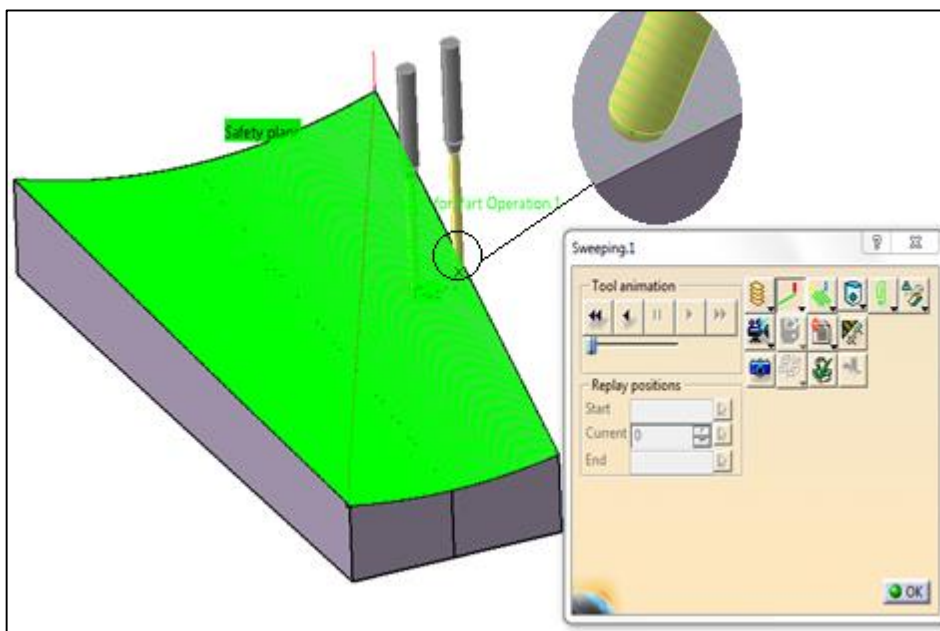


Figure 3-43. The tool path "Sweeping" machining simulation.

CATIA can also display a video simulating the three operations, as shown in Figure 3-44 and Figure 3-45. With this simulation, one can easily observe the movement of the tool and identify any inefficiency in the machine's operation. The previous settings are modified to obtain the best solution if any inefficiency is recorded.

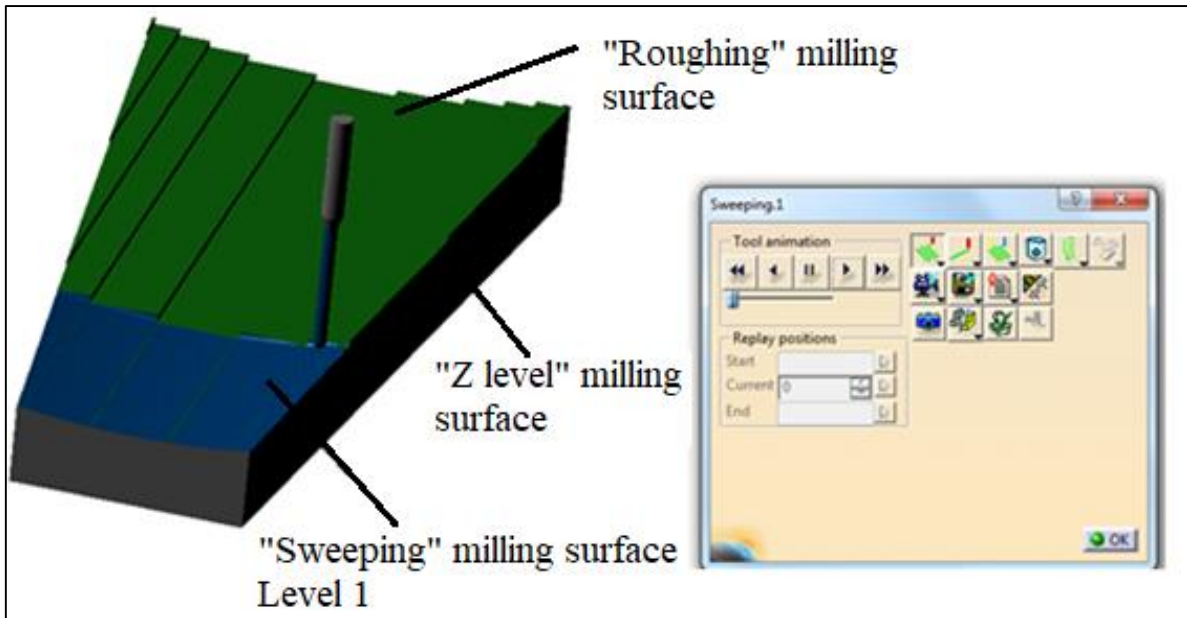


Figure 3-44. Screenshot during the "Sweeping" Level 1 in the video simulation.



Figure 3-45. Screenshot during the "Sweeping" Level 2 in the video simulation.

Figure 3-46 shows the remaining Material Analysis of the upper die available within the simulation, where the deviation was 0.1mm and acceptable for the design and manufacturing requirements of the Sail's die.

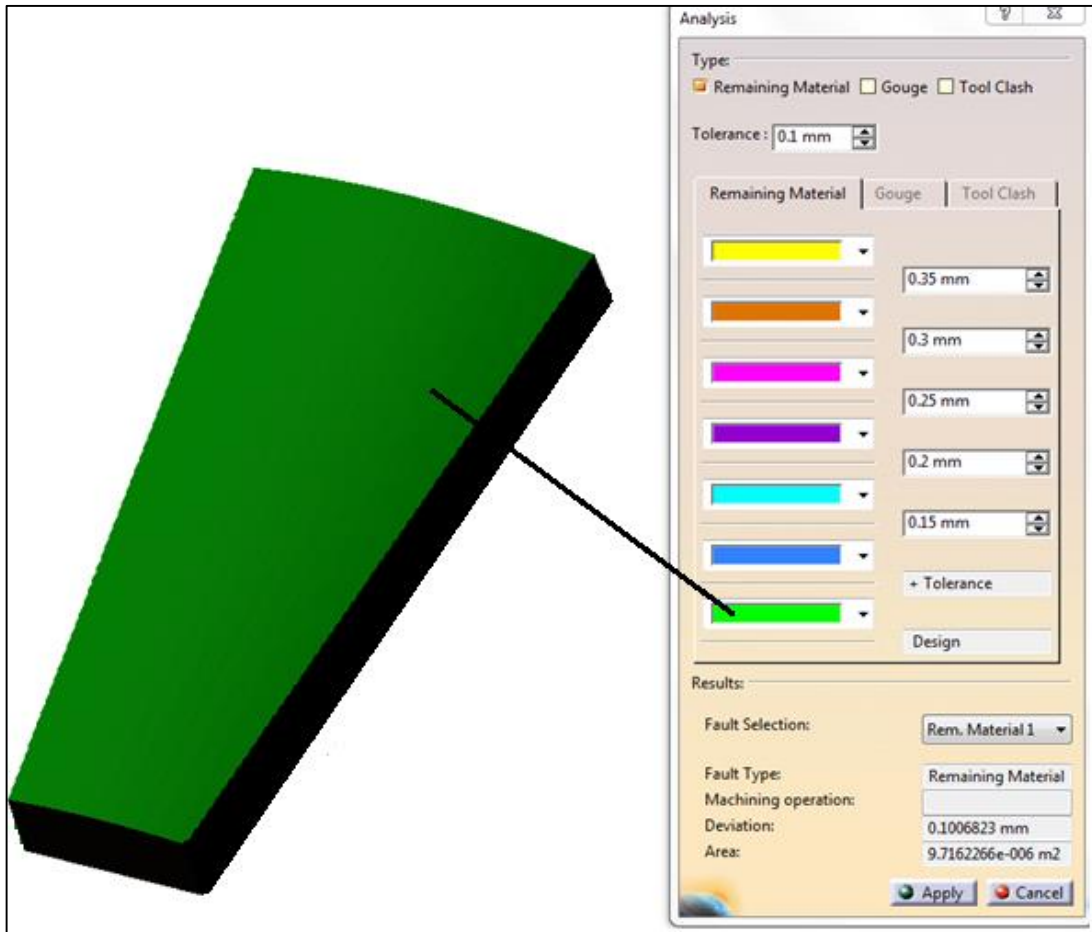


Figure 3-46. Machining analysis of upper part.

3.13.2.4 CNC machine code generation

After the success of the simulation process using Generating NC Code function in CATIA, the NC program for each part of the die in ISO format (G codes) is generated, followed by post-processing for the appropriate CNC machine and CNC control system. Using a memory card for transferring the NC programs to the 3-axis milling center control (FANUC OM model C).

3.13.2.5 Die parts CNC machining

Figure 3-47 shows the "Z" level" operation to realize contour during machining one of the lower Sail's die parts on the CNC machine. In contrast, Figure 3-48 shows the "Roughing" and the "Sweeping" as finishing operations.



Figure 3-47. "Z-level" operation of lower Sail die.

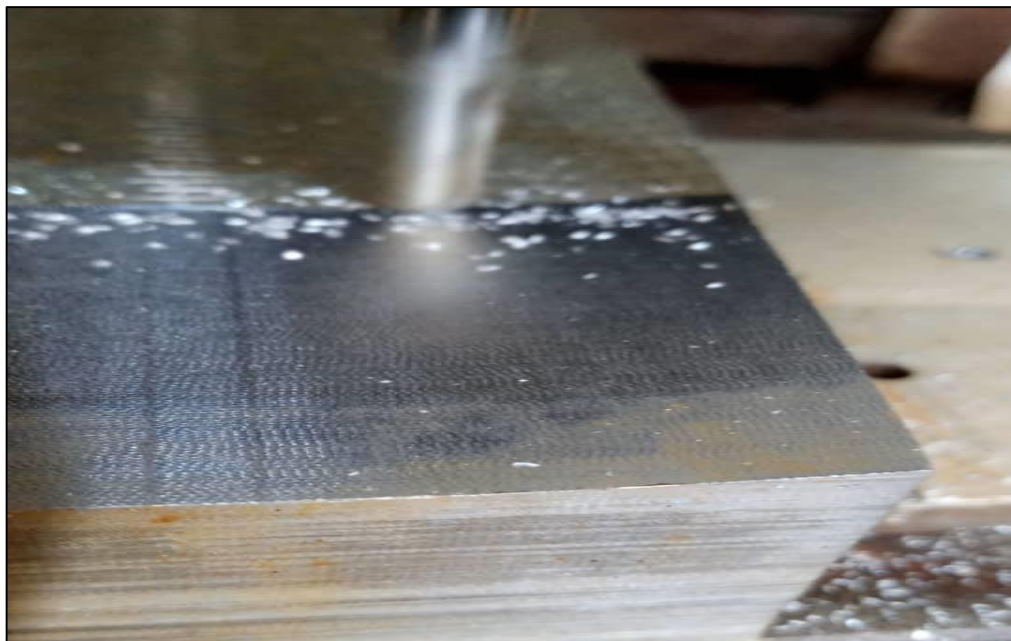


Figure 3-48. "Roughing" and "Sweeping" operations of lower Sail die.

3.13.2.6 The die testing

Once the die is correctly dimensioned and designed, the next step is to be tested. Making the first Sail sample was subjected to verification and testing.

Given the die's problems, the designer must carry out these tests to increase his (her) experience and seek a possible solution to these problems in close collaboration with the workshop staff. For future planning, all modifications made to the die must then be reproduced on the drawing to avoid losses due to repeated errors involving unnecessary

expenses. The die was successfully manufactured and installed on the appropriate hydraulic press bending machine, as shown in Figure 3-49, during the manufacturing of the prototypes. The Sail prototypes were manufactured, and the needed die tuning was made.



Figure 3-49. Sails curving die installed on the bending machine.

3.14 Manufacturing the Rotor Prototype Components

Manufacturing the Rotor prototype started from manufacturing all the Rotor components according to the requirements shown in Table 3-14. Then to start the Rotor assembly operations by assembling the sections of the Sails, Sail Ribs, and inner and outer Rotor Bands, and finally, the assembly of the complete Rotor prototype.

All the Rotor prototype components are manufactured according to the working schedule in Table 3-14. This table illustrates the complete Sail working schedule (as an example), and it must be attached with the complete Sail drawing.

Table 3-14. The Complete Sail's Working Schedule.

WORKING SCHEDULE				No. GROUP	
				99Win00100	
Object: Sail for Rotor	Code No. 20Win004		Modification	Page #	Analyst
Drawing No. Win004	Execution	Position		1/4	
Material: Sheet 2000X1000X1.5 mm ASTM (A36)					
Equipments	Tools		Calipers		
	Double smooth file of 8" (200 mm)		Meter and caliper		
	Scraper				
	Matrix and die for Sail no. 000x				
	Point D=8.5 mm				
	Point D=9 mm				
OPERATION INDEX					
No. op.	Operation		No. op.	Operation	
20	Laser cutting				
20	Laser perforation				
150	Deburing with scraper				
50	Bending				
10	Shears cutting				
50	Bending piece				
30	Marking				
80	Drilling				
150	Deburing with scraper				
190	Riveting				
200	Galvanized proofing.				

Origin	Material movement								Dest.	WORKING SCHEDULE	No. GROUP	
Mag.	2	18	5	1	5	18	8	18	Z		Mont.	99Win00100
Object: Sail for Rotor			Code No. 20Win004				Modifications	Page #		Analyst		
Drawing No. Win004			Execution		Position			2/4				
Q.ty	Description of the operations											
18	Cut with the plasma cutting machine the sheet thickness 1.5 mm as drawing.											
Equip. Tools Calipers											No. opera.	20
Meter and caliper											Machinery	2
18	Perforation with laser of two holes passing as drawing.											
Equip. Tools Calipers											No. opera.	20
Meter and caliper											Machinery	2
18	Deburring with scraper of the executed holes, and with double smooth file of 8" of cutting surfaces.											
Equip. Tools Calipers											No. opera.	150
											Machinery	18
18	Bending of the piece on die and matrix No.000X.											
Equip. Tools Calipers											No. opera.	50
											Machinery	5
18	Execute galvanized proofing.											
Equip. Tools Calipers											No. opera.	200
											Machinery	Z

Origin	Material movement								Dest.	WORKING SCHEDULE	No. GROUP	
Mag.	2	18	5	1	5	18	8	18	Z		Mont.	99Win00100
Object: Sail for Rotor			Code No. 20Win004				Modifications		Page #	Analyst		
Drawing No. Win004			Execution		Position				3/4			
Q.ty			Description of the operations									
18	Equip.	Tools	Calipers	Cut with shears (as drawing Win003), from sheet residual (thick = 1.5 mm) in A36 a strip width 57 mm long 83 mm with cuttings of 5 mm on a side at the length 57 mm.						No. opera.	10	
			Meter and caliper							Machinery	1	
18	Equip.	Tools	Calipers	Execute the two bends of the piece, one to 90° perpendicular to the piece and the second still to 90° but with the inclined piece between 15 and 48 mm from the edge realized with the first bend.						No. opera.	50	
			Meter and caliper							Machinery	5	
18	Equip.	Tools	Calipers	Mark the position of the three holes as drawing.						No. opera.	130	
										Machinery	18	
18	Equip.	Tools	Calipers	Drill with point = 8.5 mm two holes with the distance between centers of 35 mm and distant 7 mm from the edge.						No. opera.	80	
										Machinery	8	
18	Equip.	Tools	Calipers	Drill with point = 9 mm a passing hole placed to 30 mm from the bigger base of the trapezium and to 12 mm from the bended edge where the previous holes have been executed.						No. opera.	80	
										Machinery	8	

Origin	Material movement								Dest.	WORKING SCHEDULE	No. GROUP	
Mag.	2	18	5	1	5	18	8	18	Z		Mont.	99Win00100
Object: Sail for Rotor			Code No. 20Win004				Modifications	Page #		Analyst		
Drawing No. Win004			Execution		Position			4/4				
Q.ty			Description of the operations									
18	Deburring with scraper of the executed holes, and with double smooth file of 8" of cating surfaces.								No. opera.	150		
Equip. Tools Calipers									Machinery	18		
Meter and caliper												
18	Rivet the sail ties to the sails.								No. opera.	190		
Equip. Tools Calipers									Machinery	18		
Meter and caliper												
18	Execute galvanized proofing.								No. opera.	200		
Equip. Tools Calipers									Machinery	Z		
18									No. opera.			
Equip. Tools Calipers									Machinery			
18									No. opera.			
Equip. Tools Calipers									Machinery			

The following sections give details of the manufacturing of all the Rotor components; namely, the complete Sails, the Sail Ribs, the complete Rotor Arms, and the Inner and Outer Rotor Bands:

3.14.1 Manufacturing of the complete Rotor Sails

- 1- Cut 18 pieces (Rotor Sails) with the plasma cutting machine, the sheet 1500x2000mm, thickness 1.5mm, and the material specification (ASTM A36, 0.25 wt.% carbon) steel as present in the following drawing in Figure 3-50.
- 2- The holes' perforation passes with the plasma cutting machine, as shown in Figure 3-50. The picture in Figure 3-51 shows cutting the Rotor Sails using the plasma cutting machine located at the T.B.Co.

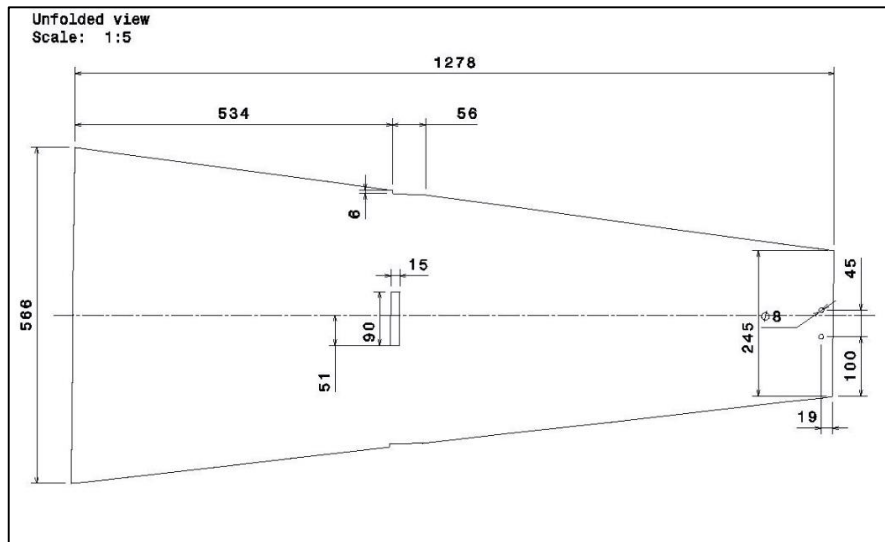


Figure 3-50. Unfolded view of the Sail.



Figure 3-51. Cutting the Sails using a CNC plasma machine.

- 3- Deburring with a scraper of the executed holes and a double smooth file of 8" of cutting surfaces.
- 4- Control all the dimensions of the executive part using Meter and caliper.
- 5- Bend the piece using the temporary die to curving the prototype Sails only, and the die was designed and manufactured to be attached to the bending machine, as shown in Figure 3-52. The picture was taken in one of Al-Inma's workshops in Tajoura while bending the Sails used to manufacture the Rotor prototype.



Figure 3-52. Curving Sails die attached to the bending machine.

- 6- Execute galvanized proofing of all the components by Al-Inma's galvanizing bath.
- 7- Cut with shears from a 4mm thick sheet (material used is ASTM A36, 0.25 wt.% carbon) steel eighteen strips width of 65mm and length of 97mm, as shown in Figure 3-53.

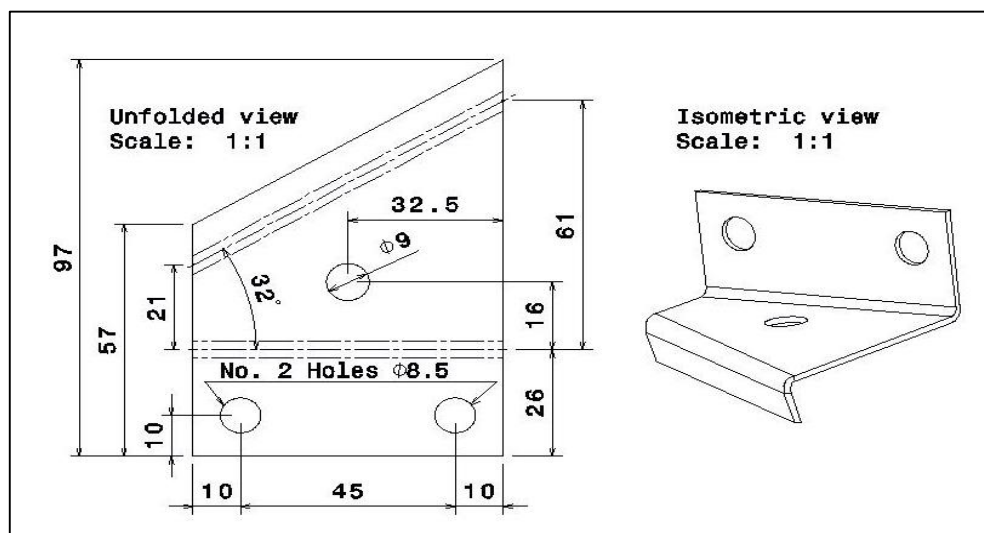


Figure 3-53. Isometric and unfolded view of the Sail Tie.

- 8- Mark the position of the three holes as in Figure 3-53.

9- Drill with point = 8.5mm two holes with the distance between centers of 45mm and a distance of 10mm from the edge.

10- Drill with point = 9mm a passing hole placed to 32.5mm from the bigger base of the trapezium and 16mm from the bent edge where the previous holes have been executed.

After executing the three holes, the Sail Tie became as shown in Figure 3-54.

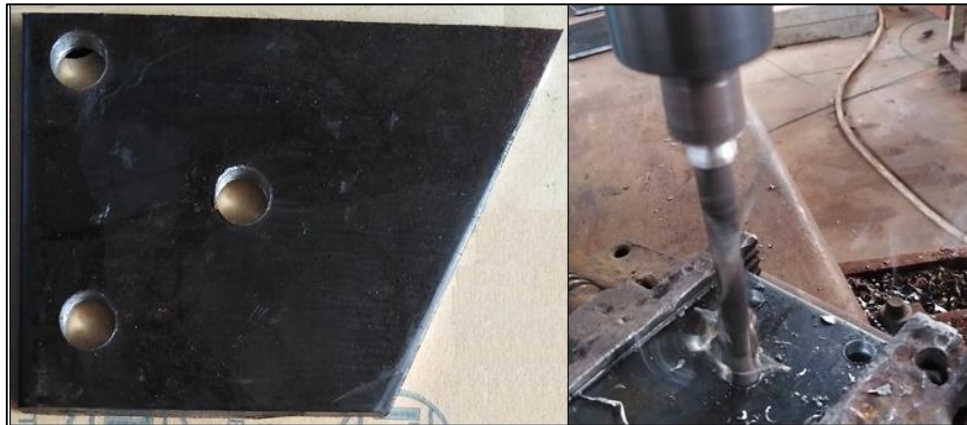


Figure 3-54. A picture of the Sail Tie while executing the three holes.

11- Deburring with a scraper of the executed holes and a double smooth file of 8" (200mm) of cutting surfaces.



Figure 3-55. The bending process of the Sail Tie by the bending press machine.

12- Executing two bends, the first and second to 90°, but the workpiece inclined between 21 and 61mm from the edge for the second. Figure 3-55 shows the two bending processes of the Sail Tie carried out on the bending press machine at the T.B.Co.

13- Control all the dimensions of the executive part using a meter and caliper.

14- Rivet the Sail Ties to the Sails.

3.14.2 Manufacturing the Sail Rib

1. Cut 18 pieces with the plasma cutting machine, the sheet 1000x2000mm, thickness 1.5mm, and the material specification is (ASTM A36, 0.25 wt.% carbon) steel as present in unfolded view in Figure 3-56.
2. The holes' perforation passes with the plasma cutting machine located at the T.B.Co., as shown in Figure 3-56.
3. Deburring with a scraper of the executed holes and a double smooth file of 8" of cutting surfaces.
4. Controlling all the dimensions of the executive part using Meter and caliper.
5. Executing two bends; the first and second to 90°, on the bending axes presented in the unfolded view in Figure 3-56, the distance is 13.1mm from the edge for the first bend, and 17.1mm from the edge for the second bend. The two bending processes of the Sail Rib were performed on the bending press machine at the T.B.Co.
6. Execute galvanized proofing of all the Ribs by Al-Inma's galvanizing bath.

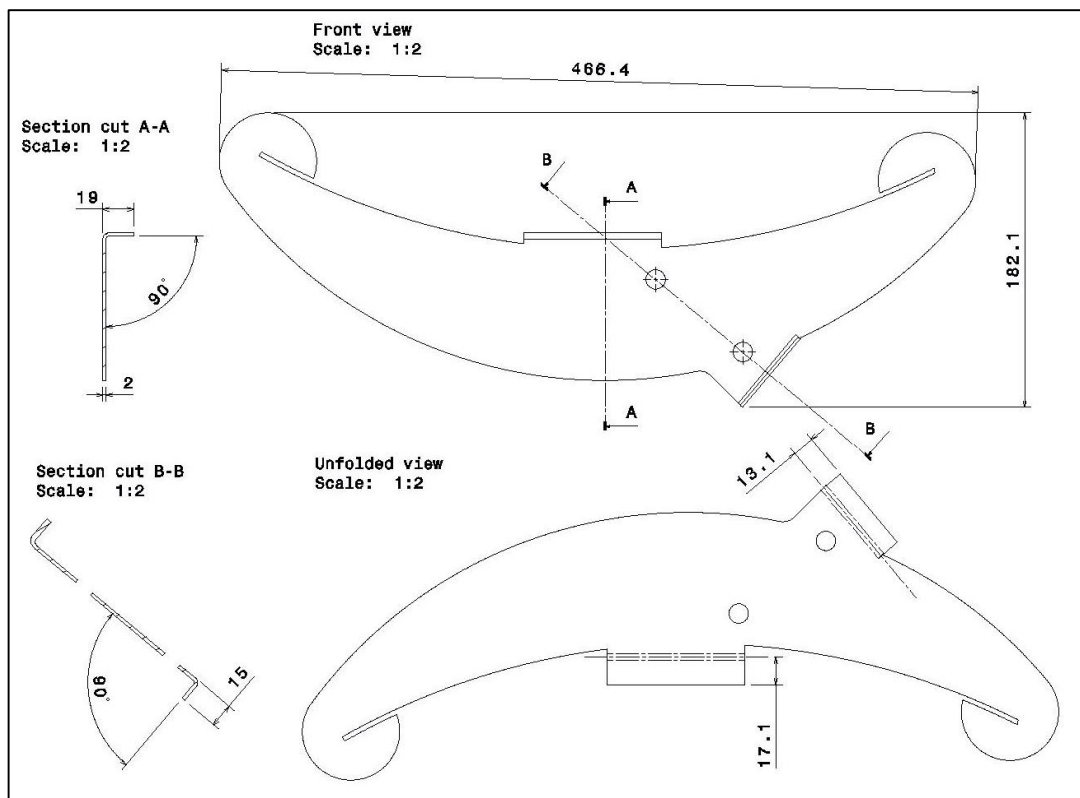


Figure 3-56. Front and Unfolded view of the Sail Rib.

3.14.3 Manufacturing the outer Rotor Bands

- 1- Cut (ASTM A36, 0.25 wt.% carbon) steel plate into six strips with dimensions of length (L) =1761mm and 45 x 10mm with cropper.

- 2- Mark the position of the ten holes as shown in Figure 3-57.
- 3- Drill with point 13mm a hole passing to 22mm from the external edge, previously marked, and a second hole $D=13\text{mm}$ passing to 99mm from the external (Outer) edge.
- 4- Rotate the piece 180° in the operation record, and drill with point 13mm a hole passing to 1532mm from the external edge, which was previously marked, and a second hole $D=13\text{mm}$ passing to 1458mm from the external edge as shown in Figure 3-57.

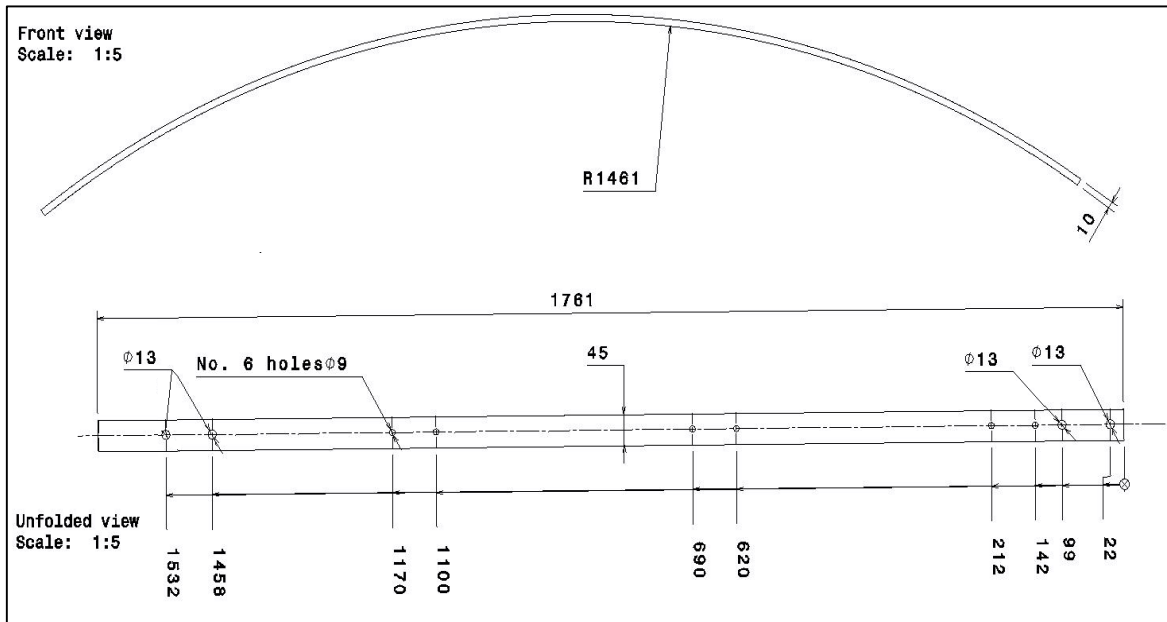


Figure 3-57. Front and unfolded view of the outer Rotor Bands.



Figure 3-58. Drilling passing holes of the Outer Rotor Bands.

- 5- Drill with point D=9mm of six holes, previously marked. Figure 3-57 shows the drilling passing holes of the outer Rotor Bands. Figure 3-58 shows the drilling process to execute the outer Rotor Band passing holes.
- 6- Deburring with a scraper of the executed holes and a double smooth file of 8" (200mm) of the cutting surfaces.
- 7- Control all the dimensions of the executive part using a meter and caliper.
- 8- Bend the piece using the CNC rolling machine, as shown in Figure 3-59 during bending.



Figure 3-59. Bending the outer Band by CNC rolling machine.

3.14.4 Manufacturing the Inner Rotor Bands

1. Cut plate 45x10mm in ASTM A36, 0.25 wt.% carbon steel into six strips L=942mm with cropper.
2. Mark the position of the five holes as shown in Figure 3-60.
3. Drill with point 13mm a hole passing to 42mm from the external edge, previously marked.
4. Rotate the piece 180° in the operation record, and drill with point 13mm a hole passing to 859mm from the external edge, which was previously marked as shown in Figure 3-60.
5. Drill with point D=9mm of three holes, previously marked.
6. Deburring with a scraper of the executed holes and a double smooth file of 8" of the cutting surfaces.
7. Control all the dimensions of the executive part using a meter and caliper.
8. Bend the piece using the rolling machine.

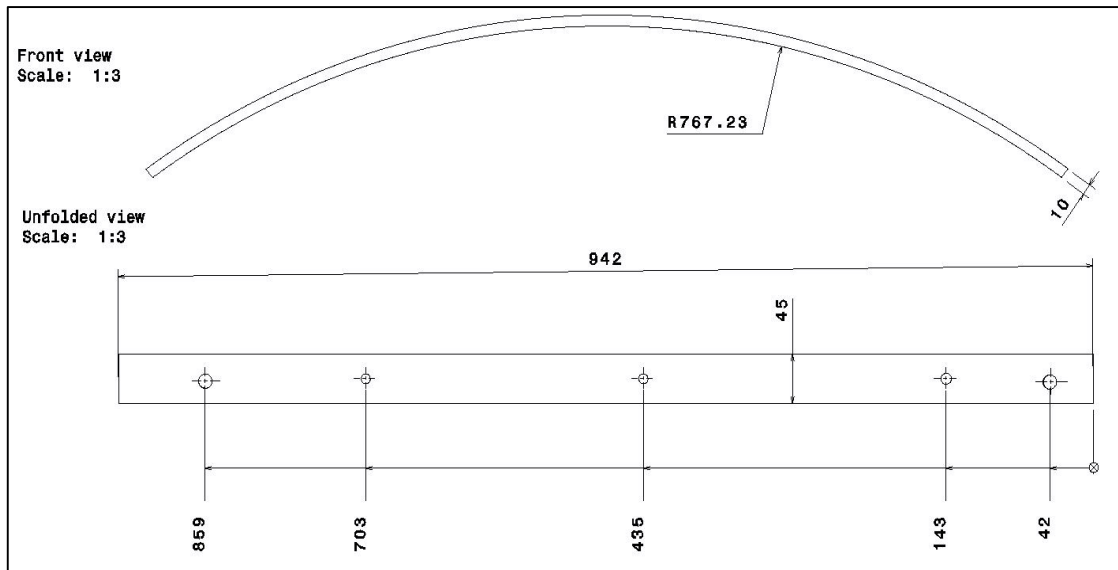


Figure 3-60. Front and unfolded view of the Rotor Inner Bands.

3.14.5 Manufacturing the complete Rotor Arms

1. Using a cutting machine, cut a steel (ASTM A36, 0.25 wt.% carbon) rod diameter of 16mm and 1472mm.
2. Threading one end of the rod of 55mm long, as shown in Figure 3-61, and threading the other end to a length of 45mm.
3. Bend the bar at 72mm from the edge of the threaded end to a length of 55mm at an angle of 6 from the rod axis, as shown in Figure 3-61.
4. Weld the cross-section Tie at a distance of 587mm from the cube's edge and in the position shown in Figure 3-61.

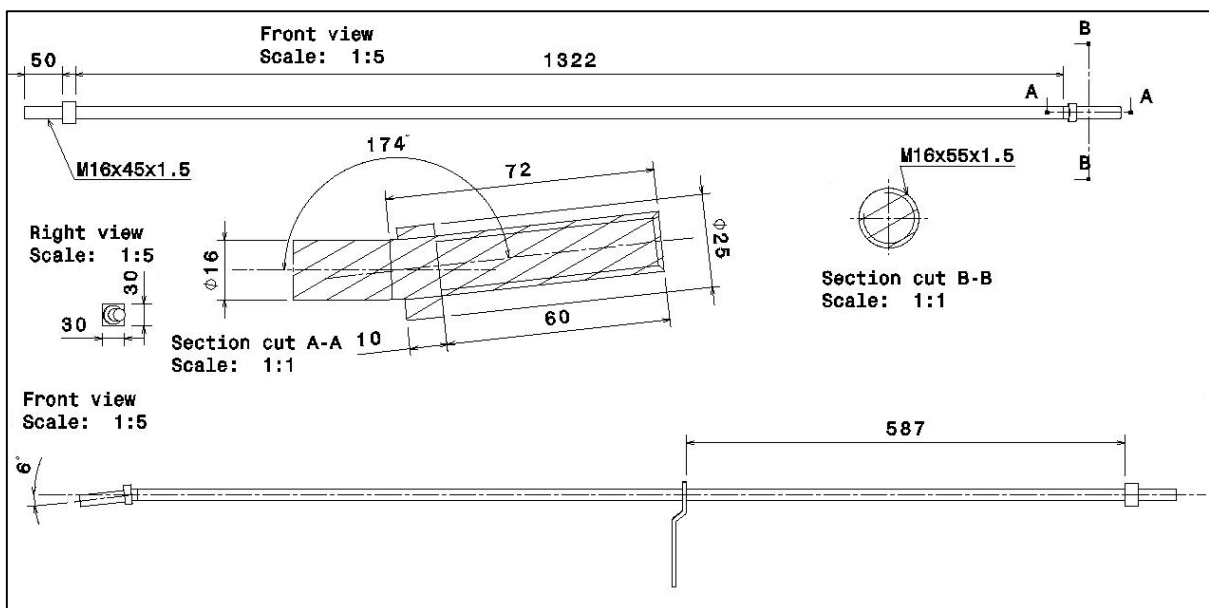


Figure 3-61. Complete Rotor Arms 2D drawing.

5. Weld the cube with sides of 30mm and perforated with a diameter of 17mm at a distance of 50mm from the unbent end, as shown in Figure 3-61, and the welding shall be on the other end far from the thread.
6. Weld a bushing with a 10mm thickness, an inner diameter of 17mm, and an outer diameter of 25mm, at a distance of 60mm from the edge of the other end, as shown in Figure 3-61.
7. Clean the welding places using an electric angle grinder.

3.15 Sails Section Assembly

The assembly of the windmill Rotor requires the preparation of the sub-assembly of the Rotor Sails (Sails section), which is described in the following steps:

- 1- Slide a Sail Rib (005) over the small end of the Sail toward the large end until it fits into the rectangular hole in the Sail (004), as indicated in Figure 3-62. Repeat this process for all eighteen Sails.

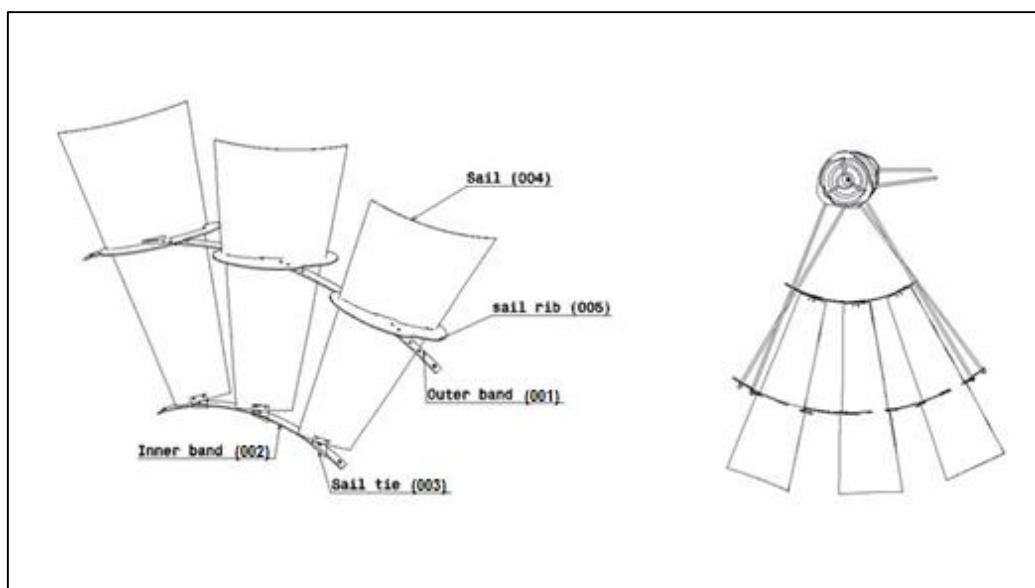


Figure 3-62. Sail section and Rotor assembly.

- 2- Lay three Sails in position, as shown in Figure 3-62. Connect the Inner Band (002) to the Sail Tie with bolts and locknuts. Do not tighten the lock nuts yet.
- 3- Slide the Outer Band (001) through the rectangular hole in the Sails until the Outer Band's bolt holes match the Sail Ribs' bolt holes.
- 4- Tighten all lock nuts in the Rotor section and repeat this procedure until all six sections are completed, as shown in Figure 3-63.



Figure 3-63. The complete Rotor Sails section assembly.

3.16 Complete Windmill Rotor Assembly

The following steps describe the assembly process of the complete windmill Rotor on the Hub:

- 1- Install the 12 Rotor Arms into the Hub assembly of the motor. The end of the Rotor Arms with the screws into the Hub. Use a wrench with smooth jaws to tighten them into the Hub. Then after the second arm is tight, tighten the first Arm so that the tabs are parallel and the offset ends are aligned to receive the inner Rotor Band. Figure 3-64 shows a picture during the installation of the Rotor Arms into the Hub. The Outer ends of the Rotor Arms will all stand straight out and in line, allowing them to slip through the holes in the outer Rotor Bands without bending. The Arms cross at the Inner Band and the cross Ties stand at right angles to the Band, so they cross the Inner Band.



Figure 3-64. Installing the Rotor Arms into the Hub.



Figure 3-65. Installing the 4th Sails section.

- 2- With a pair of Rotor Arms mounted in the front holes of the Hub facing down, place a Rotor section on, so that the ends of the Rotor Arms from the front of the Hub go through

the outer holes of the section. Rotate the Rotor to the left, and place a section onto the Arms mounted in the rear holes of the Hub. The Rotor Arms for this section will go through the Outer holes of this section, and the third section will go on the Arms from the front holes on the Hub.

- 3- Rotate the three assembled sections to the top, so they will balance, as shown in Figure 3-65, and then install the 4th section that goes on the Arms from the back holes of the Hub. Rotate again to install the fifth section onto the front holes of the Hub.



Figure 3-66. Installing the 6th Sails section.

- 4- When the technician puts the sixth and last Rotor section in place, as in Figure 3-66, the point where the first section meets the sixth requires temporarily removing the Outer end of the first Band and placing the end of the sixth section Band on the first. Then replace the first section Band so each joint is assembled with the same lap.
- 5- After all the six Rotor sections have been assembled to Rotor Arms and all the Inner Bands are bolted together, the technician should begin tightening each set of nuts on the Outer Bands a couple of turns at a time. Then rotate the Rotor and tighten the next set a couple of turns. Continue this until all the nuts are tightened fully. Figure 3-67 shows the complete windmill Rotor assembly.

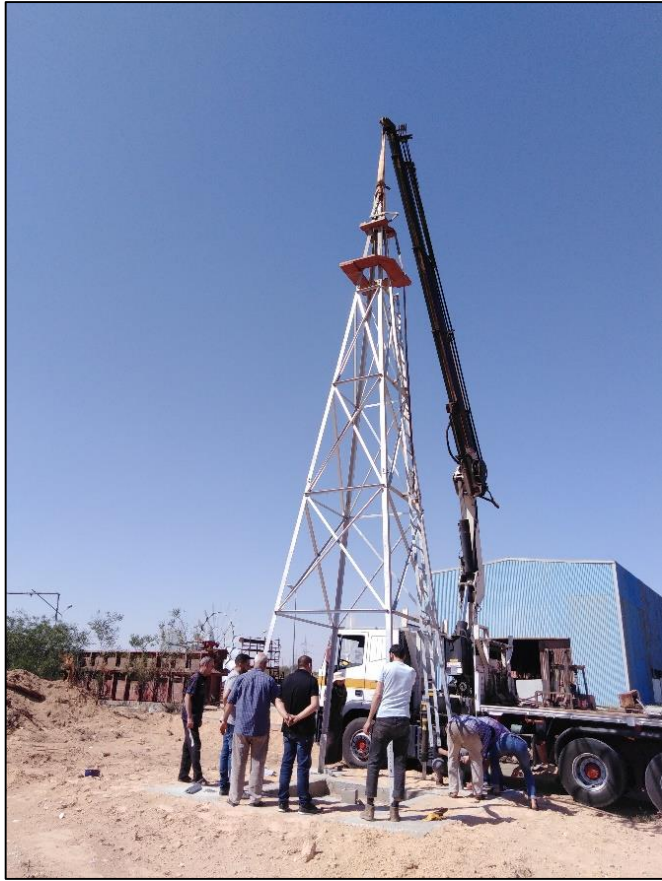


Figure 3-67. The complete windmill Rotor assembly.

3.17 Performance Testing:

The actual testing of the Rotor Components has been done to confirm that these RE components were produced successfully and fulfill their intended function. The windmill Rotor was installed on a tower (12 meters) manufactured by Al-Anma Company on the well dedicated for the experiment.

Figure 3-68 shows some pictures during the installation process of the Rotor and the tower on the well located at the company headquarters in Tajoura. Figure 3-69 shows the extraction of groundwater from the well by the windmill system at the moment the picture was taken, at a wind speed of 2.7m/sec, measured at 2m from the ground, was a success, and the water flow rate evaluated was 1liter/10s.



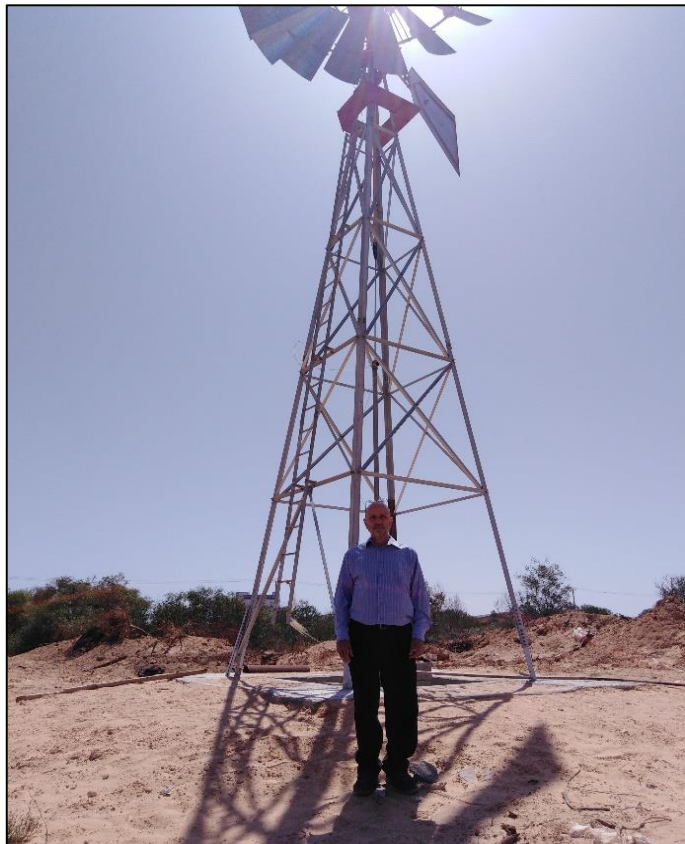
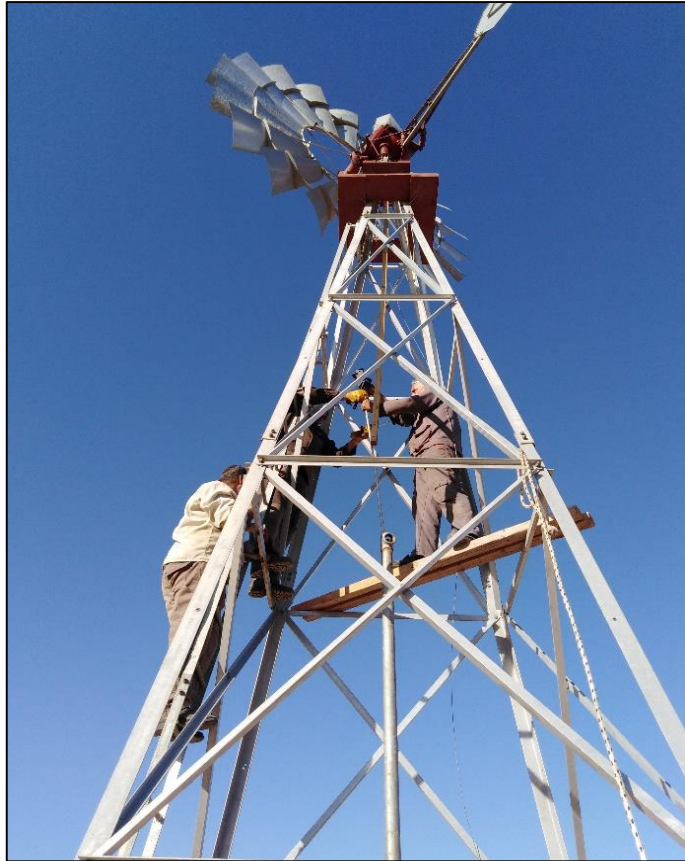




Figure 3-68. Rotor and tower installation.

By testing the entire windmill system, it is possible to deduce the success of the reverse engineering application to manufacture the rotary components of the windmill system and achieve all the objectives of this thesis.



Figure 3-69.Extracting water from the well by the windmill system.

Based on this study, Al-Anma Company decided to complete manufacturing the remaining components of the windmill system locally by adopting a Reverse Engineering approach suggested by the researcher.

CHAPTER FOUR:

**CONCLUSIONS AND
RECOMMENDATIONS**

4 CONCLUSIONS AND RECOMMENDATIONS

4.1 Conclusions

The conclusions that can be summarized are as follows:

- 1- From the wind speed data analysis, the researcher found that the city of Tajoura has sufficient wind potential that can be used for water pumping.
- 2- The appropriate diameter of the Rotor to supply the water demand on the site of 5m³/day was found from the wind analysis to be 4.7m. The closest size in the standard range, i.e., 4.88m (16ft), was selected for practical purposes.
- 3- By using digitized dimensional scanning systems to perform RE and machining process simulation in a virtual environment within an integrated CAD/CAM system, one can reduce design time and avoid errors or modifications that increase costs and CNC machining time.
- 4- The single operation die for curving the Sails was successfully designed and manufactured using integrated CAD/CAM/CNC.
- 5- The complete windmill Rotor assembly was done successfully with no problems.
- 6- The windmill system's extraction of groundwater from the well at a wind speed of 2.7m/sec, measured at 2m from the ground, was accomplished, and the water flow rate evaluated was 1 liter/10s.
- 7- Generally, from both the literature and this research study, the researchers concluded that the windmills for water pumping could not be manufactured solely by just applying the reverse engineering without determining; (i) water requirements, (ii) wind characteristics, (iii) proper evaluation of wind resources on the chosen site, and (iv) sizing the system.
- 8- All materials used to construct the windmill are locally accessible and inexpensive, making the model economically feasible.

4.2 Recommendations:

- 1- The researcher highly recommends conducting an economic feasibility study for the various alternatives (i.e., fossil fuels, photovoltaic, wind-electric generation and windmills) used to extract groundwater before deciding to choose any of these alternatives.
- 2- A research study is highly recommended for designing and manufacturing the gearbox using Reverse Engineering.
- 3- Libyan Research Centers with the Manufacturing Companies, the University of Tripoli, and other high education institutions can coordinate their efforts to manufacture spare parts using Reverse Engineering.

5 REFERENCES

- [1] R. K. Singh and A. Yadav, "Application of Reverse Engineering on CAD Modelling Using Least Square Fitting Technique," *International Journal of Advance Research in Science and Engineering*, pp. 459–470, 2017.
- [2] A. Satish, D. K. Rambabu, and M. Ramji, "Centrifugal Pump Impeller Modeling With Reverse Engineering," *International Journal of Research in Mechanical Engineering and Technology*, vol. 4, no. 1, pp. 7–13, 2013.
- [3] A. Giannelis, I. Symeonidou, D. Tzetzis, G. Kaisarlis, and P. Kyratsis, "Laser scanning and CAD conversion accuracy correction of a highly curved engineering component using a precision tactile measuring system," in *MATEC Web of Conferences*, vol. 112, 2017.
- [4] R. J. Abella, J. M. Daschbach, and R. J. McNichols, "Reverse engineering industrial applications," *Computers and Industrial Engineering*, vol. 26, no. 2, pp. 381–385, 1994.
- [5] W. Wang, *Reverse engineering : technology of reinvention*, vol. 15, pp.7. 2010.
- [6] M. Harries, "Disseminating wind pumps in rural Kenya - Meeting rural water needs using locally manufactured wind pumps," *Energy Policy*, vol. 30, no. 11–12, pp. 1087–1094, 2002.
- [7] J. Van Meel and P. Smulders, *Wind pumping: a handbook*. Washington: The International Bank for Reconstruction and Development/THE WORLD BANK, 1987.
- [8] P. T. Smulders and J. de Jongh, "Wind water pumping: Status, prospects and barriers," *Renewable Energy*, vol. 5, no. 1–4, pp. 587–594, 1994.
- [9] J. A. Carta, P. Ramírez, and S. Velázquez, "A review of wind speed probability distributions used in wind energy analysis. Case studies in the Canary Islands," *Renewable and Sustainable Energy Reviews*, vol. 13, no. 5. pp. 933–955, 2009.
- [10] S. E. Tuller and A. C. Brett, "The characteristics of wind velocity that favor the fitting of a Weibull distribution in wind speed analysis.," *Journal of Climate & Applied Meteorology*, vol. 23, no. 1, pp. 124–134, 1984.
- [11] H. Shreif, W. El-Osta, and A. Yagub, "Wind Resource Assessment for southern part of Libya: Case Study of Hun," *Solar Energy and Sustainable Development journal*, vol. 8, no. 1, 2019.
- [12] F. Castellanos and V. I. Ramesar, "Characterization and estimation of wind energy

- resources using autoregressive modelling and probability density functions,” *Wind Engineering*, vol. 30, no. 1, pp. 1–14, 2006.
- [13] M. Alzubaidi, K. N. Hasan, and L. Meegahapola, “Identification of Suitable Probability Density Function for Wind Speed Profiles in Power System Studies,” *2020 Australasian Universities Power Engineering Conference, AUPEC 2020 - Proceedings*.
- [14] M. T. Islam, A. B. Abdullah, and M. Z. Mahmud, “Reverse engineering of B-pillar with 3D optical scanning for manufacturing of non-uniform thickness part,” in *MATEC Web of Conferences*, vol. 90, 2016.
- [15] T. D. Short and P. Thompson, “Breaking the mould: Solar water pumping—the challenges and the reality,” *Solar Energy*, vol. 75, no. 1, pp. 1–9, 2003.
- [16] G. I. Ghionea, A. L. Ghionea, and I. Tanase, “Analysis of milling the parts with thin walls using CAM-FEM methods,” in *Annals of DAAAM and Proceedings of the International DAAAM Symposium*, pp. 265–266, 2009.
- [17] S. Klancnik, M. Brezocnik, and J. Balic, “Intelligent CAD/CAM system for programming of CNC machine tools,” *International Journal of Simulation Modelling*, vol. 15, no. 1, pp. 109–120, Mar. 2016.
- [18] J. Balic, “Intelligent CAD/CAM systems for CNC programming—an overview,” *Advances in Production Engineering & Management*, vol. 1, no. 1, 2006.
- [19] R. Dubovská, “The quality control of machining process with CAD/CAM systems support,” in *Proceedings of the International Conference of DAAAM Baltic*, pp. 27–32, 2012.
- [20] S. Kafandaris and T.-C. Chang, “Expert Process Planning for Manufacturing,” *J. Oper. Res. Soc.*, vol. 43, no. 1, p. 72, 1992.
- [21] L. I. Culda, E. S. Muncut, D. Mortoiu, and G. Sima, “CAD / CAM Modeling and Simulation, With the Catia Software,” *ANNALS OF THE ORADEA UNIVERSITY. Fascicle of Management and Technological Engineering*, vol. XXII (XII), no. 1, pp. 63-66, 2013.
- [22] C. Bin, G. Dingjie, Q. I. Jiyan, and J. Bingxue, “Sequence optimization of machining elements for process model based on the genetic algorithm of matrix constrained,” in *Journal of Physics: Conference Series*, , vol. 1678, no. 1, 2020.
- [23] T. Várady, R. R. Martin, and J. Cox, “Reverse engineering of geometric models - An introduction,” *CAD Computer Aided Design*, vol. 29, no. 4, pp. 255-268, 1997.
- [24] P. Moriarty and D. Honnery, “Global renewable energy resources and use in 2050,”

- Managing Global Warming: An Interface of Technology and Human, Issues*, no. November, pp. 221–235, 2018.
- [25] Z. Tasneem *et al.*, “An analytical review on the evaluation of wind resource and wind turbine for urban application: Prospect and challenges,” *Developments in the Built Environment*, vol. 4, 2020.
- [26] N. K. Roy and A. Das, “Prospects of Renewable Energy Sources,” pp. 1–39, 2018.
- [27] I. Odesola and L. G. Adinoyi, “Development of Wind powered water pump,” *International Journal of Engineering Science and Computing*, vol. 7, no. 4, pp. 10341–10345, 2017.
- [28] M. Cloutier and P. Rowley, “The feasibility of renewable energy sources for pumping clean water in sub-Saharan Africa: A case study for Central Nigeria,” *Renewable Energy*, vol. 36, no. 8, pp. 2220–2226, 2011.
- [29] F. Buonamici, M. Carfagni, R. Furferi, L. Governi, A. Lapini, and Y. Volpe, “Reverse engineering of mechanical parts: A template-based approach,” *Journal of Computational Design and Engineering*, vol. 5, no. 2, 2018.
- [30] G. Šag, Z. Lulić, and I. Mahalec, “Reverse engineering,” in *Concurrent Engineering in the 21st Century: Foundations, Developments and Challenges*, pp. 319–353, 2015.
- [31] M. Burston, R. Sabatini, A. Gardi, and R. Clothier, “Reverse engineering of a fixed wing Unmanned Aircraft 6-DoF model based on laser scanner measurements,” in *2014 IEEE International Workshop on Metrology for Aerospace, MetroAeroSpace 2014 - Proceedings*, pp. 144–149, 2014.
- [32] W. B. Thompson, J. C. Owen, H. J. De St. Germain, S. R. Stark, and T. C. Henderson, “Feature-based reverse engineering of mechanical parts,” *IEEE Trans. Robot. Autom.*, vol. 15, no. 1, pp. 57–66, 1999.
- [33] K. A. Ingle, *Reverse Engineering*. McGraw-Hill, 1994.
- [34] M. Sokovic and J. Kopac, “RE (reverse engineering) as necessary phase by rapid product development,” *Journal of Materials Processing Technology*, vol. 175, no. 1–3, pp. 398–403, 2006.
- [35] N. S. Ali, “Reverse Engineering of Automotive Parts Applying Laser Scanning and Structured Light Techniques,” *The University of Tennessee, Knoxville*, no. May, 2005.
- [36] D. Li, “Application of coordinate measuring machine in reverse engineering,” in *Advanced Materials Research*, vol. 301–303, pp. 269–274, 2011.
- [37] V. Raja and K. J. Fernandes, *Reverse Engineering An Industrial Perspective*. 2009.

- [38] M. Kettner, P. Schmidt, S. Potente, F. Ramsthaler, and M. Schrodt, "Reverse engineering-rapid prototyping of the skull in forensic trauma analysis," *Journal of Forensic Sciences*, vol. 56, no. 4, pp. 1015–1017, 2011.
- [39] A. Kumar, P. K. Jain, and P. M. Pathak, "Machine Element Reconstruction Using Integrated Reverse Engineering and Rapid Prototyping Approach," in *5th International & 26th All India Manufacturing Technology, Design and Research Conference*, no. AIMTDR 2014, pp. 123-(1-5), 2014.
- [40] K. H. Lee and H. Woo, "Use of reverse engineering method for rapid product development," *Computers and Industrial Engineering*, vol. 35, no. 1–2, pp. 21–24, 1998.
- [41] N. Singh, "Review Article Reverse Engineering- A General Review," *International Journal of Advanced Engineering Research*, pp. 1–5, 2012.
- [42] N. Troussier, M. Bricogne, A. Durupt, F. Belkadi, and G. Ducellier, "A knowledge-based reverse engineering process for CAD models management," *8th International Conference on Integrated Design and Manufacturing in Mechanical Engineering, IDMME'010*, 2010.
- [43] Ö. VERİM and M. YUMURTACI, "Application of reverse engineering approach on a damaged mechanical part," *International Advanced Researches and Engineering Journal*, vol. 4, no. 1, pp. 21–28, 2020.
- [44] S. Motavalli, "Review of Reverse Engineering Approaches," *Computers and Industrial Engineering*, vol. 35, no. 1–2, pp. 25–28, 1998.
- [45] A. Kumar, P. K. Jain, and P. M. Pathak, "Reverse Engineering in Product Manufacturing: An Overview," pp. 665–678, 2013.
- [46] N. Anwer and L. Mathieu, "From reverse engineering to shape engineering in mechanical design," *CIRP Annals - Manufacturing Technology*, vol. 65, no. 1, pp. 165–168, 2016.
- [47] Z. M. Bia and L. Wang, "Advances in 3D data acquisition and processing for industrial applications," *Robotics and Computer-Integrated Manufacturing*, vol. 26, no. 5, pp. 403–413, 2010.
- [48] T. Segreto, A. Bottillo, A. Caggiano, and M. Martorelli, "Integration of reverse engineering and ultrasonic non-contact testing procedures for quality assessment of CFRP aeronautical components," in *Procedia CIRP*, vol. 79, pp. 343–348, 2019.
- [49] B. Bidanda, S. Motavalli, and K. Harding, "Reverse engineering: An evaluation of prospective non-contact technologies and applications in manufacturing systems,"

- International Journal of Computer Integrated Manufacturing*, vol. 4, no. 3, pp. 145–156, 1991.
- [50] A. K. Jain, “Segmentation and Classification of Range Images,” *IEEE Transactions on Pattern Analysis and Machine Intelligence*, vol. PAMI-9, no. 5, pp. 608–620, 1987.
- [51] D. Lesage, J. C. Leon, and P. Veron, “Discrete curvature approximations and segmentation of polyhedral surfaces,” *International Journal of Shape Modeling*, vol. 11, no. 2, pp. 217–252, 2005.
- [52] J. Dan and W. Lancheng, “An algorithm of NURBS surface fitting for reverse engineering,” *International Journal of Advanced Manufacturing Technology*, vol. 31, no. 1–2, pp. 92–97, Nov. 2006.
- [53] R. Hartson and P. S. Pyla, *The UX Book: Process and Guidelines for Ensuring a Quality User Experience*. Elsevier Inc., 2012.
- [54] G. Döllner, P. Kellner, and O. Tegel, “Digital mock-up and rapid prototyping in automotive product development,” *Journal of Integrated Design and Process Science*, vol. 4, no. 1, pp. 55–66, 2000.
- [55] O. Bellart, “The multi facets of Reverse Engineering,” in *Reverse Engineering*, pp. 103–107, 1996.
- [56] G. Sequenzia, G. Fatuzzo, S. M. Oliveri, and R. Barbagallo, “Interactive re-design of a novel variable geometry bicycle saddle to prevent neurological pathologies,” *International Journal on Interactive Design and Manufacturing*, vol. 10, no. 2, pp. 165–172, 2016.
- [57] H. J. Wagner, “Introduction to wind energy systems,” in *EPJ Web of Conferences*, vol. 189, 2018.
- [58] R. Gasch and J. Twele, *Wind power plants: Fundamentals, design, construction and operation, second edition*. pp. 1–548, 2012.
- [59] Groover, *Fundamentals of Modern Manufacturing* . 2010.
- [60] S. Kalpakjian and S. R. Schmid, *Manufacturing Engineering & Technology*. 2010.
- [61] Y. Nukman, A. Farooqi, O. Al-Sultan, A. R. A. Alnasser, and M. S. H. Bhuiyan, “A Strategic Development of Green Manufacturing Index (GMI) Topology Concerning the Environmental Impacts,” in *Procedia Engineering*, vol. 184, pp. 370–380, 2017.
- [62] H. A. Youssef and H. El-Hofy, *Machining technology: Machine tools and operations*. 2008.
- [63] S. Kalpakjian and S. R. Schmid, “Manufacturing engineering and technology,”

- Journal of Materials Processing Technology*, vol. 25, no. 1, pp. 112–113, 1991.
- [64] B. Arezoo, K. Ridgway, and A. M. A. Al-Ahmari, “Selection of cutting tools and conditions of machining operations using an expert system,” *Computers in Industry*, vol. 42, no. 1, pp. 43–58, 2000.
- [65] M. C. Frank, “Implementing rapid prototyping using CNC machining (CNC-RP) through a CAD/CAM interface,” in *18th Solid Freeform Fabrication Symposium, SFF 2007*, pp. 112–123, 2007.
- [66] S. H. Ryu, D. K. Choi, and C. N. Chu, “Roughness and texture generation on end milled surfaces,” *International Journal of Machine Tools and Manufacture*, vol. 46, no. 3–4, pp. 404–412, 2006.
- [67] R. Ramesh, K. S. Ravi Kumar, and G. Anil, “Automated intelligent manufacturing system for surface finish control in CNC milling using support vector machines,” *International Journal of Advanced Manufacturing Technology*, vol. 42, no. 11–12, pp. 1103–1117, 2009.
- [68] D. Veeramani and Y. S. Gau, “Selection of an optimal set of cutting-tools for a general triangular pocket,” *International Journal of Production Research*, vol. 35, no. 9, pp. 2621–2638, 1997.
- [69] T. Kuragano, “FRES DAM system for design of aesthetically pleasing free-form objects and generation of collision-free tool paths,” *Computer-Aided Design*, vol. 24, no. 11, pp. 573–581, 1992.
- [70] L. Lennings, “Selecting Either Layered Manufacturing or CNC Machining to Build Your Prototype,” Jul. 2000.
- [71] P. Nikam, “Application of Subtractive Rapid Prototyping (SRP) For RSP Tooling,” *Mechanical Engineering Department, Cleveland State University*, pp.33–34. Jan. 2005.
- [72] S. Akula and K. P. Karunakaran, “Hybrid adaptive layer manufacturing: An Intelligent art of direct metal rapid tooling process,” *Robotics and Computer-Integrated Manufacturing*, vol. 22, no. 2, pp. 113–123, 2006.
- [73] A. B. Savarese, *Manufacturing engineering*. pp. 1-171, 2011.
- [74] V. BOLJANOVIC, *Sheet metal forming processed and die design, 2nd ed.* United States of America, 2009.
- [75] J. Jin and J. Shi, “Automatic feature extraction of waveform signals for in-process diagnostic performance improvement,” *Journal of Intelligent Manufacturing*, vol. 12, no. 3, pp. 257-268, 2001.

- [76] www.custompartnet.com, “<https://www.custompartnet.com/wu/images/sheet-metal/press-brake.png>” .
- [77] O. Badran, “Wind Energy Research and Development in Jordan,” *Al-Balqa' Applied University Faculty of Engineering Technology, Department of Mechanical Engineering, Amman –Jordan*, pp. 2360–2363, Dec. 2000.
- [78] O. O. Ajayi, R. O. Fagbenle, J. Katende, and J. O. Okeniyi, “Availability of wind energy resource potential for power generation at Jos, Nigeria,” *Frontiers in Energy*, vol. 5, no. 4, pp. 376-385, 2011.
- [79] O. S. Ohunakin, “Assessment of wind energy resources for electricity generation using WECS in North-Central region, Nigeria,” *Renewable and Sustainable Energy Reviews*, vol. 15, no. 4. pp. 1968–1976, 2011.
- [80] S. Mathew, *Wind energy: Fundamentals, resource analysis and economics*. 2007.
- [81] F. A. L. Jowder, “Weibull and Rayleigh distribution functions of wind speeds in Kingdom of Bahrain,” *Wind Engineering*, vol. 30, no. 5, pp. 439–446, 2006.
- [82] T. P. Chang, “Performance comparison of six numerical methods in estimating Weibull parameters for wind energy application,” *Applied Energy*, vol. 88, no. 1, pp. 272–282, 2011.
- [83] C. Carrillo, J. Cidrás, E. Díaz-Dorado, and A. F. OBando-Montaño, “An approach to determine the weibull parameters for wind energy analysis: The case of Galicia (Spain),” *Energies*, vol. 7, no. 4, pp. 2676–2700, 2014.
- [84] S. Saravanan, D. Anbazahan, G. S. Manikandan, M. Mathavan, A. M. Afrith, and K. Prakash, “Design and Fabrication of Wind Energy Water Pump,” *International Journal of Engineering Research & Technology (IJERT)*, vol. 6, no. 04, pp. 4–7, 2018.
- [85] S. Balamurali, P. Chinnamani, B. Hariharan, S. M. Hariprakas, and B. Haswin, “Design and Fabrication of Windmill Reciprocating Water Pumping System,” *International Journal of Advance Research and Innovative Ideas in Education*, vol. 2, no. 3, pp. 2395–4396, 2016.
- [86] A. I. Borok, M., S. Johnson, Z., & J. Agandu, “Design and Simulation of Wind Pump System for Ban Village,” *International Journal of Engineering Trends and Technology*, vol. 35, no. 2, pp. 80–84, 2016.
- [87] M. Jadhao, P. Patne, V. Ruiwale, A. Kadam, and S. Kulkarni, “Design of Windmill for lifting Water,” *International Journal of Current Engineering and Technology*, vol. 7, no. 7, pp. 325–330, 2017.
- [88] T. Aized, S. M. Sohail Rehman, S. Kamran, A. H. Kazim, and S. Ubaid ur Rehman,

- “Design and analysis of wind pump for wind conditions in Pakistan,” *Advances in Mechanical Engineering*, vol. 11, no. 9, 2019.
- [89] A. W. Manyonge, R. M. Ochieng, F. N. Onyango, and J. M. Shichikha, “Mathematical modelling of wind turbine in a wind energy conversion system: Power coefficient analysis,” *Applied Mathematical Sciences*, vol. 6, no. 89–92, 2012.
- [90] J. Wieringa, “Updating the Davenport roughness classification,” *Journal of Wind Engineering and Industrial Aerodynamics*, vol. 41, no. 1–3, pp. 357–368, 1992.
- [91] J. Wieringa, “Roughness-dependent geographical interpolation of surface wind speed averages,” *Quarterly Journal of the Royal Meteorological Society*, vol. 112, no. 473, pp. 867–889, 1986.
- [92] N. I. Ramli, M. I. Ali, M. S. H. Saad, and T. A. Majid, “Estimation of the Roughness Length (Z_0) in Malaysia using satellite image,” *7th Asia-Pacific Conference on Wind Engineering, APCWE-VII*, 2009.
- [93] D. S. Hammond, L. Chapman, and J. E. Thornes, “Roughness length estimation along road transects using airborne LIDAR data,” *Meteorological Applications*, vol. 19, no. 4, pp. 420–426, 2012.
- [94] Frederick Wheaton, *CIGR Handbook of Agricultural Engineering*, vol. 5, no. Dec. 1999.
- [95] Aermotor Windmill Corporation, “Installation, operation, and maintenance,” Arizona, USA, Publication no. 28140, 1978.
- [96] C. F. Gillis, Harris, “Still Turning: A History of Aermotor Windmills,” *Great Plains Research*, vol. 26, no. 2, pp. 148–148, 2016.
- [97] H. J. van Dijk, “Calculation of The Required Storage Tank Capacity in Windpump Irrigation Systems.,” *Wind Engineering*, vol. 10, no. 4, pp. 209-214, 1986.
- [98] M.Arturo,“Baces3d_brochure”www.baces3d.com/download/Baces3d_brochure_en.pdf.
- [99] G. Pei, “Current status and progress of digital orthopaedics in China., ” *Journal of Orthopaedic Translation*, vol. 2, no.3, pp. 107-117, 2019.
- [100] R. Zhou, L. Zhang, X. Pang, and L. Zhou, “Smooth piecewise spline surfaces over arbitrary control polyhedron,” *Chinese Journal of Aeronautics*, vol. 14, no. 1, pp. 57-64, 2001.
- [101] X. Zhang, X. Feng, P. Xiao, G. He, and L. Zhu, “Segmentation quality evaluation using region-based precision and recall measures for remote sensing images,” *ISPRS Journal of Picturegrammetry and Remote Sensing*, vol. 102, pp. 73-84, 2015.
- [102] N. Jyothirmayi and B. V. S. Rao, “The design and fabrication of a compound die to

- make hexagonal washer,” *International Journal of Mechanical and Production Engineering Research and Development*, vol. 9, no. 4, pp. 517–528, 2019.
- [103] V. V. Reddy, “Modelling and Manufacturing of Progressive die for Mechanical Press Operations,” *Turkish Journal of Computer and Mathematics Education (TURCOMAT)*, vol. 12, no. 3, pp. 3662–3671, 2021.
- [104] X. Zhang, Z. Zhao, Z. Guo, and W. Zhao, “Research on machining parameter optimization in finishing milling with multiple constraints,” *Proceedings of the Institution of Mechanical Engineers, Part B: Journal of Engineering Manufacture*, vol. 236, no. 6-7, pp. 968-980, 2021.
- [105] G. Sun, C. H. Sequin, and P. K. Wright, “Operation decomposition for freeform surface features in process planning,” *CAD Computer Aided Design*, vol. 33, no. 9, pp. 621–636, 2001.
- [106] L. T. Tunç, O. M. Ozkirimli, and E. Budak, “Machining strategy development and parameter selection in 5-axis milling based on process simulations,” *International Journal of Advanced Manufacturing Technology*, vol. 85, no. 5–8, pp. 1483–1500, 2016.
- [107] Y. Quinsat and L. Sabourin, “Optimal selection of machining direction for three-axis milling of sculptured parts,” *International Journal of Advanced Manufacturing Technology*, vol. 27, no. 11–12, pp. 1132–1139, 2006.
- [108] Z. Liu *et al.*, “FEM-based optimization approach to machining strategy for thin-walled parts made of hard and brittle materials,” *International Journal of Advanced Manufacturing Technology*, vol. 110, no. 5–6, pp. 1399–1413, 2020.
- [109] X. Zhang, T. Pan, A. Ma, and W. Zhao, “High efficiency orientated milling parameter optimization with tool wear monitoring in roughing operation,” *Mechanical Systems and Signal Processing*, vol. 165, 2022.
- [110] L. CHEN, P. HU, M. LUO, and K. TANG, “Optimal interface surface determination for multi-axis freeform surface machining with both roughing and finishing,” *Chinese Journal of Aeronautics*, vol. 31, no. 2, pp. 370–384, 2018.

Appendices

Appendix (1): CATIA V5 HTML Deviation Analysis report of the Sail

GENERAL INFORMATION

- [Project Information](#)
- [Company Information](#)
- [Inspector Information](#)

DIGITIZATION INFORMATION

- [Digitization Information](#)

DEVIATION CHECK RESULTS

- [Deviation Analysis Input Parameters](#)
- [Deviation Analysis Statistic Result](#)
- [3DXML Result](#)
- [Main Result](#)
- [Annotation Set 3](#)



GENERAL INFORMATION



Project Information

Project Title	Sail Scanning
Creation Date	Thursday, October 29, 2020 6:46:11 PM
Part Name	deviation_check
Comment	For documentation

Company Information

Company Name	T.B.Co.
Company Webpage	

Inspector Information

Inspector Name	Bibi
Phone Number	00218-92-500
E-mail Address	is_bibi@yahoo.it
Organization	University of Tripoli
Office Address	Tripoli

DIGITIZATION INFORMATION

Digitization Information

System	Baces3d Scanner
Comment	For documentation

DEVIATION CHECK RESULTS

Deviation Analysis Input Parameters

Reference Data	Mesh Creation.1
Data To Measure	Surface.1
Accuracy	0.01
Only Orthogonal	0
Absolute	0

Deviation Analysis Statistic Results

Total Number of Selected Points	1197
Number of Points Used in Computation	1197
Number of Points with Positive Deviation	5
Number of Points with Negative Deviation	1192
Positive Maximum Deviation Value	0.75mm
Negative Maximum Deviation Value	-3.01mm
Mean Deviation	-0.51mm
Standard Deviation	0.21mm
Positive Mean Deviation	0.61mm
Negative Mean Deviation	-1.27mm
Positive Tolerance	1.00mm
Negative Tolerance	-1.00mm
Percentage In Tolerance	97.33

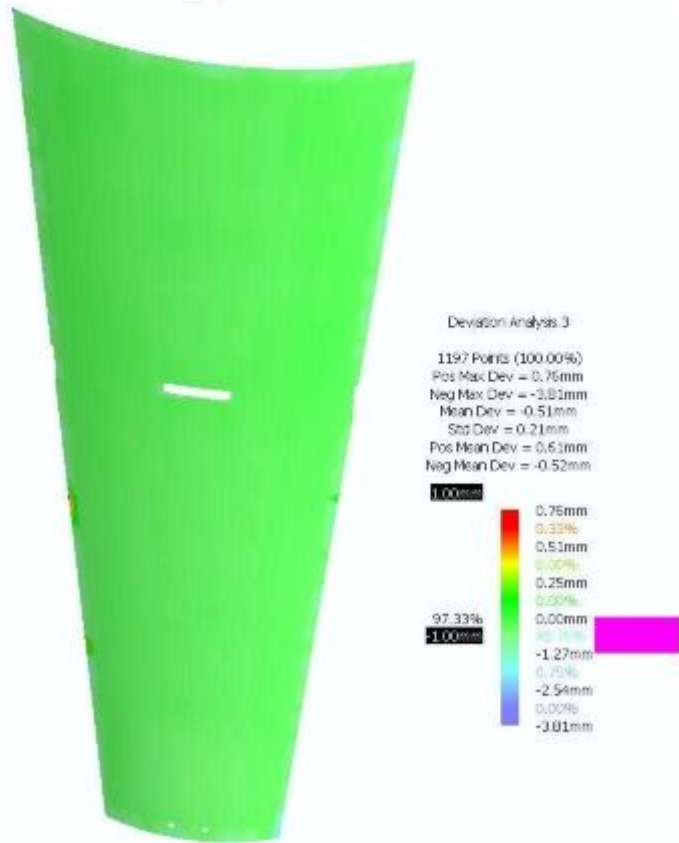


Figure 3.1 Deviation Results Distribution

[3DXML Resu...](#)

Figure 3.2

[Main Result](#)



Figure 3.3

[Annotation Set 3](#)

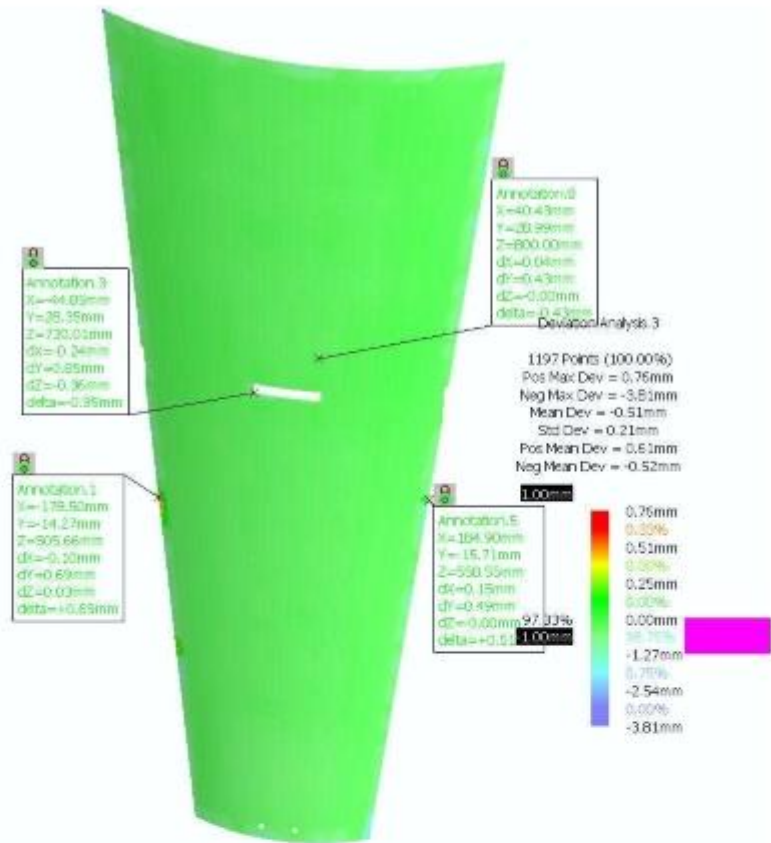


Figure 34

Appendix (2): CATIA V5 HTML Deviation Analysis report of the Sail Tie

GENERAL INFORMATION

- [Project Information](#)
- [Company Information](#)
- [Inspector Information](#)

DIGITIZATION INFORMATION

- [Digitization Information](#)

DEVIATION CHECK RESULTS

- [Deviation Analysis Input Parameters](#)
- [Deviation Analysis Statistic Result](#)
- [3DXML Result](#)
- [Main Result](#)

USER DEFINED RESULTS

- [Figure 4,1 Sail Tie Deviation Analysis1](#)
- [Figure 4,2 Sail Tie Deviation Analysis4](#)
- [Figure 4,3 Sail Tie Deviation Analysis3](#)
- [Figure 4,4 Sail Tie Deviation Analysis6](#)
- [Figure 4,5 Sail Tie Deviation Analysis5](#)



DIGITIZATION INFORMATION

Digitization Information

System	Baces3D
Comment	For documentation

DEVIATION CHECK RESULTS

Deviation Analysis Input Parameters

Reference Data	Surface1
Data To Measure	Mesh Creation1
Accuracy	0.01
Only Orthogonal	0
Absolute	0

Deviation Analysis Statistic Results

Total Number of Selected Points	3704
Number of Points Used in Computation	3704
Number of Points with Positive Deviation	614
Number of Points with Negative Deviation	397
Positive Maximum Deviation Value	0.15mm
Negative Maximum Deviation Value	-0.12mm
Mean Deviation	0.01mm
Standard Deviation	0.03mm
Positive Mean Deviation	0.05mm
Negative Mean Deviation	-0.02mm
Positive Tolerance	1.00mm
Negative Tolerance	-1.00mm
Percentage In Tolerance	100.00

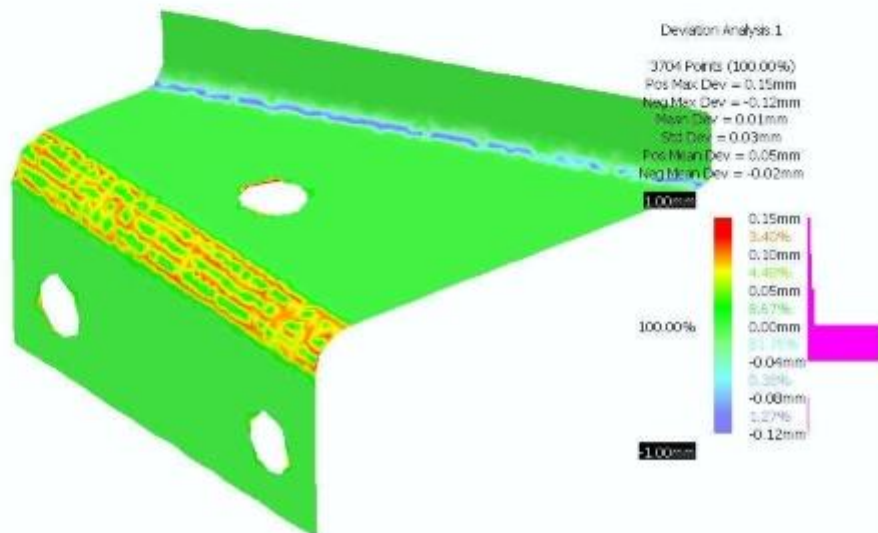


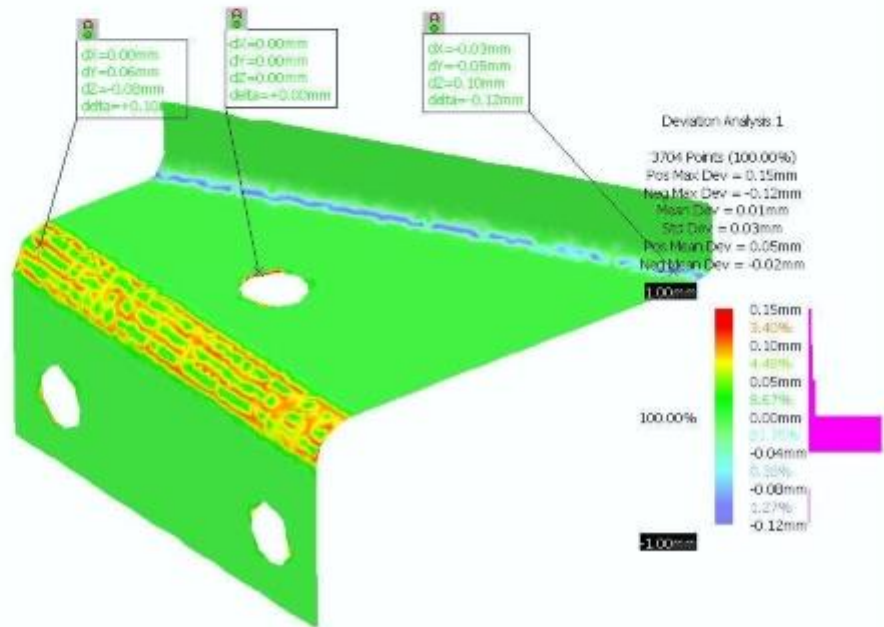
Figure 3.1 Deviation Results Distribution

[3DXML Result](#)



Figure 3.2

[Main Result](#)



USER DEFINED RESULTS

Figure 4.1 Sail Tie Deviation Analysis1

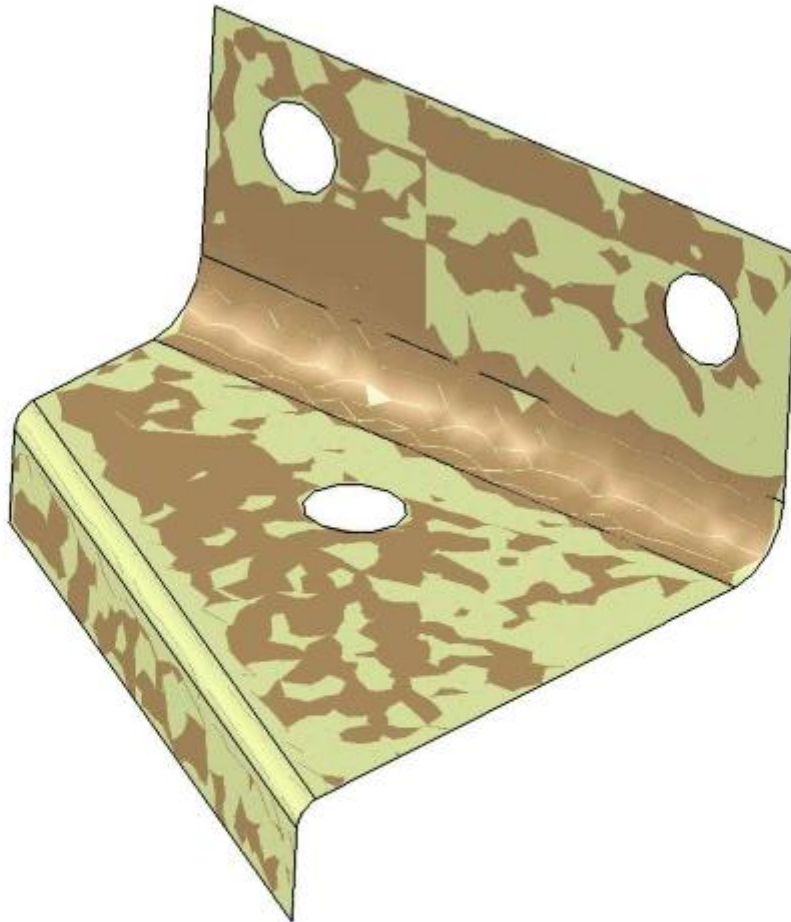


Figure 4.2 Sail Tie Deviation Analysis4

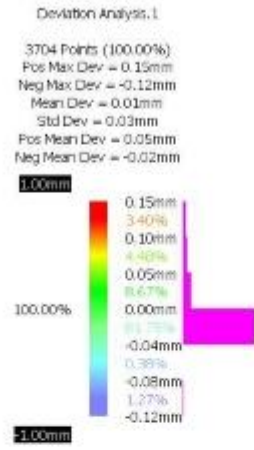
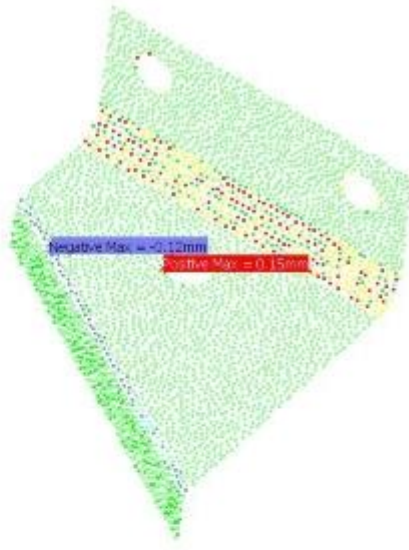


Figure 4.3 Sail_Tie_Deviation Analysis3

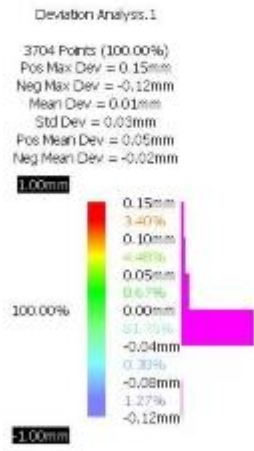
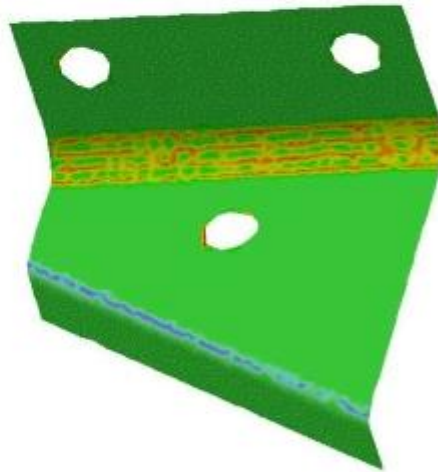


Figure 4.4 Sail_Tie_Deviation Analysis6



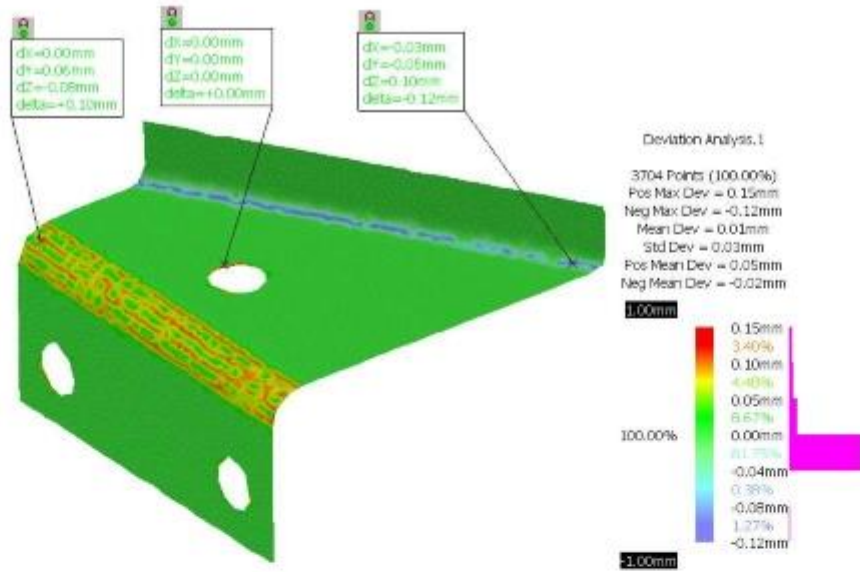
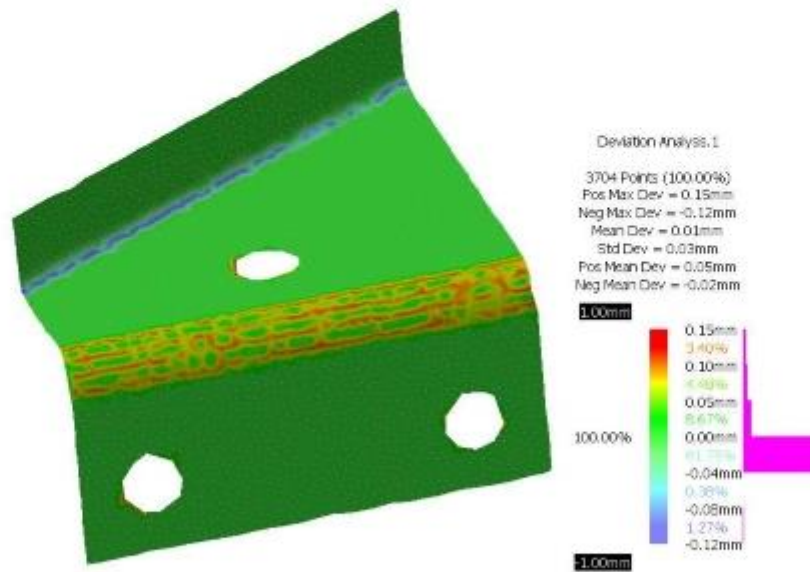


Figure 4.5 Sail Tie Deviation Analysis5





جامعة طرابلس
كلية الهندسة
قسم الهندسة الميكانيكية و الصناعية

تطبيق الهندسة العكسية في تصنيع النموذج الأولي لمكونات الدوار لطاحونة ريحية لضخ المياه

مقدم من الطالب: اسماعيل محمد حسين بلال

تحت إشراف: الدكتور عبد الباسط علي فريفر
أستاذ مشارك

قدمت الاطروحة استكمالاً لمتطلبات الإجازة العليا (الماجستير) في الهندسة الصناعية

ربيع 2021-2022

الملخص

تعد طواحين الهواء التي تعمل بضخ المياه بدائل موثوقة لتوفير المياه في بعض المناطق المعزولة عن شبكة الكهرباء، خاصة تلك التي تعاني من ضعف مصادر الرياح التي لا تكفي لتشغيل توربينات الرياح لتوليد الكهرباء. يتطلب التصميم الناجح لطواحين الهواء لضخ المياه دراسة متأنية للعديد من المعلمات المتغيرة اعتماداً على نمط الرياح وتضاريس الموقع. في هذه الدراسة، اعتمد الباحثون على تطبيق نهج متكامل بين بعض الأنشطة التي تستخدم عادة في تصميم الطواحين الريحية والهندسة العكسية (RE)، بهدف الحصول على نموذج (CAD) ثلاثي الأبعاد لنظام طاحونة ضخ المياه. سيكون هذا النموذج ثلاثي الأبعاد أساساً لتصنيع النموذج الأولي لطاحونة الهواء التي سيتم تثبيتها في موقع تجريبي في إحدى ضواحي مدينة تاجوراء ضمن مشروع بحثي. لا يمكن إهمال تلك الأنشطة التي تستخدم في تصميم الطواحين الريحية عند تطبيق الهندسة العكسية للتصنيع الناجح للطواحين؛ تم استخدام بيانات الرياح المسجلة في مركز أبحاث ودراسات الطاقة الشمسية (CSERS) لعدة سنوات لحساب متوسط سرعة الرياح اليومية والشهرية ودراسة نمط الرياح اليومي. أظهر تحليل بيانات الرياح التي تم جمعها أن الحد الأدنى والحد الأقصى لمتوسط سرعة الرياح اليومية في تاجوراء يتراوح من 2.35 م / ث إلى 4.69 م / ث، ومتوسط سرعة الرياح السنوي 3.24 م / ث. من بين أنشطة التصميم الأمامية تقدير موارد الرياح المتاحة في الموقع لتحديد حجم النظام لتوفير متطلبات المياه بالموقع البالغة 5 متر مكعب / يوم. من هذه النقطة فصاعداً، تم اختيار طاحونة هوائية تجارية لضخ المياه يبلغ ارتفاعها 4.88 متراً (16 قدماً) وارتفاع برج قياسي يبلغ 12 متراً لتكون هدفاً لتطبيق (RE) للحصول على نموذج (CAD). يتم يتم إنجاز الهندسة العكسية على ثلاث مراحل: رقمنة الجزء المستهدف، ومعالجة البيانات المقاسة، ثم إنشاء نموذج (CAD). لاعتماد النموذج ثلاثي الأبعاد لجميع الأجزاء. لاعتماد النموذج ثلاثي الأبعاد لجميع الأجزاء، يجب مقارنتها بالبيانات الأصلية المسوحة ضوئياً باستخدام تحليل الانحراف في CATIA. بعد اعتماد النماذج ثلاثية الأبعاد لجميع مكونات الدوار، تم إنشاء نماذج التجميع ثلاثية الأبعاد بناءً على النهج المتكامل للهندسة العكسية. بالنسبة للأشعة المنحنية، فقد قام الباحث بتطبيق مثلاً عملياً متكاملًا لأحد تطبيقات الهندسة العكسية لتصميم قالب ثني لتقويس أشعة طاحونة ريحية (هوائية) لضخ المياه باستخدام برمجة محاكاة آلات التحكم العددي بالكمبيوتر (CNC) باستخدام أنظمة التصميم بمساعدة الحاسب والتصنيع (CAD / CAM) وتقنية التصنيع باستخدام الحاسب الآلي لتصنيع القالب. تم استخدام التطبيق التفاعلي ثلاثي الأبعاد بمساعدة الحاسب V5 (CATIA) كنظام CAD / CAM متكامل لتصميم وتطوير القالب ومحاكاة العملية من خلال النماذج الرسومية ثلاثية الأبعاد. نظرًا لصعوبة تصنيع تقوس الأشعة يدويًا بناءً على العمالة المتاحة، وعدد الأشعة المستخدمة لإنتاج وحدة واحدة من طاحونة ضخ المياه، وأهمية الأشعة في تحسين كفاءة نظام الطاحونة الهوائية، فقد تم اتخاذ قرار بتصميم وتصنيع قالب أحادي العملية. يتكون هذا القالب من أربعة أجزاء لتلائم سعة ماكينة (CNC) المتاحة لتقويس الأشعة باستخدام نموذج الشراع ثلاثي الأبعاد من الهندسة العكسية (Sail's 3D) من (RE). تم إعداد نموذج التصنيع بمساعدة الحاسب (CAM) لآلة أجزاء القالب، وتم إجراء محاكاة لمسار الأداة باستخدام (CATIA V5)، وتمت برمجة جميع عمليات المعالجة. وباستخدام مركز آلة CNC، تم تشكيل جميع أجزاء القالب وتجميعها باستخدام اللحام، وتم تصنيع نماذج الأشعة الأولية. وأخيرًا، تجدر الإشارة إلى أن طواحين الهواء الخاصة بضخ المياه لا يمكن تصنيعها فقط من خلال تطبيق الهندسة العكسية.

تطبيق الهندسة العكسية في تصنيع النموذج الأولي لمكونات الدوار لطاحونة ريحية لضخ المياه

مقدم من الطالب: إسماعيل محمد حسين بلال

أجيزت هذه الأطروحة من قبل لجنة المناقشة:

الاسم:..... العضو الخارجي

(مكان العمل و عنوانه).

الاسم:..... العضو الداخلي

(قسم الهندسة الميكانيكية و الصناعية-طرابلس).

الاسم: د. عبدالباسط علي فريفر المشرف الاول

(قسم الهندسة الميكانيكية و الصناعية-طرابلس).

الإعتماد

د. د.

عميد الكلية

مدير مكتب الدراسات العليا و التدريب

تاريخ الإعتماد/...../..... .